

REPORT DOCUMENTATION PAGE

Form Approved
OMB No. 0704-0188

1a. REPORT SECURITY CLASSIFICATION UNCLASSIFIED		1b. RESTRICTIVE MARKINGS	
2a. SECURITY CLASSIFICATION AUTHORITY		3. DISTRIBUTION / AVAILABILITY OF REPORT Approved for public release; distribution unlimited.	
2b. DECLASSIFICATION / DOWNGRADING SCHEDULE			
4. PERFORMING ORGANIZATION REPORT NUMBER(S)		5. MONITORING ORGANIZATION REPORT NUMBER(S)	
6a. NAME OF PERFORMING ORGANIZATION Research Laboratory of Electronics Massachusetts Institute of Technology	6b. OFFICE SYMBOL (If applicable)	7a. NAME OF MONITORING ORGANIZATION	
6c. ADDRESS (City, State, and ZIP Code) 77 Massachusetts Avenue Cambridge, MA 02139		7b. ADDRESS (City, State, and ZIP Code)	
8a. NAME OF FUNDING / SPONSORING ORGANIZATION Office of Naval Research	8b. OFFICE SYMBOL (If applicable)	9. PROCUREMENT INSTRUMENT IDENTIFICATION NUMBER N00014-80-C-0941	
8c. ADDRESS (City, State, and ZIP Code) 800 North Quincy Street Arlington, VA 22217		10. SOURCE OF FUNDING NUMBERS	
		PROGRAM ELEMENT NO.	PROJECT NO. NR 395-066
		TASK NO.	WORK UNIT ACCESSION NO.
11. TITLE (Include Security Classification) Communications: Fiber-Coupled External-Cavity Semiconductor High-Power Laser: Final Report			
12. PERSONAL AUTHOR(S) R.H. Rediker et al.			
13a. TYPE OF REPORT Final	13b. TIME COVERED FROM 7/1/80 TO 12/31/88	14. DATE OF REPORT (Year, Month, Day) June 30, 1989	15. PAGE COUNT 96 pp.
16. SUPPLEMENTARY NOTATION			
17. COSATI CODES		18. SUBJECT TERMS (Continue on reverse if necessary and identify by block number)	
FIELD	GROUP	SUB-GROUP	
19. ABSTRACT (Continue on reverse if necessary and identify by block number) Work by R. H. Rediker and his collaborators is summarized here.			
20. DISTRIBUTION / AVAILABILITY OF ABSTRACT <input type="checkbox"/> UNCLASSIFIED/UNLIMITED <input type="checkbox"/> SAME AS RPT. <input type="checkbox"/> DTIC USERS		21. ABSTRACT SECURITY CLASSIFICATION UNCLASSIFIED	
22a. NAME OF RESPONSIBLE INDIVIDUAL Barbara Passero - RLE Contract Reports		22b. TELEPHONE (Include Area Code) (617) 253-2500	22c. OFFICE SYMBOL

February 1981

REPORTS DISTRIBUTION LIST FOR ONR PHYSICS PROGRAM OFFICE
UNCLASSIFIED CONTRACTS

Director Defense Advanced Research Projects Agency Attn: Technical Library 1400 Wilson Blvd. Arlington, Virginia 22209	3 copies
Office of Naval Research Physics Program Office (Code 421) 800 North Quincy Street Arlington, Virginia 22217	3 copies
Office of Naval Research Director, Technology (Code 200) 800 North Quincy Street Arlington, Virginia 22217	1 copy
Naval Research Laboratory Department of the Navy Attn: Technical Library Washington, DC 20375	3 copies
Office of the Director of Defense Research and Engineering Information Office Library Branch The Pentagon Washington, DC 20301	3 copies
U. S. Army Research Office Box 12211 Research Triangle Park North Carolina 27709	2 copies
Defense Technical Information Center Cameron Station Alexandria, Virginia 22314	⁴ 12 copies
Director, National Bureau of Standards Attn: Technical Library Washington, DC 20234	1 copy
Commanding Officer Office of Naval Research Western Regional Office 1030 East Green Street Pasadena, California 91101	3 copies

Commandant of the Marine Corps Scientific Advisor (Code RD-1) Washington, DC 20380	1 copy
Naval Ordnance Station Technical Library Indian Head, Maryland 20640	1 copy
Naval Postgraduate School Technical Library (Code 0212) Monterey, California 93940	1 copy
Naval Missile Center Technical Library (Code 5632.2) Point Mugu, California 93010	1 copy
Naval Ordnance Station Technical Library Louisville, Kentucky 40214	1 copy
Commanding Officer Naval Ocean Research & Development Activity Technical Library NSTL Station, Mississippi 39529	1 copy
Naval Explosive Ordnance Disposal Facility Technical Library Indian Head, Maryland 20640	1 copy
Naval Ocean Systems Center Technical Library San Diego, California 92152	1 copy
Naval Surface Weapons Center Technical Library Silver Spring, Maryland 20910	1 copy
Naval Ship Research and Development Center Central Library (Code L42 and L43) Bethesda, Maryland 20084	1 copy
Naval Avionics Facility Technical Library Indianapolis, Indiana 46218	1 copy

LIBRARY
RESEARCH REPORTS DIVISION
NAVAL POSTGRADUATE SCHOOL
MONTEREY, CALIFORNIA 93940

RESEARCH LABORATORY OF ELECTRONICS
MASSACHUSETTS INSTITUTE OF TECHNOLOGY-
" CAMBRIDGE, MASSACHUSETTS 02139

Communications: Fiber-Coupled External-Cavity
Semiconductor High-Power Laser

Final Report

Period Covered July 1, 1980 - December 31, 1988

Submitted to the Office of Naval Research
Contract N00014-80-C-0941

by Dr. Robert H. Rediker, Principal Investigator

June ~~30~~, 1989

Table of Contents

I.	Introduction	1
II.	External cavity controlled operation of a semiconductor diode gain element in series with an optical fiber	6
	A. Experimental apparatus	6
	B. Experimental results	11
	1. Stimulated emission (lasing) spectra	11
	2. Temporal stability of external cavity output	14
	3. Threshold behavior	18
	C. Analysis of threshold data to obtain insertion loss of fibers in the cavity	21
	D. Determination of factor A	25
III.	Operation of five individual lasers as a coherent ensemble controlled by a spatial filter within an external cavity	31
	A. Development of experimental facilities at RLE on M.I.T. campus	31
	B. The external cavity	32
	C. The gain elements	37
	D. Experimental results	38
	E. Theory	44
IV.	High-spectral-purity cw and pulse operation of the coherent ensemble	53
	A. Improvements to the experimental apparatus	53
	B. Improvements to the external cavity	53
	C. Experimental results – high spectral purity	54
	D. Experimental results – power amplification	60
V.	Validation of the model of the external-cavity semiconductor laser	63
	A. Improvements to the experimental apparatus	63
	B. Improvements to the external cavity	63
	C. The experimental results – the intensity distribution	65
	D. The experimental results – the phase distribution	67
VI.	Preparations for fiber-coupled operation	73
	A. Effect of changing the polarization of the radiation at the input to the cavity	73
	B. Quantification of coupling with one-meter fiber	78
	C. Modifications to the five-element external cavity	88
VII.	Epilogue	91

COMMUNICATIONS: FIBER-COUPLED EXTERNAL-CAVITY
SEMICONDUCTOR HIGH-POWER LASER

Final Report to the Office of Naval Research
Contract N00014-80-C-0941

July 1, 1980 - December 31, 1988

Robert H. Rediker

Massachusetts Institute of Technology
Department of Electrical Engineering and Computer Science
and Research Laboratory of Electronics

I. Introduction

When this program was initiated in July, 1980, the state-of-the-art in semiconductor lasers had reached the point where as stated in the proposal "these lasers must be given serious consideration for satellite-borne operation where reliability and power conversion efficiency are of prime concern. The key technical question which needs to be answered is whether a large number of these low-power semiconductor lasers can be coupled in parallel to produce a high-average power (~ 1 kW) coherent laser beam." During the 8-1/2 years of this contract this state-of-the-art has improved even more than forecasted in the proposal. Monolithic broad area or stripe-array lasers have been reported with output power of the order of 10 watts (compared to of the order of 10 milliwatts in 1980). In this program the coherent coupling of an array of individual semiconductor lasers by an external cavity has been demonstrated, a model of operation has been developed, and the model validated so one can extrapolate easily to the number of lasers needed for the 1 kW originally proposed. The concept upon which this program is based is shown in Fig. 1.1. Illustrated in the figure starting from left to right are:

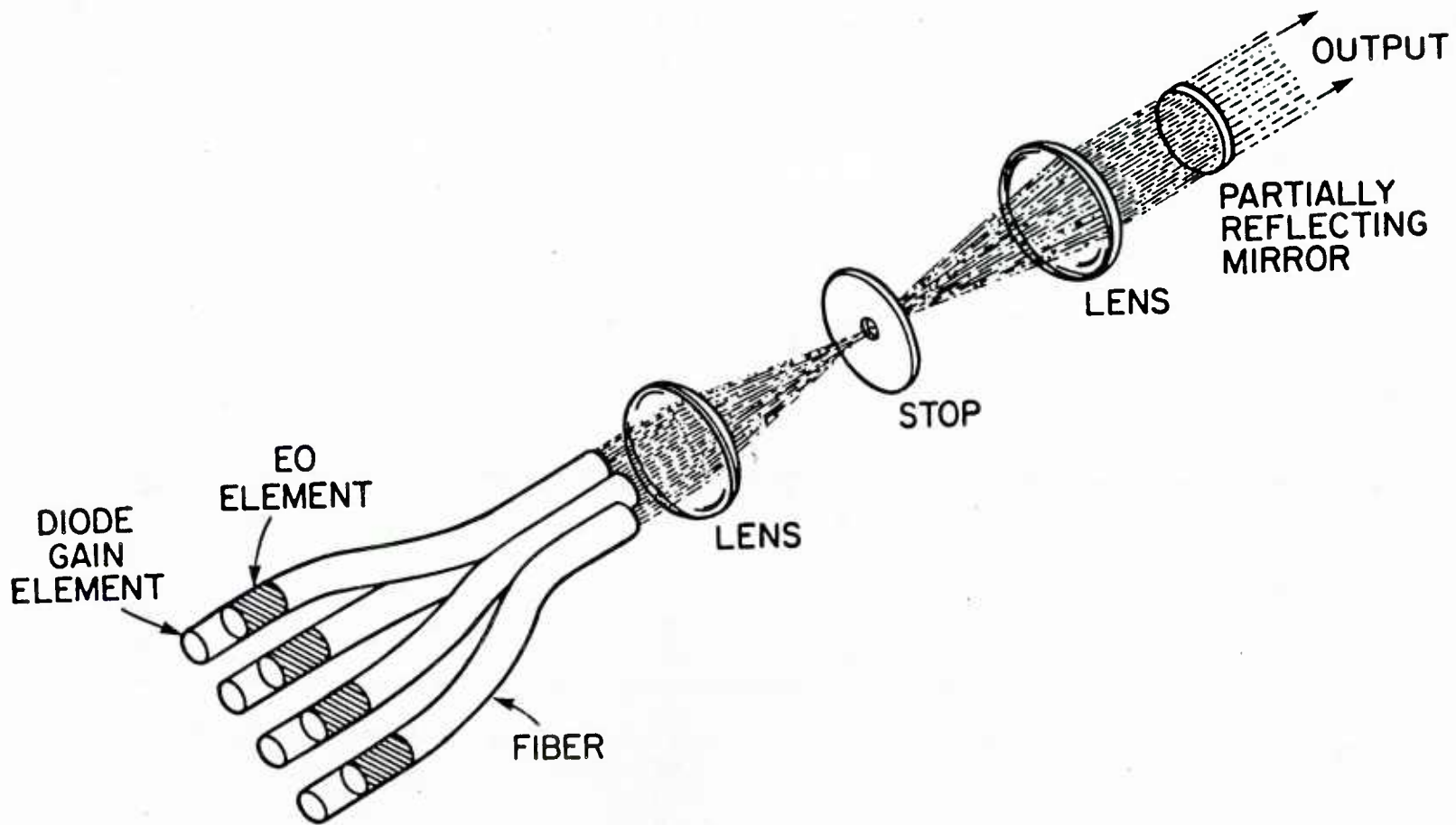


Fig. 1.1 Concept of the fiber-coupled external-cavity semiconductor high-power laser.

the semiconductor-diode gain element whose left facet is coated for near unity reflectivity and whose right facet is antireflection coated; electrooptic element for phase shifting; focusing lens; the appropriate spatial filter to assure coherence of wavefront across entire fiber bundle emitter (illustrated schematically as a stop); focusing lens to recollimate beam; and a partially reflecting mirror. The external cavity is bounded on the left by the reflecting facets of the semiconductor gain elements and on the right by the partially reflecting mirror.

The proposed fiber coupling may be essential because the density of the heat dissipation is prohibitive for monolithic or hybrid laser arrays on a single heat sink. The advantage of the external cavity in assuring coherence between a multitude of semiconductor lasers, whether they be on monolithically integrated or separated discrete lasers is discussed below. While in 1980, semiconductor lasers were being developed for the relatively high-price telecommunications market, the subsequent development and commercial introduction of the compact disc with semiconductor laser stylus has resulted in a low-price mass market with annual production of semiconductor lasers in tens of millions of units.

The results described in this report have been obtained with collaboration at no cost to the contract with various industrial concerns and with M.I.T. Lincoln Laboratory. The semiconductor lasers for the early experiments were supplied at no cost by Bell Telephone Laboratories. The semiconductor lasers for experiments in the five-laser external cavity were made especially for this program at no cost by Philips Research Laboratories, Eindhoven, The Netherlands. The Philips Corporation and the Sony Corporation are the co-inventors of the compact disc system (Philips markets compact disc players in the U.S.A. under the various labels of U.S. companies they own as well as receiving royalties

on all players marketed.) The spatial filters placed in the external cavity to assure coherence between the lasers were made especially for this program by the microelectronics group at Lincoln Laboratory. Recently, we were taught at Bell Telephone Laboratories how to efficiently couple the output from semiconductor lasers into fibers. This acknowledgment paragraph to these major contributors is placed here rather than at the end of this report because it would have been inappropriate to attempt this program or for ONR to have started to sponsor this program if this collaboration had not been either planned or expected at the beginning of the program.

The complete unknown when this program was initiated was whether the external cavity could control the operation of the series combination of a semiconductor gain element [a semiconductor laser with one or both of its facets anti-reflection (AR) coated] and an optical fiber. Since the electromagnetic mode of a semiconductor-diode gain element is TE and the electromagnetic mode of an optical fiber is HE, both different from the free space mode, it was important to make certain that this series combination of a semiconductor gain element and an optical fiber perform appropriately in an external cavity. The results demonstrating the desired control of this series combination by the external cavity are described in Section II of this report.

At the beginning of this program, the use of a spatial filter as was proposed in this program to assure coherent output from an array of semiconductor lasers had been demonstrated.¹ Three lasers were forced into coherence by placing reflective strips where the maxima of the interference pattern would occur if the three lasers used were coherent. The optical peak pulse power at room temperature was measured to be 5 W, three times the peak power of a single laser in the array. The use of an external cavity to control the wavelength

at which a semiconductor-diode gain element in the cavity will lase had also been demonstrated. It had been shown² that, with an external cavity, the laser radiation is produced in a single mode with no spectral or spatial hole-burning in the spontaneous spectrum. Thus the 35-nm spontaneous line is homogeneously broadened and the energy in this line is fed into the one mode. In these experiments the cw power in the laser line was 5 mW and its spectral width was less than 3.5 MHz or 8×10^{-6} nm.

Section III of this report describes the operation of five individual lasers as a coherent ensemble controlled by a spatial filter within an external cavity. Locking occurred with lasers whose output wavelength when operated individually with the spatial filter removed from the cavity differed by 6 nm.

The high-spectral-purity cw and pulse output from this ensemble of discrete diode lasers is described in Section IV. The validation of the model of the external-cavity semiconductor laser which allows extrapolation from 5-elements to a multitude of lasers is described in Section V. In the results presented in Sections III through V the semiconductor gain elements were at the input endplate of the external cavity. In Section VI, the design fabrication and installation of the fixtures to hold the fibers in the endplate is described as well as the jigs to efficiently couple output of the gain elements into the fiber.

References - Section I

1. E.M. Philipp-Rutz, "Spatially Coherent Radiation from an Array of GaAs Lasers," Appl. Phys. Lett. 26, 475 (1975).
2. M.W. Fleming and A. Mooradian, "Spectral Characteristics of External-Cavity-Controlled Semiconductor Lasers," IEEE J. Quant. Electron. 17, 44 (1981).

II. External Cavity Controlled Operation of a Semiconductor Diode Gain Element in Series with an Optical Fiber

A. Experimental Apparatus

Figure 2.1 is an artist's conception of the experimental arrangement showing the components inside the four-bar external cavity. Figure 2.2 is a photograph of the cavity. The Super-Invar four-bar structure supports and aligns the separate components. The use of the structure employing Super-Invar rods with their extremely low coefficient for thermal expansion was essential to obtain stable monochromatic output. The lens was AR coated at 820 nm on all surfaces. The semiconductor diode gain element is a (AlGa)As stripe geometry double heterostructure diode laser, supplied by Bell Telephone Laboratories, whose laser output was at ~ 820 nm. The laser was gain-guided in the dimension parallel to the plane of the junction. After the laser was characterized it was AR coated with ZrO_2 and the reflectivity per facet reduced to less than 0.5 percent from 810 to 840 nm.

To the right of the gain element is a cylindrical lens which compensates for the astigmatism inherent in the gain-guided/index-guided semiconductor diode gain element. This lens is a drawn quartz fiber of 40 μ m diameter, and is cemented to a miniature four-axis positioner which is mounted on the same stage as the diode. The lens is adjusted to obtain a far-field pattern that is roughly circular. The separation of the lens from the diode is on the order of the diameter of the lens.

The next element in the cavity is a graded-index (GRIN) rod lens used to change the now circular beam from diverging to converging. The lens is held in an arm attached to an x-y-z micropositioner mounted on two bars of the four-bar structure. Alignment in the horizontal and vertical directions is aided by

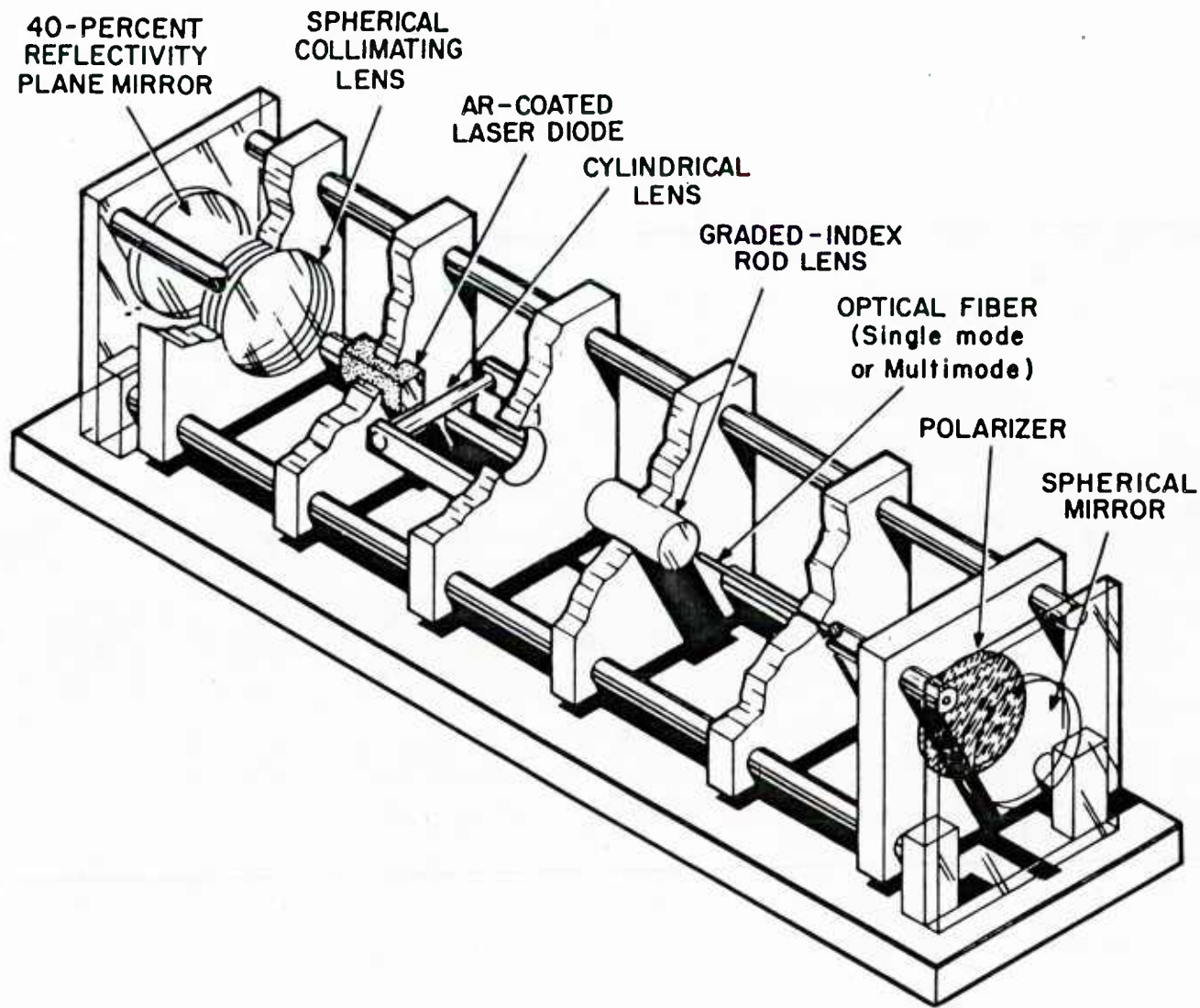


Fig. 2.1 Artist's sketch illustrating the experimental arrangement of components inside four-bar Super-Invar external cavity. From left to right: the 40-percent-reflectivity plane mirror; the spherical lens that focuses the collimated radiation from the plane mirror into the active area at the left facet of the AR-coated diode gain element; the cylindrical lens that compensates for the astigmatism of the radiation from the right facet of the AR-coated diode gain element; the graded-index rod lens that focuses the now spherical beam into the optical fiber; the optical fiber with a polarizer shown at its output; and the spherical mirror that reflects the radiation back into the fiber.

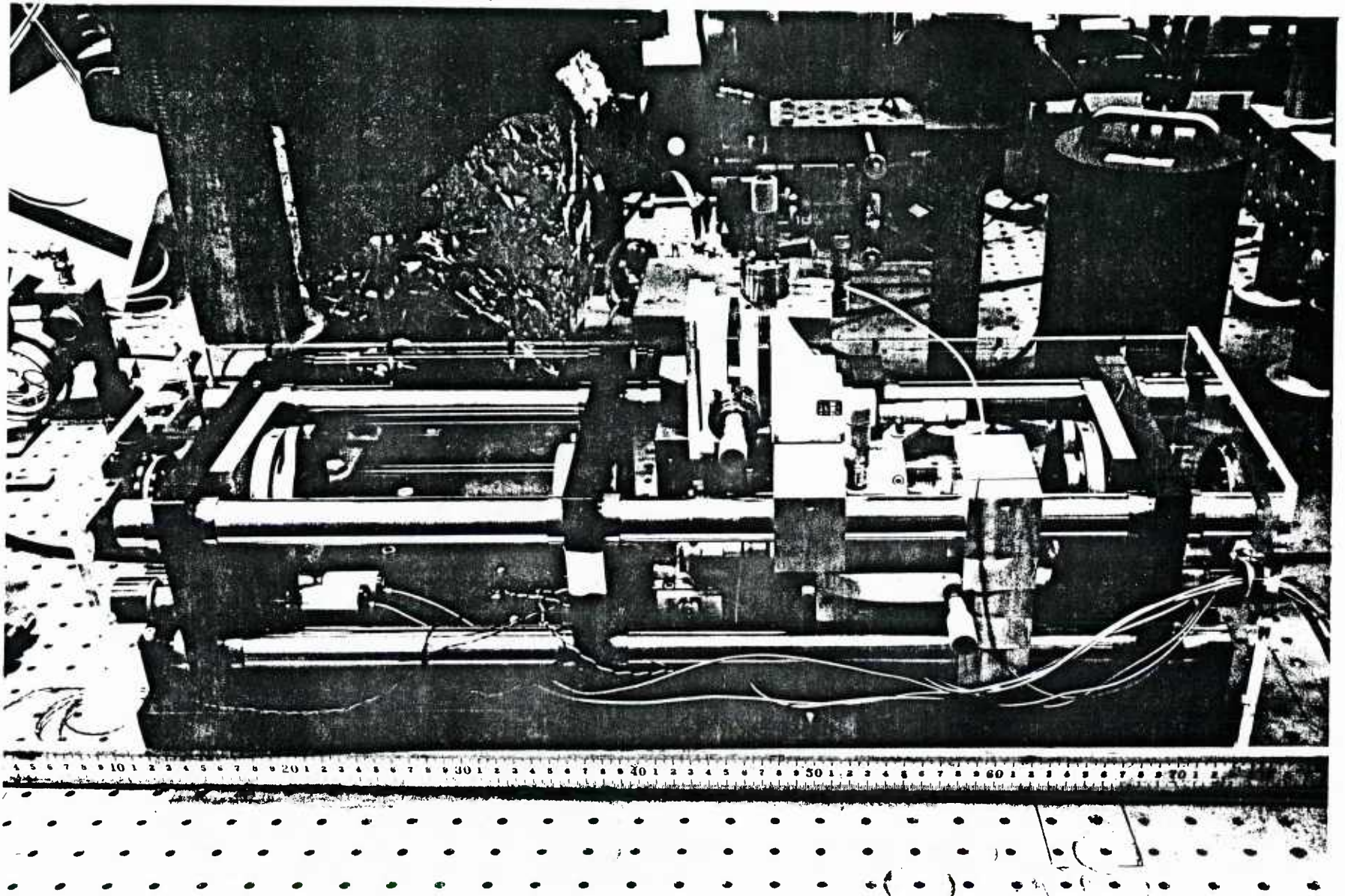


Fig. 2.2 Photograph of experimental arrangement showing micromanipulators used to align cavity. The experimental results were obtained with the cavity inside a suitable plexiglas enclosure.

the use of piezoelectrics on the x and y axes of the positioner. The axial (z-axis) position of the lens is optimized at the same time as the axial position of the optical fiber, to be described next.

Results for two types of optical fibers will be presented in the paper. The first type was a Corning 4834 fiber which was single mode with a 9.3 μm -diameter core. The second was Corning 8020 graded index fiber with a 63 μm core. The following characteristics of the fibers were supplied to us. The Type 4834 single-mode fiber was coded 2-01-4, had an absorption coefficient (α) of 2.53 dB/km at 820 nm, and had a cutoff wavelength (λ_c) of 720 nm. The multimode Type 8020 fiber was from Lot #60665105, had an α of 7.9 dB/km at 820 nm and had a 3-dB-cutoff frequency of 750 MHz-km.

Fibers of 14-cm length were prepared by cleaving to obtain optical quality end faces. In an attempt to prevent temperature fluctuations and stresses from affecting the fiber, and thereby the operation of the external cavity, the fiber was placed at the center of 2.36 cm-diameter split Super Invar rod. The preparation of the fibers required great care (e.g., the fibers were "threaded" into hollow stainless-steel tubes before cleaving so no damage would occur to the cleaved end faced). Only very short (0.5 cm) ends of the fibers protrude from the end of the Invar rod. The Super Invar rod, along with the fiber, is positioned by an x-y-z micropositioner fixed to two rods of the four-bar Super-Invar structure.

Because of the importance of the state of polarization in the spatially filtered multiple-gain-element fiber-coupled external-cavity laser, such as shown in Fig. 1.1, it is important to investigate the operation of the series combination of a single semiconductor diode gain element and optical fiber in the presence of a polarization-selective element. The next-to-last element in Fig. 2.1 is a polarizer. The objective of the polarizer is to preserve a

constant state of polarization at the output of the fiber in the external cavity laser. The polarizer is the infrared film type mounted on a rotary stage. It is the only element not connected to the four-bar structure. Instead, the polarizer is supported from a post in the optical table next to the four-bar structure.

The last element in the external cavity laser is a spherical mirror. It has a 7.5-cm radius of curvature, centered on the output end of the optical fiber. The mirror, coated for maximum-reflectivity, is held in a two-axis gimbal mount, with fine adjustment of tilt accomplished by piezoelectric activated positioners. The gimbal mount is fixed to a plate through which the four rods of the cavity structure pass.

The light path in the external cavity is as follows. Light emitted from the left side of the AR-coated laser diode is collimated by the spherical lens onto the plane mirror. The reflected beam is reimaged onto the diode facet by the spherical lens. The emission from the right side of the diode passes through the cylindrical lens, the graded-index rod lens and into the fiber (single-mode or multimode). A polarizer, when present, filters the output of the fiber. The spherical mirror reflects and converges the diverging light, sending it back through the polarizer, and into the fiber. The emission of the fiber end nearest the diode is then focused into the diode by the action of the graded-index rod lens and the cylindrical lens.

The diagnostics used to measure the output of the cavity included a back-biased EG&G type SGD-440 photodiode for taking light output (lux)-current curves, and a Spex Model 1400-11 3/4 meter spectrometer or a Tropel Model 240-2 scanning Fabry-Perot Spectrum Analyzer for measuring spectra. The resolution of the spectrometer was 0.05 nm and that of the Scanning Fabry-Perot 1.7×10^{-5} nm (7.5 MHz).

B. Experimental Results

1. Stimulated Emission (Lasing) Spectra

The semiconductor diode laser used in the experiments was gain-guided in the plane of the junction and exhibited a spectral output which consisted of a multiplicity of longitudinal modes.¹ After anti-reflection coating its facets to a reflectivity of less than 0.5 percent, the semiconductor diode was operated as a gain element in an external cavity similar to that used by Fleming and Mooradian.² The measured output spectrum of the external cavity now consisted of a single spectral line consistent with the results of reference 2. Mirrors were used to define both ends of the cavity: one mirror had 98-percent reflectivity; the other mirror had 40-percent reflectivity and served as the output coupler.

The semiconductor diode gain element was then placed in the experimental apparatus described in Section A and shown in Figs. 2.1 and 2.2. The output spectrum of the external cavity shown in Fig. 2.3 is for the diode gain element in series with the single-mode fiber, with the polarizer shown in Fig. 2.1 not in the cavity. The spectrum is shown in the figure both as measured using a spectrometer and as measured using a scanning Fabry-Perot interferometer. The top trace shown for the scanning interferometer covers its entire 1500 MHz free spectral range and demonstrates that the cavity output contains only a single spectral line. The bottom trace shows the spectral line on an expanded scale. The full-width at half-maximum (FWHM) of the line is indistinguishable from the 7.5-MHz resolution of the scanning interferometer.

The single-mode fiber of Fig. 2.3 was replaced with the multimode fiber to obtain the results of Fig. 2.4. (The optical fibers are

SPECTROMETER

SCANNING FABRY-PEROT INTERFEROMETER 7.5 MHz (1.7×10^{-5} nm) IS INSTRUMENT RESOLUTION

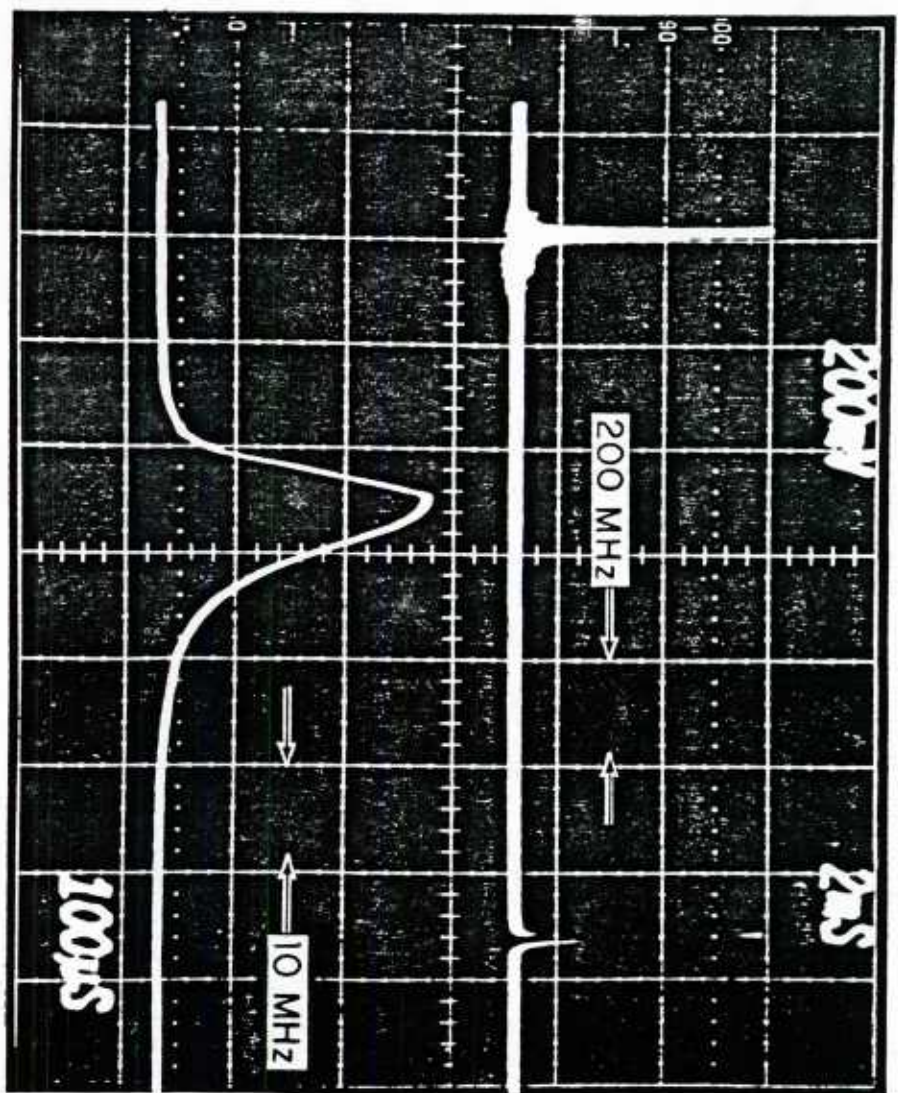
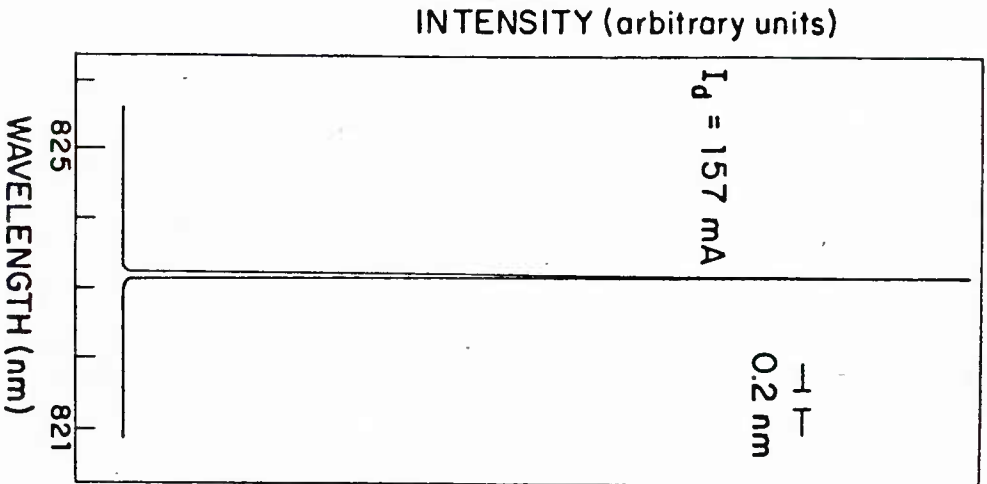
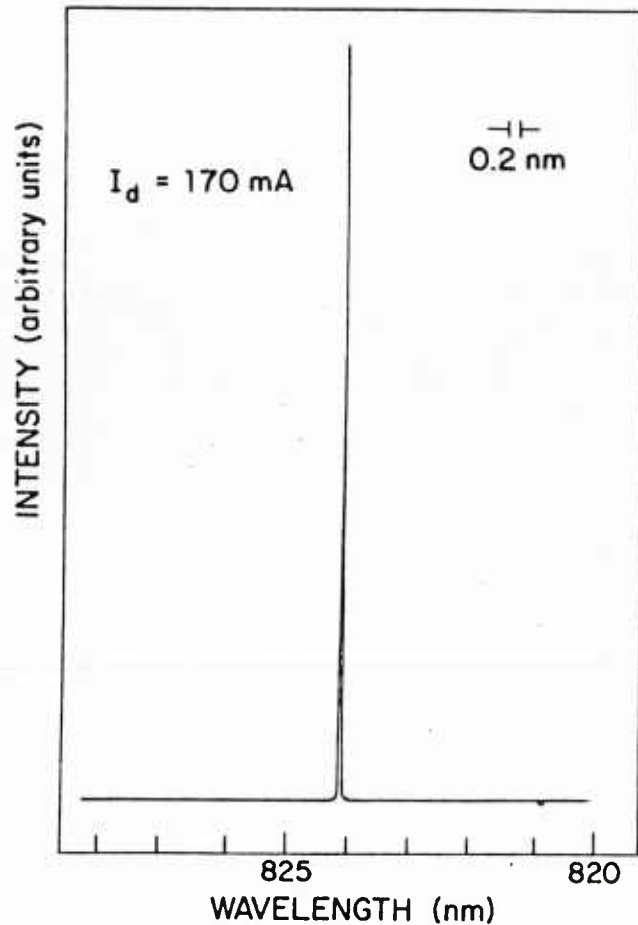


Fig. 2.3 a) Output spectrum of external cavity containing series combination of a single-mode fiber and a diode gain element b) Fabry-Perot-interferometer scan of this spectrum. Top trace shows entire 1500-MHz free spectral range, bottom trace shows that the FWHM of the line is indistinguishable from 7.5-MHz instrument resolution.

SPECTROMETER



SCANNING FABRY-PEROT INTERFEROMETER

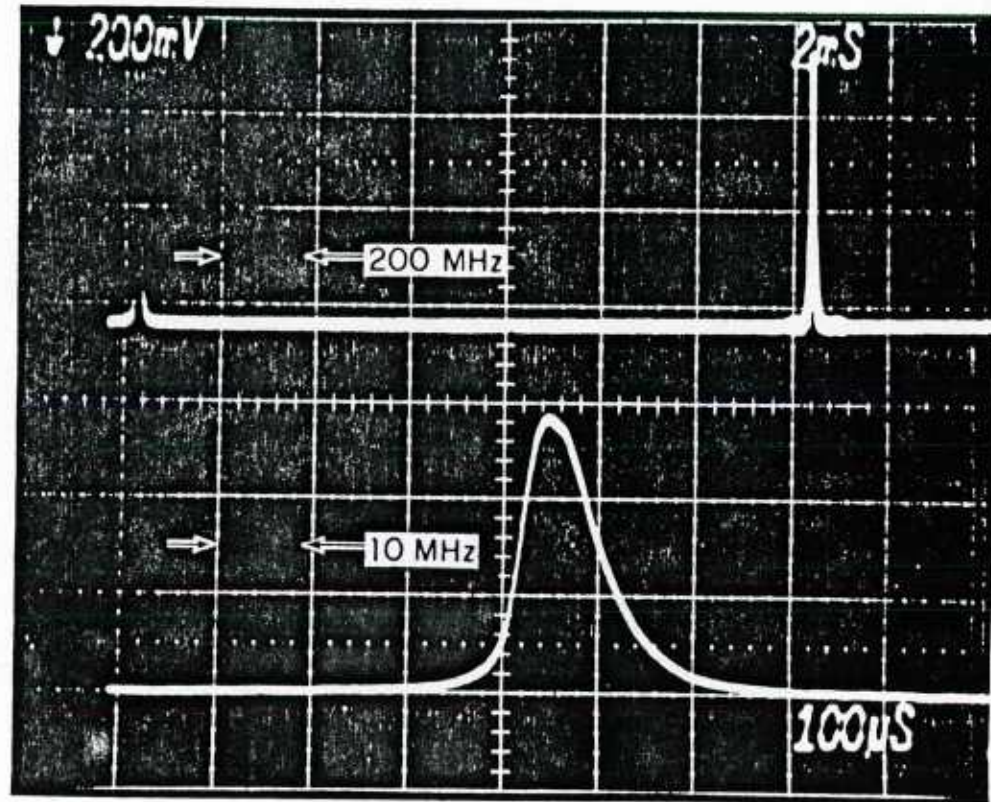


Fig. 2.4 a) Output spectrum of external cavity containing series combination of a multimode fiber and a diode gain element. b) Fabry-Perot-interferometer scan of this spectrum. Top trace shows entire 1500-MHz free spectral range, bottom trace shows that the FWHM of the line is indistinguishable from 7.5-MHz instrument resolution.

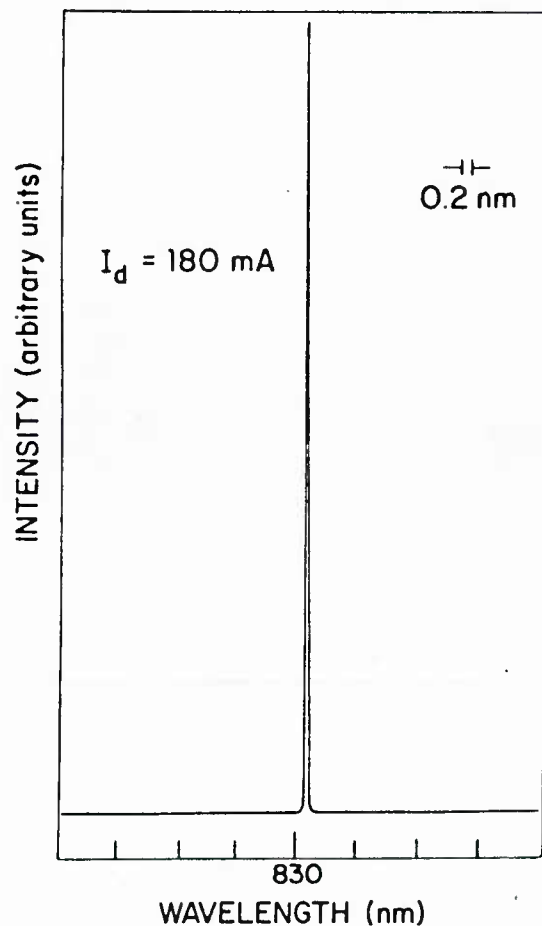
described in detail in Section A above.) Again the cavity output consists of a single spectral line and its FWHM is indistinguishable from the 7.5-MHz resolution of the scanning Fabry-Perot interferometer. The output in Fig. 2.4 is at a longer wavelength than that of Fig. 2.3 because, as indicated in the figure captions, the diode current is higher in the former case (170 mA compared to 157 mA) and the diode is consequently operating at a higher equilibrium temperature. The single spectral line output of Fig. 2.4 was *a priori* not expected and the data presented shows that this result is still obtained well above the threshold current. As will be discussed in Section B-3 below, the threshold currents for both the single-mode and multimode fiber in series with the gain element are very similar.

The output spectrum of the external cavity is shown in Fig. 2.5 for the diode gain element in series with the multimode fiber and polarizer placed in the cavity at the output of the fiber (see Fig. 2.1). The polarizer was aligned parallel to the diode-gain-element polarization. The spectrum again consists of a single spectral line and has a linewidth limited by the resolution of the scanning Fabry-Perot interferometer.

2. Temporal Stability of External Cavity Output

It is essential to confirm that the measurements reported in the paper are not averages of fluctuations and that there was no spiking, short pulses or any other such phenomena in the output of the external-cavity laser. The output of the cavity as measured with a wide-bandwidth photodetector was displayed on an oscilloscope and there were no spikes or fluctuations within the limiting 225-MHz bandwidth of the oscilloscope. The temporal variation was measured over a large range of sweep speeds on the oscilloscope. Results for 20 nsec per horizontal

SPECTROMETER



SCANNING FABRY-PEROT INTERFEROMETER

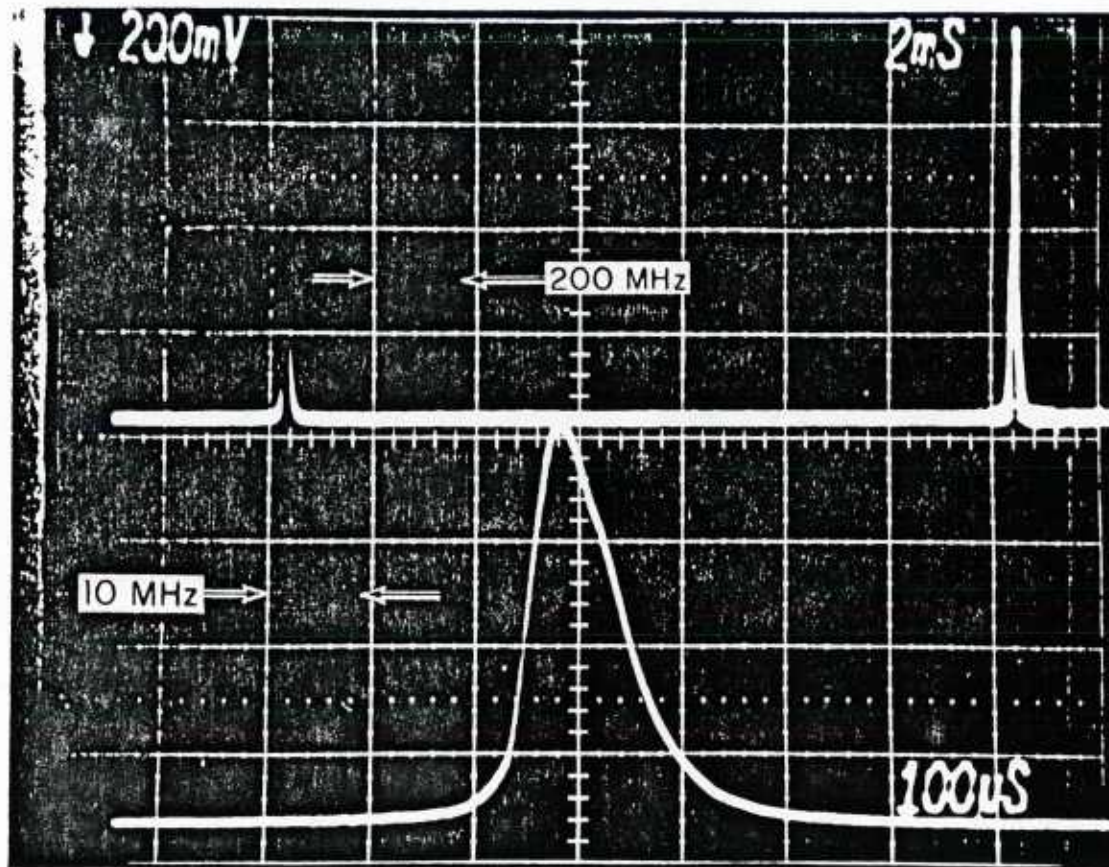
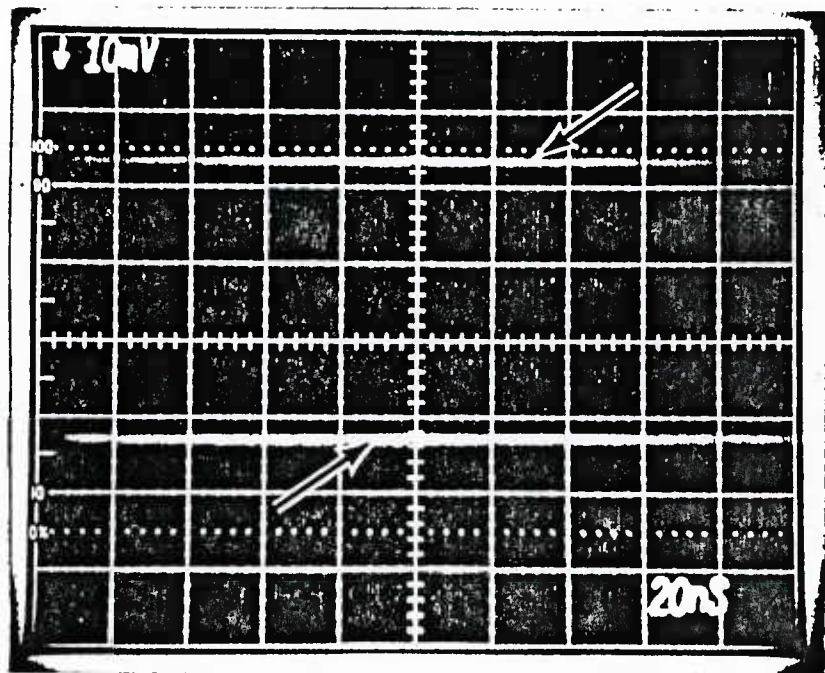


Fig. 2.5 a) Output spectrum of external cavity containing series combination of a multimode fiber and a diode gain element and with polarizer oriented with its polarization parallel to that of diode in series at other end of fiber. b) Fabry-Perot-interferometer scan of this spectrum. Top trace shows entire 1500-MHz free spectral range, bottom trace shows that the FWHM of the line is indistinguishable from 7.5-MHz instrument resolution.

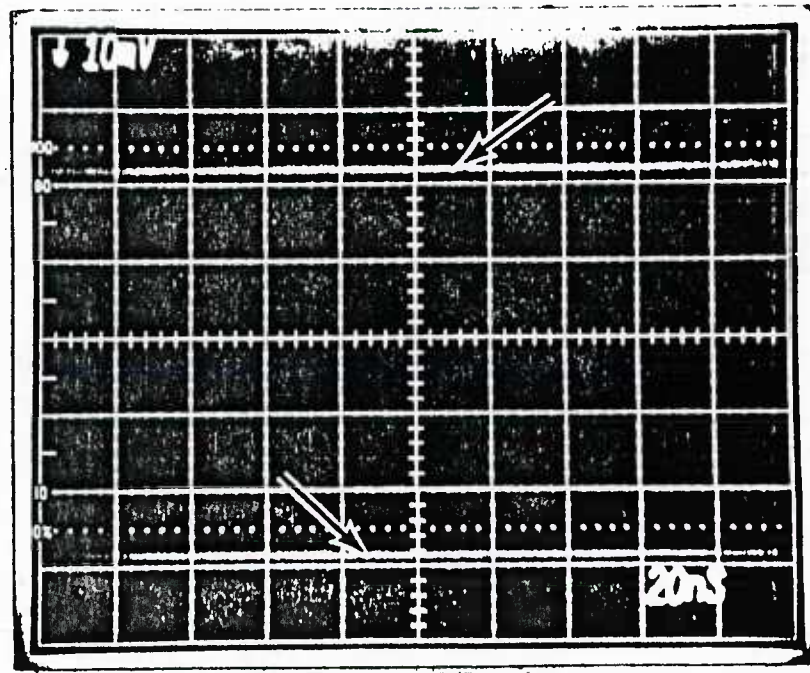
division are shown on Fig. 2.6. The top traces are for the detector in the dark, the bottom traces are measurements of the external cavity output. The left oscilloscope picture is for the diode gain element in series with the multimode fiber. For the results shown in the right oscilloscope picture, the polarizer was placed in the cavity at the output of the fiber. The polarizer was aligned parallel to the diode-gain-element polarization. The results of Fig. 2.6, which show a single trace, demonstrate that the short term stability of the cavity output is temporally invariant to at least one part in fifty up to the bandwidth of the oscilloscope.

The output (approximately 1 mW) was also measured using a spectrum analyzer with system noise of 10 nW within any 300-kHz-bandwidth interval. No noise above this level was measurable up to 100 MHz and at the cavity mode-beat frequency of 280 MHz. These results are consistent with the results for a semiconductor diode gain element in an external cavity² and are also consistent with the recent results reported for semiconductor diode lasers operating with an external mirror.^{3,4} The pulsing previously reported was explained to be related to laser defects causing regions of saturable absorption in the diode laser.^{3,4}

The results were particularly gratifying for the configuration with the polarizer in place, as they showed that there was no fluctuation in the polarization of the output from the multimode fiber when it was used inside the external cavity. The stability of this polarization is important for coherent coupling of semiconductor diode gain elements in parallel using fibers as shown in Fig. 1.1, and thus for the overall program.



(a)



(b)

Fig. 2.6 Temporal variation of output from external cavity containing series combination of multimode fiber and a diode gain element. a) No polarizer in cavity; b) Polarizer oriented with its polarization parallel to that of diode at output end of fiber. In both oscilloscope photographs, at 20 ns per horizontal division and 10 mV per vertical division, the wideband detector signal shows as a negative deflection. The top trace is for the detector in the dark. The diode gain element current is larger in (b) resulting in a larger detector output.

The temporal stability of the spectral output from the cavity was investigated for periods of the order of one minute. The external cavity was enclosed in a plexiglass box for the experiments described in this paper. No other thermal, acoustic, or magnetic isolation was used as has been used for ultra-stable CO₂ lasers.⁵ The stability over the period of one minute is illustrated by the results shown in Fig. 2.7. These results are for the diode gain element in series with the single-mode fiber. The maximum fluctuation in the output frequency of the external cavity was 2 MHz over the 1-minute interval.

A note of caution needs to be mentioned concerning temporal stability. To obtain the results presented in this report, correct alignment of the components within the cavity was essential. Incorrect alignment caused a large variety of temporal variations and could also be an explanation of the results of others showing these temporal variations.

3. Threshold Behavior

Figure 2.8 shows the effect of inserting the fibers into the cavity on the light output - current curves for the cavity and consequently on the diode threshold current. Curve A is for the diode laser before anti-reflection coating its facets, and curve B is for the same diode, now an AR-coated gain element, in the external cavity with the cavity defined at one end by a 98-percent-reflectivity mirror and the other end with a 40-percent-reflectivity mirror. For the other curves, the experimental arrangement is that illustrated in Figs. 2.1 and 2.2. The 40-percent-reflectivity mirror was again used to define one end of the cavity and to serve as the output coupler. Curve C is for the multimode fiber in series with the gain element and curve D is for the single-mode fiber

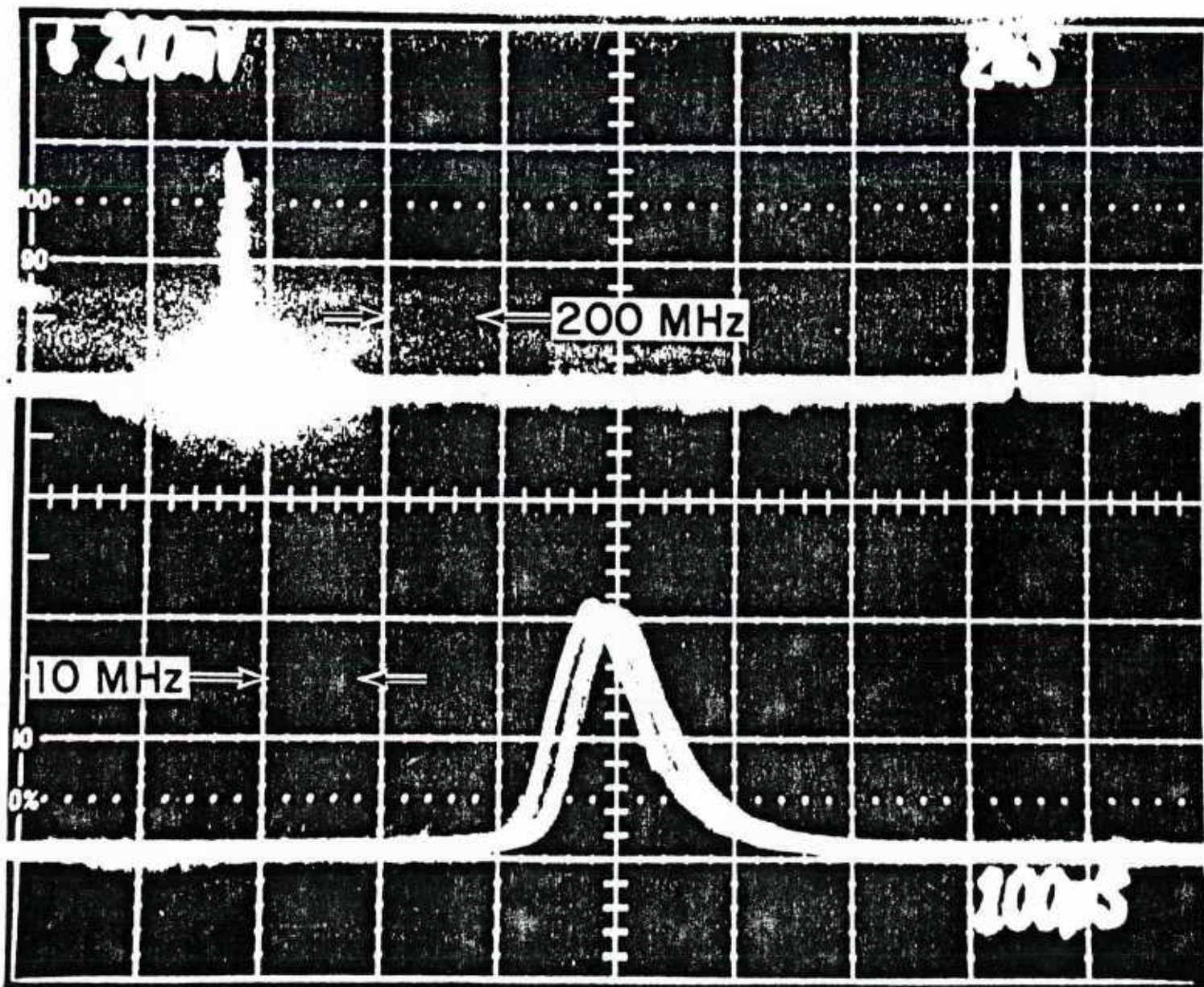


Fig. 2.7 Measurement of stability of laser over a 1-min. time interval. Traces are made up of 13 Fabry-Perot scans of spectrum, each taken 5 s apart. As in Figs. 2.3, 2.4 and 2.5, top trace shows entire 1500-MHz free spectral range, and abscissa is expanded by a factor of 20 in bottom trace. For results illustrated, external cavity contained series combination of a diode gain element and a single-mode fiber.

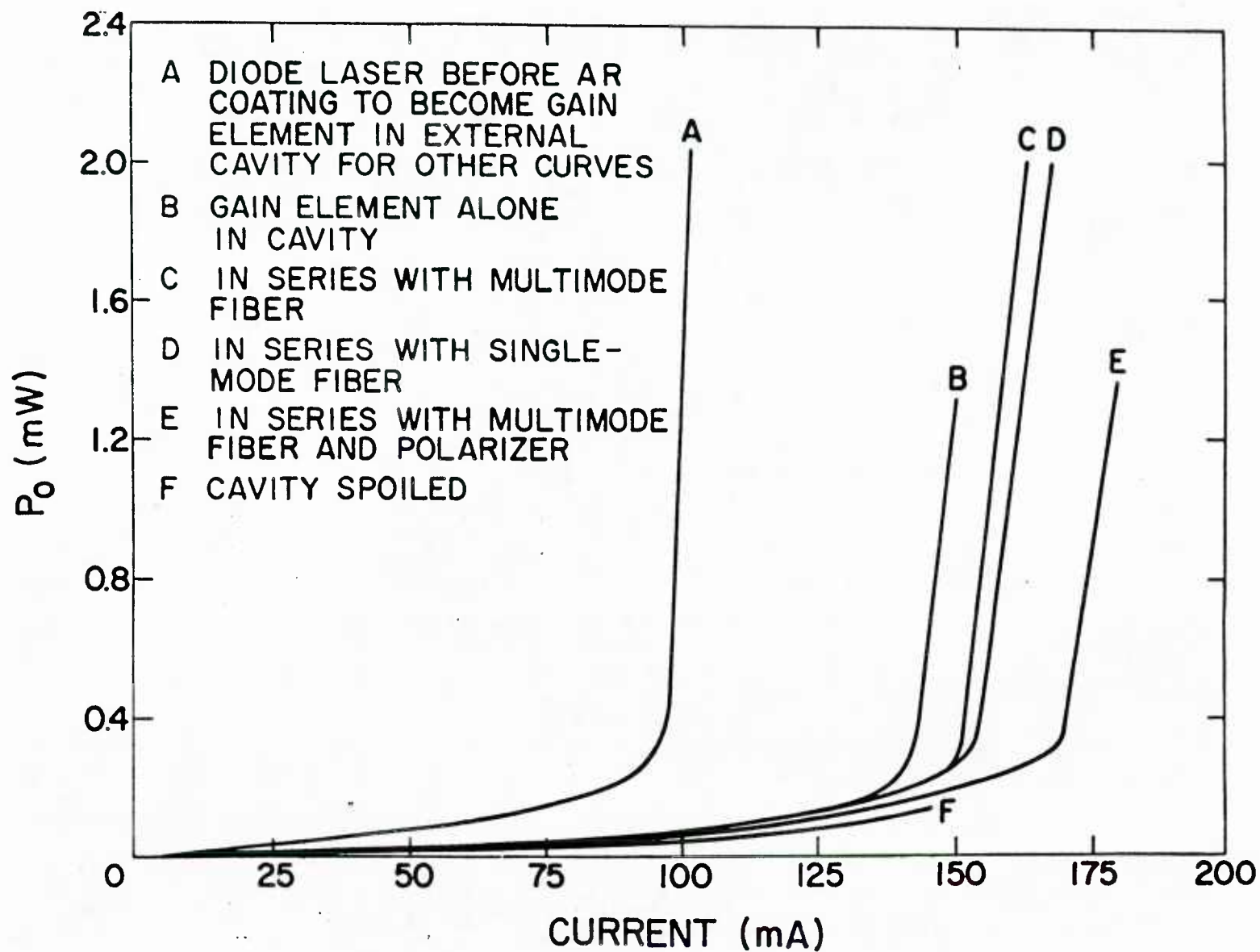


Fig. 2.8 Single-ended power output as a function of diode gain element current, for six experimental configurations described in inset of figure.

in series with the gain element. Note that the difference in the diode-gain-element threshold current for curves C and D is relatively very small. For curve E the polarizer was placed in the cavity at the output of the multimode fiber and it was aligned parallel to the diode gain element polarization. The cavity mirror was blocked to obtain curve F.

C. Analysis of Threshold Data to Obtain Insertion Loss of Fibers in the Cavity

In this section we develop a simple model of the external-cavity laser and find values of the losses in the laser consistent with the measured threshold current. The gain constant of the electromagnetic mode in the diode gain element can be approximated for the gain region of interest by

$$\Gamma g \ell = \frac{\eta_i \beta \Gamma}{s d} I - \Gamma \beta \ell J_0 \quad (1)$$

where Γ is the confinement factor for the mode in the diode gain region, g is the gain per unit length in the cavity, η_i is the internal quantum efficiency, I is the diode current, ℓ is the length of the diode, s is the width of the current distribution passing through the active region, d is the thickness of the active region, and β and J_0 are constants.

The external-cavity-laser model used in the analysis is shown in Fig. 2.9. In this model, the internal loss per unit length due to free-carrier absorption or other causes in the diode gain element is characterized by α and the loss elements are characterized by $\frac{1}{\kappa T}$, where for the fiber, κ is the fraction of the radiation coupled into the fiber and T is the transmission of the fiber. The value of κ is the mean of the coupling coefficient for coupling between the diode and one end of the fiber and the coefficient for coupling between the mirror and the other end of the fiber. The threshold gain must

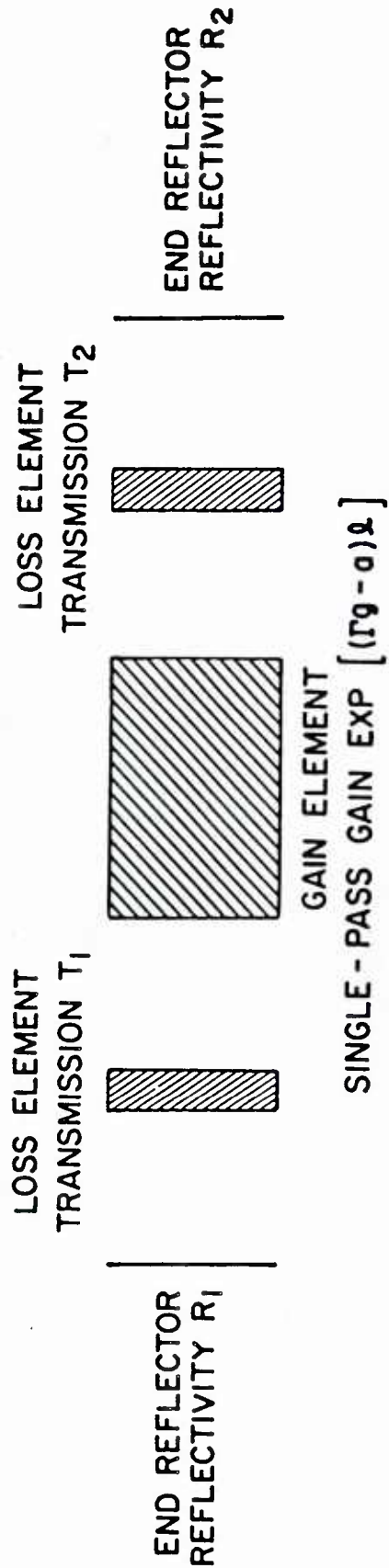


Fig. 2.9 Simple model of external-cavity laser used in analyzing threshold currents observed for various configurations. The loss elements are characterized by $1/\kappa T$ where T is the transmission, and κ is the mean of the coupling coefficients for coupling from the gain element and coupling from the end reflector.

satisfy the condition

$$R_1 R_2 \kappa_1^2 T_1^2 \kappa_2^2 T_2^2 \exp[2(\Gamma g_t - \alpha)l] = 1 . \quad (2)$$

Defining $\frac{sd}{\eta_i \beta \Gamma} \equiv A$ and substituting the value for threshold gain into Equation 1, the threshold current is

$$I_t = A \left[\alpha l + J_0 \beta \Gamma l - \ln \sqrt{R_1 R_2 \kappa_1^2 T_1^2 \kappa_2^2 T_2^2} \right] . \quad (3)$$

For various sets of components within the cavity corresponding to different diode threshold currents, the difference in the threshold currents is given by

$$\exp \frac{I_t - I_t'}{A} = \sqrt{\frac{R_1' R_2' \kappa_1'^2 \kappa_2'^2 T_1'^2 T_2'^2}{R_1 R_2 \kappa_1^2 \kappa_2^2 T_1^2 T_2^2}} . \quad (4)$$

As the reference cavity, we will use the diode laser before its facets were antireflection (AR) coated. For this diode laser $R_1' = R_2' = 0.32$, $T_1' = T_2' = 1$, and $I_t' = 97$ mA. In the external cavity the known values of the end reflectors will be used and $\kappa_1 T_1$ and/or $\kappa_2 T_2$ will be determined from the experimental values of the threshold current using Equation 4.

In order to obtain values for $\kappa_1 T_1$ and $\kappa_2 T_2$ from Equation 4, the factor A had to be determined. The experiment and associated data used to obtain an approximate value for the factor A is described in Section D. Summarizing this experiment, it is based on the fact that the optical gain through the active region of a semiconductor diode gain element is proportional to the diode current and the proportionality factor is $1/A$.

The relative positions of the spherical collimating lens, the diode and the output coupler remained unchanged for all of the external cavity curves B through E in Fig. 2.8. For curve B, the cavity is symmetrical and the value of $\kappa_1 T_1$ for all configurations B through E was obtained from the difference in threshold current between curves A and B. This value is 0.27. The values of κT of most interest are those for the single-mode fiber and for the multi-mode fiber. For the multimode fiber, the diode threshold current is 149 mA and for the single-mode fiber it is 151 mA. The values of κT obtained from these values are shown in Table I. Also shown in Table I are the values of κT as measured with the spherical mirror at the right end of the cavity removed and replaced with a detector. Thus there is no cavity.

The values in Table I need further explanation. The values for "inside cavity" are the mean of the κT values for the forward and reverse direction, from the diode through the cylindrical lens/graded-index lens/optical fiber/spherical mirror combination in the forward direction and from the spherical mirror into the optical fiber and subsequently through all the other components to the diode in the reverse direction. The values listed in Table I under the

ELEMENT INSERTED. IN CAVITY	κT OF ELEMENT INSIDE CAVITY	κT AS MEASURED WITHOUT A CAVITY
SINGLE-MODE FIBER	0.12	0.18
MULTIMODE FIBER	0.13	0.70

Table I Values of the product of the effective coupling coefficient κ and the transmission T of optical fibers inserted in the cavity. Also shown are the values for these fibers when the diode gain element is coupled into them without any cavity present.

heading "without a cavity" were also obtained to two significant figures as the coupling coefficients to each of the two fibers when the diode gain element was replaced with a diode laser (from the same group of lasers that the gain element had been taken from to be AR coated).

The difference between the values for κT inside the cavity and with no cavity can be explained for the single-mode fiber as the difference between the overall coupling coefficients in the forward and reverse direction. The coupling from the spherical mirror back into the fundamental mode of the fiber could be significantly smaller than 18 percent. (It should be pointed out that the coupling from the diode into the single-mode fiber is itself much smaller than the values above 50 percent which have been reported by a number of workers in the field using more sophisticated optics.⁶⁻⁸)

The difference between the values for κT inside the cavity and with no cavity can be explained for the multimode fiber solely by postulating that only one or a selected number of the many modes of the multimode fiber participated in the lasing. This premise is also consistent with the spectral purity of the output of the external cavity when the multimode fiber was inside the cavity. The result is believed due to the fact that only selected mode(s) of the multimode fiber are reflected back into the fiber by the spherical mirror in appropriate phase and angle to participate in the lasing. It should be noted that the external cavity control with a single spectral line output when the multimode fiber was used, was an unexpected result of the research reported in this paper.

D. Determination of Factor A

The experiment and associated results to determine the factor $A \equiv (sd/\eta_1\beta\Gamma)$ in Equation 4 are described in this section.

The diode gain element was removed from the external cavity. While operating the diode with current I , the spontaneous emission power P leaving the front facet of the diode is measured. The power exiting the rear of the diode is proportional to the power leaving the front. This power will be denoted by cP , where c is a constant (approximately 1, although this is not necessary). Now optics are inserted behind the diode such that a fraction k of the light is re-injected into the diode gain element. (See the inset in Fig. 2.10 for the experimental arrangement.) The diode has gain g (for current I) and absorption α . The power now measured in front of the diode is $P + ckP \exp[(\Gamma g - \alpha)\ell]$. These two measurements are repeated for various currents. Figure 2.10 plots the power leaving the front facet of the diode as a function of diode current without (lower curve) and with (upper curve) a portion of the rear facet emission re-injected.

If the fractional change of power, $\Delta P/P$ (upon re-injecting some rear-facet emission), is denoted by r , then we can write the following:

$$\ln r = \ln(ck) + \Gamma g \ell = \alpha \ell . \quad (5)$$

The parameter r is related to the current I by using Equation 1 in Section C:

$$\Gamma g \ell = \frac{I}{A} - \Gamma \beta \ell J_0 . \quad (6)$$

Inserting this into Equation 5, we find

$$\ln r = \frac{I}{A} + [\ln(ck) - (\alpha + \Gamma \beta J_0)\ell] . \quad (7)$$

Thus $\ln r$ is a linear function of I whose slope is $1/A$. In Fig. 2.11 we plot $\ln \frac{\Delta P}{P} \equiv \ln r$ from Fig. 2.10 from 140 mA to 170 mA. Also indicated is the line that best fits the data. The reciprocal slope of this line, 19.8 mA, is used in Section C as the value of A . It should be emphasized that this value

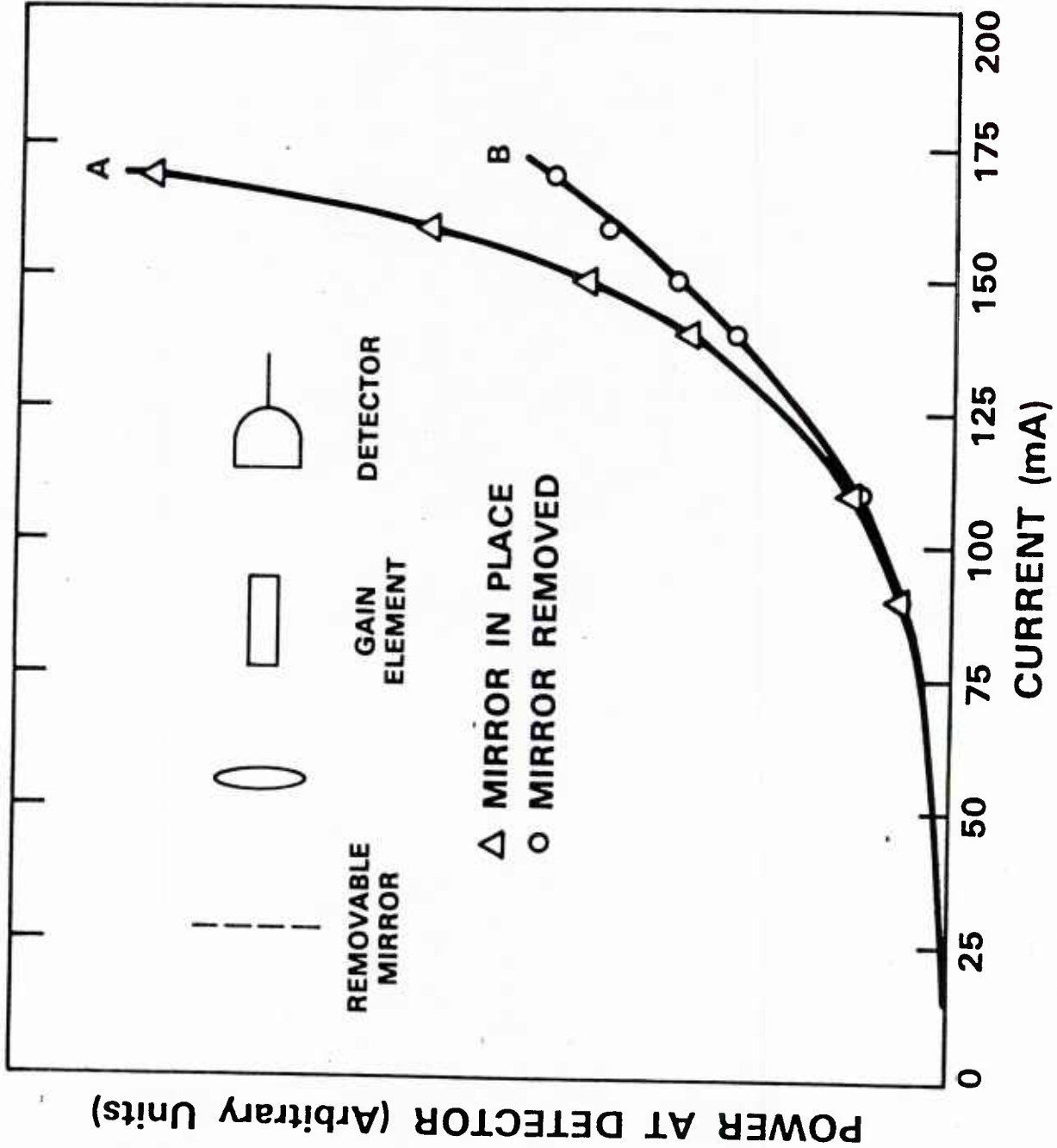


Fig. 2.10 Front-facet power output of diode gain element as a function of diode current. For the triangular points, a portion of the emission from the rear facet re-injected into the diode active region; for the circular points, the mirror shown in the inset is removed and there is no re-injection.

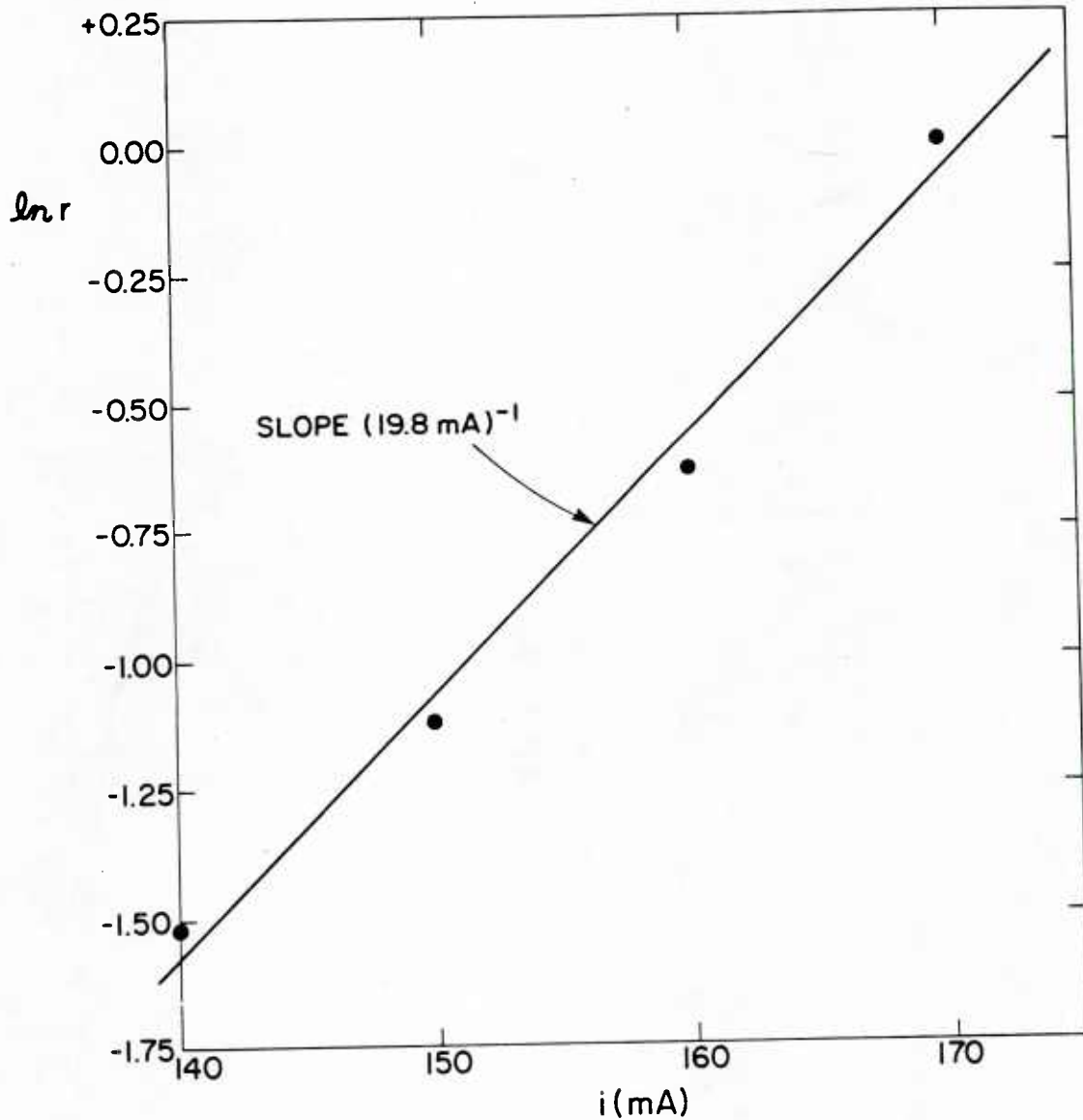


Fig. 2.11 Semi-logarithmic plot of the fractional change r in front-facet output power, $\Delta P/P$, due to the re-injection of emission into rear facet by mirror as shown in inset in Fig. 2.10. Only the interval from 140 mA to 170 mA is plotted. A least-squares fit to the data (assuming a linear relationship) is superimposed. The reciprocal slope of this line is the value of the factor A used in Section C.

represents a weighted average over the spontaneous emission and is being used as a good approximation for analyzing the onset of stimulated emission.

References — Section II

1. W. Streifer, D.R. Scifres and R.D. Burnham, "Longitudinal mode spectra of diode lasers," Appl. Phys. Lett. vol. 40, pp. 305-307, 1982 and references cited therein.
2. M.W. Fleming and A. Mooradian, "Spectral characteristics of external-cavity controlled semiconductor lasers," IEEE J. Quantum Electron. vol. QE-7 pp. 44-59, 1981.
3. L. Figueroa, "Studies of mode locking in (GaAl)As injection lasers" IEEE J. Quantum Electron. vol. QE-17, pp. 1074-1085, 1981.
4. K.Y. Lau, L. Figueroa and A. Yariv "Generation and quenching of intensity pulsations in semiconductor lasers coupled to external cavities," IEEE J. Quantum Electron. vol. QE-16, pp. 1329-1336, 1980.
5. C. Freed, "Design and short-term stability of single-frequency CO₂ lasers," IEEE J. Quantum Electron. vol. QE-4, pp. 404-408, 1968. See for example H.C. Casey Jr. and M.B. Panish, Heterostructure Lasers New York: Academic 1978.
6. M. Sarawatari and K. Nawata, "Semiconductor laser to single-mode fiber coupler," Appl. Opt. vol. 18, pp. 1847-1856, 1979.
7. J. Yamada, Y. Murakami, J. Sakai, and T. Kimura, "Characteristics of a hemispherical microlens for coupling between a semiconductor laser and single mode fiber," IEEE J. Quant. Electron. vol. QE-16, pp. 1067-1072, 1980.
8. H. Sakaguchi, N. Seki, and S. Yamamoto, "High efficiency coupling from laser diodes into single-mode fibers with quadrangular pyramid-shaped hemielliptical ends." Tech. Digest of 1981 Conf. on Int. Optics and Optical Fiber Commun. (April 1981).

III. Operation of Five Individual Lasers as a Coherent Ensemble Controlled by a Spatial Filter Within an External Cavity

A. Development of Experimental Facilities at RLE on M.I.T. Campus

The research on the series combination of semiconductor gain element and optical fiber described in Section II was performed at Lincoln Laboratory by enhancing existing equipment. Facilities at the Research Laboratory of Electronics on the M.I.T. campus were then placed in operation. These facilities included an optical table and optical diagnostic equipment such as a grating spectrometer and a scanning Fabry-Perot interferometer for more resolution. It was decided that the first major experiment would be to demonstrate that five individual gain elements within an external cavity would operate as a coherent ensemble controlled by a spatial filter in the Fourier plane of the ensemble. Five temperature controllers to control the temperature of the diode-gain-element heat sinks to 3×10^{-4} °C were built, and are operational. Since diode lasers have a wavelength variation with temperature of 0.25 nm/°C, this made it possible to control the wavelength to 7.5×10^{-5} nm (the frequency to 35 MHz). The temperature set point for each gain element can be adjusted to be $20 \text{ °C} \pm 15 \text{ °C}$, making it possible to relax the room temperature diode-laser wavelength specification to ± 3.7 nm. The spontaneous linewidth (the spectral width over which there is gain) of a diode laser is usually larger than 5 nm.

With the assurance that this temperature controller was to be built, Dr. L.J. Van Ruyven, then head of the Solid State Laser Development Department of Philips Research Laboratory, agreed to supply the program at no cost a variety of lasers in several different packages. We finally settled on using in the cavity, as described below, channelled substrate planar (CSP) lasers especially designed and fabricated for us at Philips and which we had AR coated

to make them into gain elements. It is interesting to note that in one of the leading laser laboratories in the world (with the billion-dollar compact disc business plan in hand Philips invested heavily in semiconductor laser research, development, and production), it was expected that the gain elements would only go as a coherent ensemble if they lased independently at nearly identical wavelengths. It was one of the goals of this program to determine how closely one had to specify the lasing wavelength, because the tighter the specification the more costly the lasers. We believed, as was later proven true, that all that was required is that the individual lasers have gain at the lasing wavelength of the ensemble. The spectral width at which there is gain is essentially the spontaneous emission linewidth which is usually significantly in excess of 5 nm. Fabrication of lasers within this spectral spread with high yield is easily achievable.

B. The External Cavity

The centerpiece of the facility at the Research Laboratory of Electronics is the external cavity housing the five gain elements. This cavity, described in detail below, was designed and built under subcontract to this program at M.I.T. Lincoln Laboratory. In addition to the mechanical designer paid by this contract, the design committee included an expert in classical optics, an expert in Fourier optics, and an expert in design of laser cavities, all of whom contributed their time at no cost to the contract. Their contributions to the design were, by hindsight, essential to the successful operation of the external cavity. It was possible to build the external cavity to a higher degree of sophistication and accuracy than originally planned.

A photograph of the external cavity taken in 1983 is shown in Fig. 3.1. The cavity consists of five plates supported and aligned by four super-invar

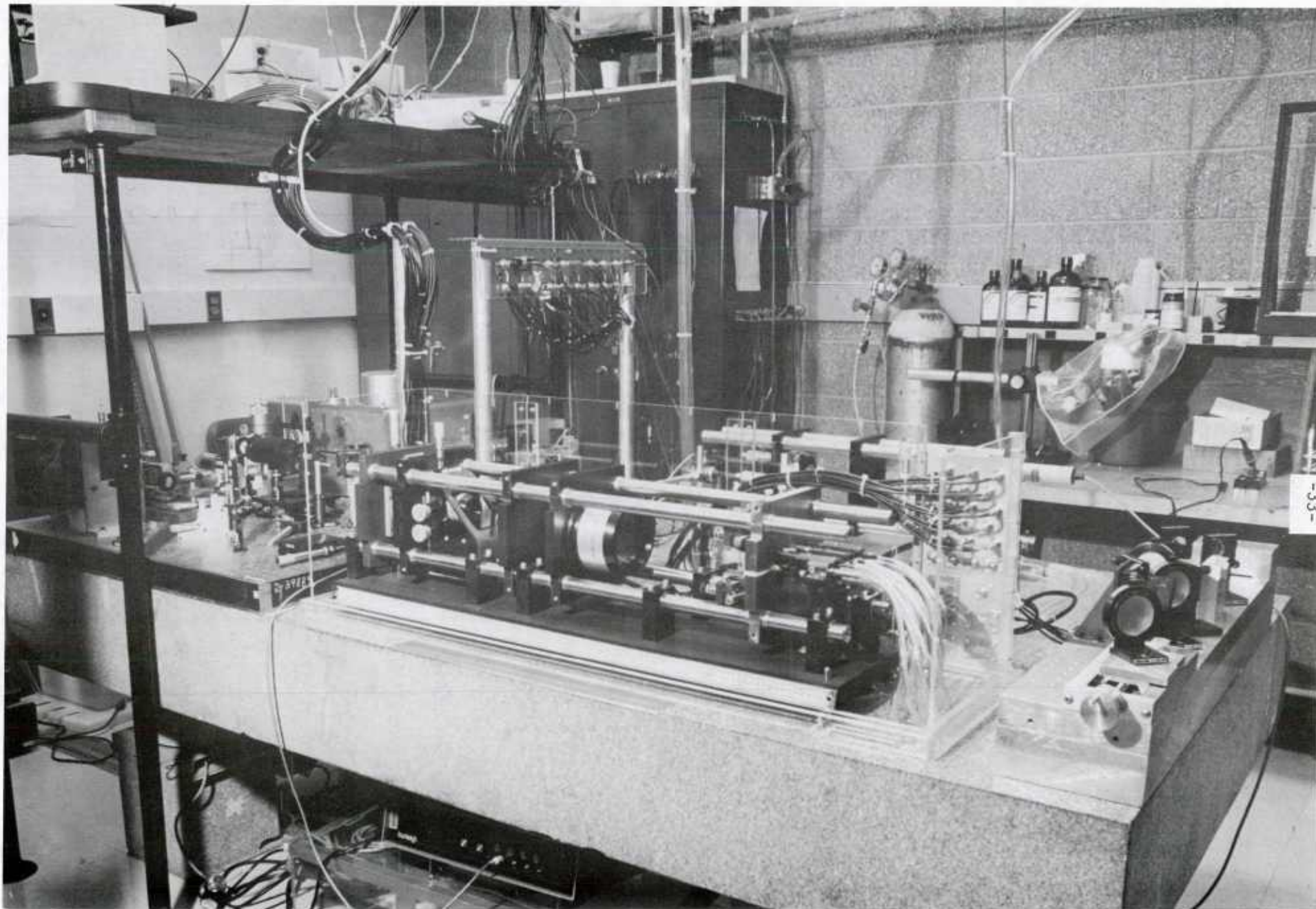


Fig. 3.1 Photograph of five-gain element external cavity on optical table. In the left background is the diagnostic system. In back of the five-gain element external cavity is single-element external cavity to test individual gain elements. To the right is optical assembly used in aligning five-gain element external cavity.

rods. As discussed in Section D below, in order to re-image the collimated gain element output back on itself after it makes a round trip through the cavity the plates are spaced such that exact Fourier transform relations hold between the various elements of the cavity. The details of the external cavity assembly shown in the figure are now described with emphasis on the areas where special precautions were taken.

Starting at the right in Fig. 3.1, the first plate holds micromanipulators and piezoelectric transducers (PZT's) used to properly orient the five collimator pen subassemblies. Each collimator pen consists of a gain element (a semiconductor diode laser which has been antireflection coated on one facet) and a collimating optic. The gain elements are discussed in Section C. The collimating optic is a 20x microscope objective, its lenses having been transferred to a customized barrel in the interests of compactness and part count reduction. Centering of the diode relative to the collimating optic is performed in a special pre-alignment jig, and then locked, prior to insertion of the collimator pen into the laser. Final focussing of the collimator optic is done after the pen is in the cavity. Errors in centering persisting past the prealignment stage may be corrected by inserting appropriate shims behind the collimator pens until pen parallelism can be attained using the pitch-yaw micromanipulators. Electrical heaters and temperature sensors are also included in each collimator pen. Heat sinking is provided by a bank of thermoelectric coolers connected to the collimator pens by flexible copper straps so as not to impede the motion of the micromanipulators. The coolers and their associated water supply/return lines are behind (i.e., to the right of) the first plate. Returning to the description of the first plate, the nominal center-to-center spacing of the collimator pens is 1.98 cm. Centering and coarse pitch-yaw adjustments are

performed by mechanical micromanipulators. Because the collimator pen outputs must be accurately parallel in order to overlap in the focal plane of the primary lens, fine pitch-yaw adjustments are accomplished with PZT's. PZT's are also used to give slight axial displacements to each collimator pen, thereby controlling the relative phase of the outputs of the collimator pens if necessary.

The second plate of the cavity holds the primary lens which focuses the collimated radiation from the gain elements onto the spatial filter. That is, it produces the Fourier transform of the output of the collimator pen ensemble. The primary lens has a 10 cm diameter aperture and a 25 cm focal length, and is antireflection coated for the wavelength range of interest. The only adjustment to lens orientation is the position of the plate along the super-invar rods. Each plate of the cavity includes this degree of freedom, in addition to any explicitly stated motions.

The third plate of the cavity carries the spatial filter. The prototype spatial filter used in 1983 consisted of eleven $3.8 \mu\text{m}$ slits on $10.47 \mu\text{m}$ centers. The slit period, together with the lens focal length and collimator pen spacing, is consistent with an operating wavelength of 830 nm. The filter is produced from a silicon wafer that has been coated with a silicon nitride film on one side. Integrated circuit techniques are used to selectively remove strips from the silicon nitride film down to the silicon substrate and to form a window in the silicon substrate up to the silicon nitride film. The result is a silicon nitride film with slits supported by a frame of solid silicon. For the prototype spatial filter one side of the film is blackened as a final step. Mechanical micromanipulators position the spatial filter at the focus of the primary lens at which point the outputs from the collimator pens converge. A rotation stage is used to align the slits of the spatial filter

parallel to the interference fringes in the transform of the coherent ensemble. A PZT is used for fine adjustment of the spatial filter in a direction perpendicular to the fringes.

The fourth plate of the cavity supports the secondary lens which recollimates the light transmitted by the spatial filter. The secondary lens has a 3.5 cm diameter aperture and an 8.75 cm focal length. Like the primary lens, it has been antireflection coated. Three translation (xyz) and two rotational (pitch-yaw) degrees of freedom allow the secondary lens to be optimally aligned with respect to the other optical elements in the cavity. The choice of a smaller focal length than the primary lens results in a reduction in the width (and height) of the output of the laser, permitting the use of smaller, less expensive optics in the diagnostic system.

The leftmost plate of the cavity holds the end mirror assembly. Initial operation was with a 90 percent reflectivity dielectric mirror. The mirror is attached to a piezoelectric aligner/translator containing three PZT stacks that can be driven differentially or in common. It, in turn, is mounted in a gimballed mechanical micromanipulator for coarse pitch-yaw adjustment.

A sixth plate, not shown in Fig. 3.1, was used only briefly. Positioned between the collimator pens and the primary lens, this plate carried five independently tiltable etalons. The plate and its components were designed to integrate with the given overall design of the external cavity laser with a minimum of inconvenience. It was at one time believed that the free-running wavelengths of the collimator pens (in the absence of the spatial filter) needed to be "near-tuned" in order that insertion of the spatial filter would cause locking. However, the lasing spectra of the uncoupled collimator pens were not all single-mode, thus complicating the concept of "near-tuning". The etalons were used to obtain tunable, single-

mode spectra. The etalon thickness was 0.03 cm, although other thicknesses could also have been used. Each etalon was packed into a small aluminum cell and affixed to a titling sub-plate. Normal incidence was avoided. One mechanical motion controlled the pitch of each sub-plate. No yaw control was necessary. After the fact, it became evident that etalon tuning was not essential to the coherent operation of the laser. The entire external cavity structure is enclosed in a plexiglass box for acoustic and thermal isolation. Part of the enclosure may be seen in Fig. 3.1. Also seen in the figure, at extreme right, is part of the optical assembly, used in aligning the cavity. Concurrent with the design of the cavity, a detailed alignment protocol was developed.

C. The Gain Elements

The semiconductor gain elements are originally channeled-substrate-planar (CSP) lasers with undoped active layers that were especially fabricated for us by Philips Research Laboratories, Eindhoven, the Netherlands. Because of the CSP structure the lasers have negligible astigmatism and because of the undoped active layers they have a gain curve which is mainly determined by the density of states functions of the unperturbed bands and therefore has a relatively broad maximum as a function of wavelength. While special slices were grown for this experiment, the lasers are not necessarily neighbors from the slice. The lasers were made from a channeled n^+ substrate with a channel width between 5 and 7 μm (top of channel) and 4 μm (bottom of channel) and a channel depth of about 1.3 μm . The n-type AlGaAs cladding layer with 33 percent Al, has a thickness of $1.62 \pm 0.04 \mu\text{m}$ inside the channel and $0.29 \pm 0.06 \mu\text{m}$ outside the channel. The flat active layer has a thickness of $0.10 \pm 0.02 \mu\text{m}$. The p-type AlGaAs cladding layer has a thickness of $3.13 \pm 0.68 \mu\text{m}$ and a p-type GaAs top layer of 0.5 μm provides good ohmic contact. The

finished diode lasers have a cavity length of 250 μm and their facets are coated with $\lambda/2$ of Al_2O_3 . The lasers were tested for lasing wavelength and for lasing threshold current. The lasers are then anti-reflection coated on their facet shown facing into the cavity in Figs. 3.1 and 3.2 with $\lambda/4$ of HfO_2 . After the anti-reflection coating (performed by Design Optics, Sunnyvale, California) the new gain elements were tested in a single-gain-element external cavity again for wavelength and for lasing threshold current. The gain-elements were also tested with the external cavity feedback mirror removed. For the five elements used in the experiments described below, the values of the threshold currents were typically about 90 ma before anti-reflection coating, increased by typically about 10 ma in the external cavity after anti-reflection coating and were yet at least another 40 ma higher with the feedback mirror removed (we did not test any of the elements at currents above 140 ma).

D. Experimental Results

Figure 3.2 is an artist's conception of the five-gain-element external cavity showing the components inside the cavity. (Figure 3.1 is a photograph of this cavity.) The distance between the large lens on the right and the collimated output from the gain element and between the lens and the spatial filter are both identically the focal length of this lens. Similarly the distance between the smaller lens on the left and the spatial filter and between the lens and the partially reflecting mirror are both identically the focal length of this lens. Thus the light in one round trip through the cavity undergoes four Fourier transforms, and four Fourier transforms is an identity operation, producing positive feedback. The magnitude-squared Fourier transform of the near-field of the five-element array in the plane of the spatial filter is shown in Fig. 3.3. The magnitude-squared Fourier transform can be variously called the Fraunhofer diffraction pattern, or the

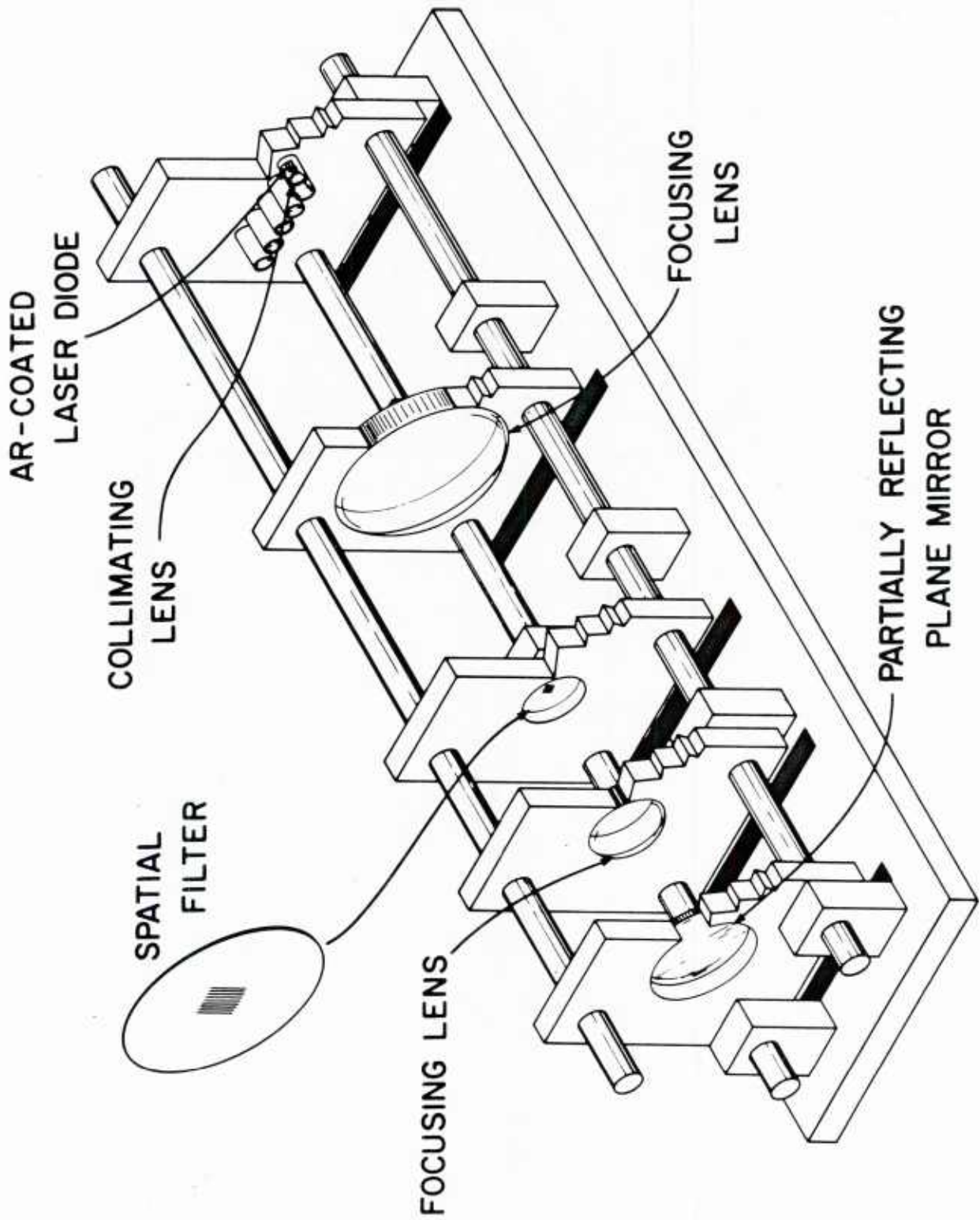


Fig. 3.2 Artist's conception of five-gain-element external cavity showing the components inside the super-invar four-bar structure.

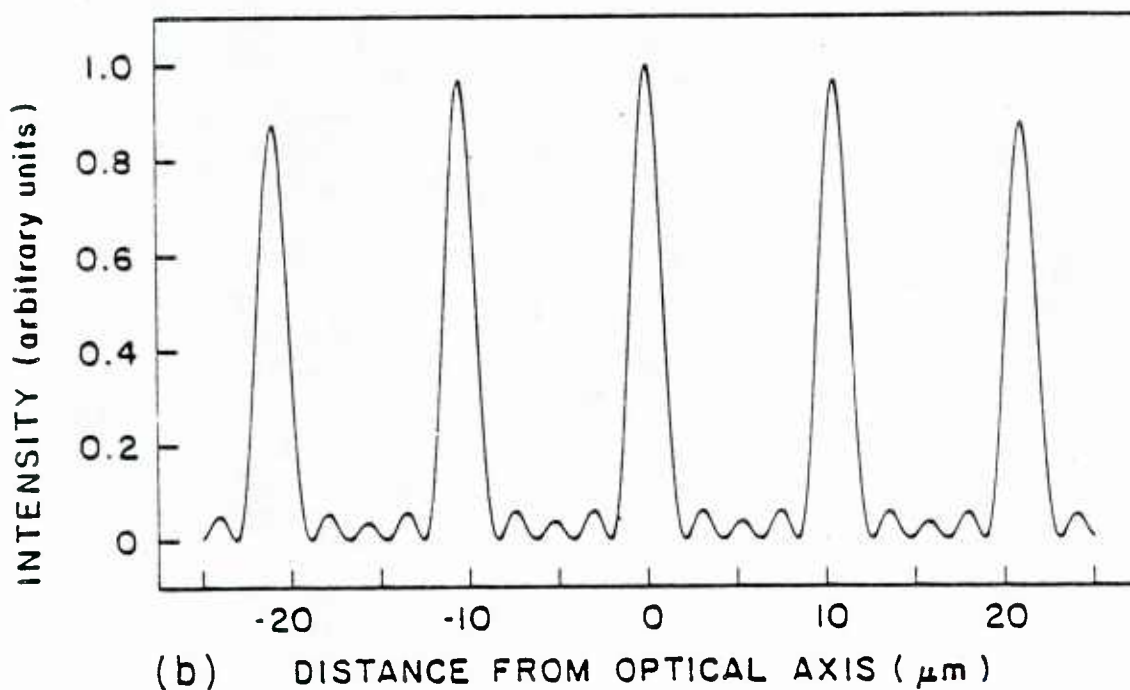
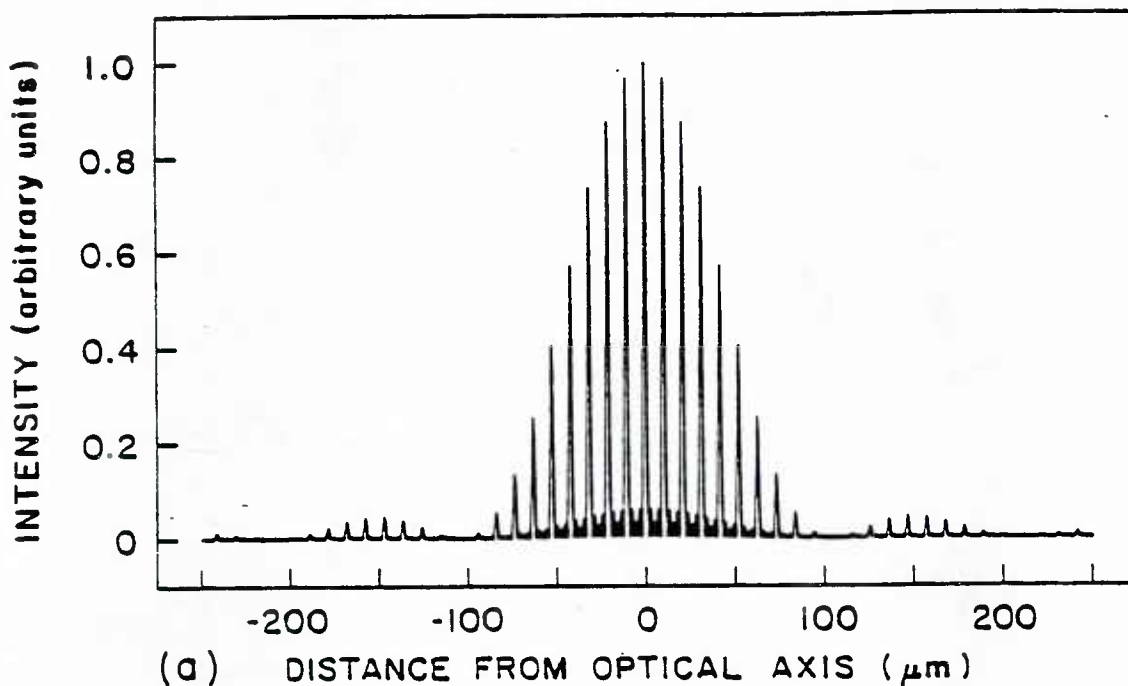
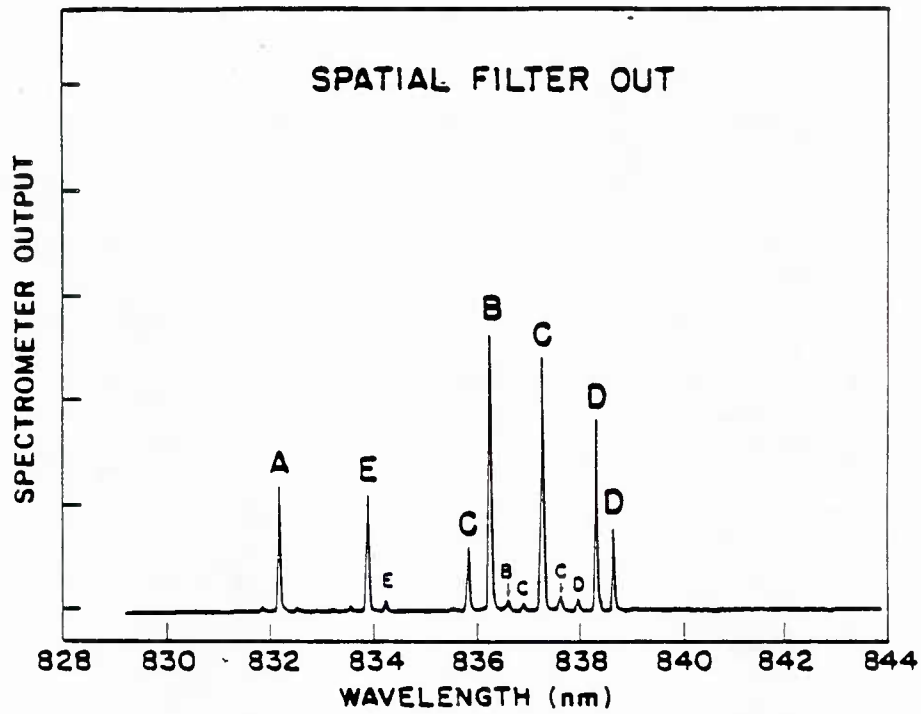


Fig. 3.3 a) Magnitude-squared Fourier transform of near-field of five-element array. Equal excitation, 0.2 cm element width, flat-top element profile, 2.0 cm element spacing, and $0.84 \mu\text{m}$ wavelength are assumed. Abscissa is transverse dimension in focal plane of 25 cm focal length lens. b) Expanded plot of central portion of pattern.

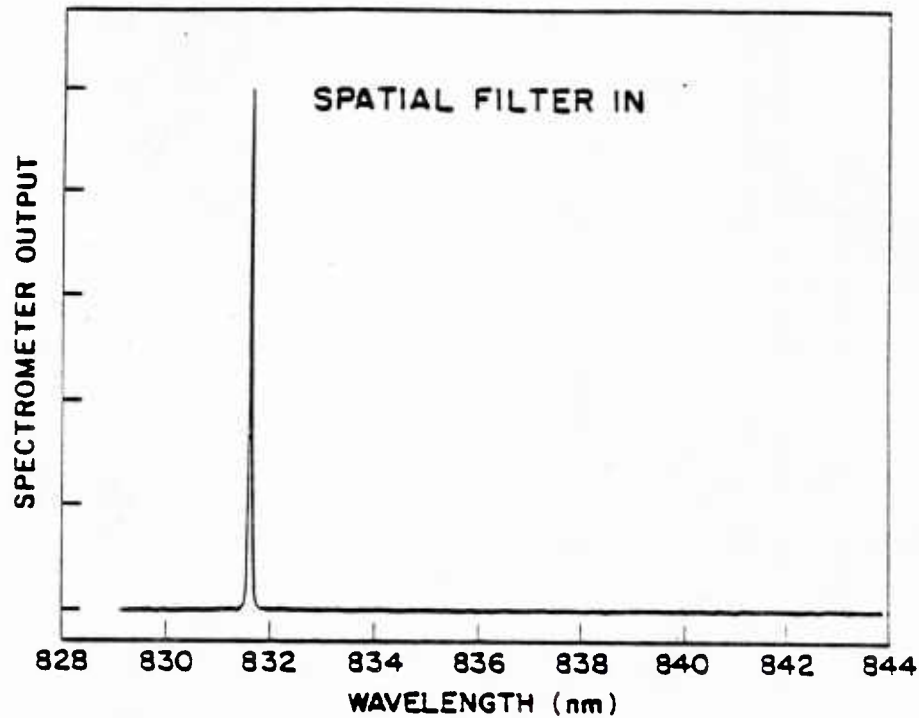
interference pattern of the five elements if they are coherent with each other. As mentioned in Section B above the prototype spatial filter used in the experiment consisted of eleven $3.8 \mu\text{m}$ slits on $10.47 \mu\text{m}$ centers. An unsophisticated explanation of the operation of the coherent ensemble is that the feedback to the five elements from the mirror on the other side of the spatial filter is greatly increased when the elements are coherent with each other and the interference pattern is transmitted through the filter. Gain elements (i.e. amplifiers) like to oscillate if they have gain at the frequency at which they also have positive feedback.

It is instructive in this final report to give a chronology of how success was achieved and the ensemble went coherent. In the experience of this investigator, it was typical of successful experimental technique, and is always omitted in the open literature. The five gain elements were placed in the cavity and with the spatial filter removed acted as individual external cavity lasers with wavelengths that varied over a range of 6 nm. It was not possible at that time to make the ensemble coherent when the filter was in place. The lasers were temperature tuned to reduce the difference in the independent wavelengths to values less than the resolution of the spectrometer, but success was still elusive. We then inserted etalons in series with each gain element so the individual wavelengths were identical and there was no reason that the ensemble should not go coherent. It did. We then removed the etalons and the ensemble remained coherent. We then turned off the temperature controllers and the ensemble still remained coherent. The moral: you get things to work when you run out of excuses of why it shouldn't. Then, of course, it continues to work when you put the excuses back in.

In Fig. 3.4a is shown the spectrum of the output from the external cavity with the five gain elements lasing individually and the spatial filter removed



(a)



(b)

Fig. 3.4 Spectrum of output form external cavity containing five gain elements: (a) Spatial filter removed from cavity. Letters over peaks indicate gain elements from which emission is occurring. (b) All experimental conditions are kept identical but spatial filter is in cavity. The scale for the ordinate is the same in (a) and (b).

from the cavity. The gain elements were operating at temperatures about 2 °C above room temperature. The width of the spectral lines is that of the model 12G Perkin-Elmer spectrometer used in the experiments. (The spectrometer has since been replaced with a Spex model 1870 computer driven spectrometer at no cost to the contract.) No gain element by itself lased with the spatial filter in the cavity. (The currents were not increased above 140 mA.) The loss due to the filter was too large. Only when the gain elements lased together coherently was the interference pattern produced, which bunched the radiation so it efficiently passed through the slits of the spatial filter. It should be pointed out that no attempt was made in obtaining Fig. 3.4a for which there are five independent external cavity lasers, to optimize the current through the gain elements for single mode operation if there is such a regime for any of the lasers.

Figure 3.4b shows the spectrum of the external cavity output with all the experimental conditions unchanged from those used to obtain the spectrum of Fig. 3.4a except the spatial filter was inserted in place. Note the single resolution-limited line and that the individual lasers had been pulled by up to above 6 nm. For the wavelength 831.8 nm the slit center-to-center spacing of 10.47 μm corresponds to Fourier transform spacing of gain elements of 1.986 cm. The spacing in the cavity design is 1.98 cm. The center-to-center spacing of the gain elements although controlled with micrometers to a precision of 0.002 cm is not known to better than ± 0.01 cm in absolute value. While the results of Fig. 3.4 are for one set of diode gain element currents and powers, they are typical for other currents and powers.

The 60Å^o pulling that was measured was limited in value because individual lasers were selected in a narrow wavelength range so the temperature control could be used to make all the lasing wavelengths identical. It should be

pointed out that the individual diode gain elements were displaced along the axis of the cavity of the order of $\pm \lambda$ (830 nm) and sensitivity to phase variation was also shown to be small.

In the experiments above the power output from the coherent ensemble is approximately 0.4 times the sum of the individual powers of the lasers when the spatial filter is out. A major part of the loss in power can be explained by the fact that the slits in the spatial filter are overfilled and there is significant diffraction loss from the use of the spatial filter.

E. Theory

It is very important to understand the operation of the external cavity laser and in particular it is important to select the best geometry for the spatial filter. One desires to obtain the maximum values with appropriate weighting factors of: 1) the ratio of the thresholds for the gain elements operating individually to the thresholds for operation as a coherent ensemble; 2) the output power; and 3) the range of the stability of the system with respect to filter duty cycle and frequency detuning.

A technical description of the operation of the laser, as for any oscillator, must consider characteristics of the amplification mechanism as well as the feedback mechanism. The laser system may be cut, so to speak, at the left focal plane of the five collimating lenses in Fig. 3.2 and the action of the two resulting subsystems considered separately and then synthesized. The feedback is supplied by the passive subsystem to the left of this cut and the amplification by the active subsystem to the right.

Standard optical matrix representations for each of the passive elements (lenses, filter, end mirror and path length between elements) are used. The theoretical treatment of the gain elements closely follows Cassidy¹ in his

model of the injection laser. In this case monochromaticity is assumed as well as one perfectly AR-coated facet. The active part of the cavity is represented with a matrix developed from rate equation and propagation equations¹ that includes phase front change through the collimating optics, passage through the real and imaginary parts of the nonlinear gain, and reflection at the rear facet. The important β factor — ratio of real to imaginary parts of the index of refraction — is included. One crucial assumption is made in the derivation: that the gain medium can be modeled as a homogeneous two-level system with negligible lower level population while in fact the gain and spontaneous emission have different dependencies on upper and lower level occupancy probabilities.² This assumption implies that situations involving absorption are not considered.

Six empirical parameters were experimentally determined through characterization (spectral and laser threshold) of the gain elements before and after antireflection coating both in and out of the external cavity. The first two describe the dependence of the gain on the current in each element: the gain threshold and scale factor in a linearized approximation of the dependence of gain on input current. They were obtained by examining the superluminescent spectra from each element³ as well as the measured threshold current before antireflection coating and after coating in the cavity with two end mirrors with different reflectivity. A third parameter is the cross section which accounts for coupling of the photons to the gain when gain saturation is included. The ratio of spontaneous emission to gain is obtained as in reference 1. Finally, the nonunity forward and backward coupling between the gain element and the end mirror is estimated by examining cavity threshold changes with different end mirror reflectivities.

Combining the passive and active matrices that represent the system and imposing the condition for unity gain provides a nonlinear matrix equation that is soluble using iterative numerical techniques. The numerical analysis was implemented in Fortran. Through solution of the nonlinear equation, the computer simulation provides information on three aspects of system operation. First, a threshold current for each element is determined for operation in the cavity through the spatial filter versus spatial filter duty cycle at the wavelength for maximum transmission through the filter. In addition the threshold for the coherent ensemble, assuming the elements run with identical currents, is determined. The result is plotted in Fig. 3.5 and shows a threshold decrease of between 30 to 40 mA for coherent operation over individual operation for 30% duty cycle filters. The difference in threshold becomes less marked as filter duty cycle is increased. Filter duty cycles below 30% show a significant threshold increase even for the coherent operation as more of the light in the intensity peaks is blocked off by the opaque regions of the filter. These results indicate filter duty cycles between 30% and 40% minimize system threshold.

The second part of the theory involves a plot of the external cavity laser output power of a set input current distribution versus wavelength detuning from the wavelength determined by system geometry to maximize filter transmission. Plotted in Fig. 3.6 for various duty cycle filters, the results indicate frequency selectivity of the filter is best for 30-40% duty cycle filters. For duty cycles less than 50 percent, the output power is monotonically decreasing with detuning, while for duty cycles between 50 and 100 percent, there is a slight increase in output power for small detuning but a decrease for large detuning. Again, filters with duty cycles less than 30% show the marked increase in system threshold which produces the lower output powers.

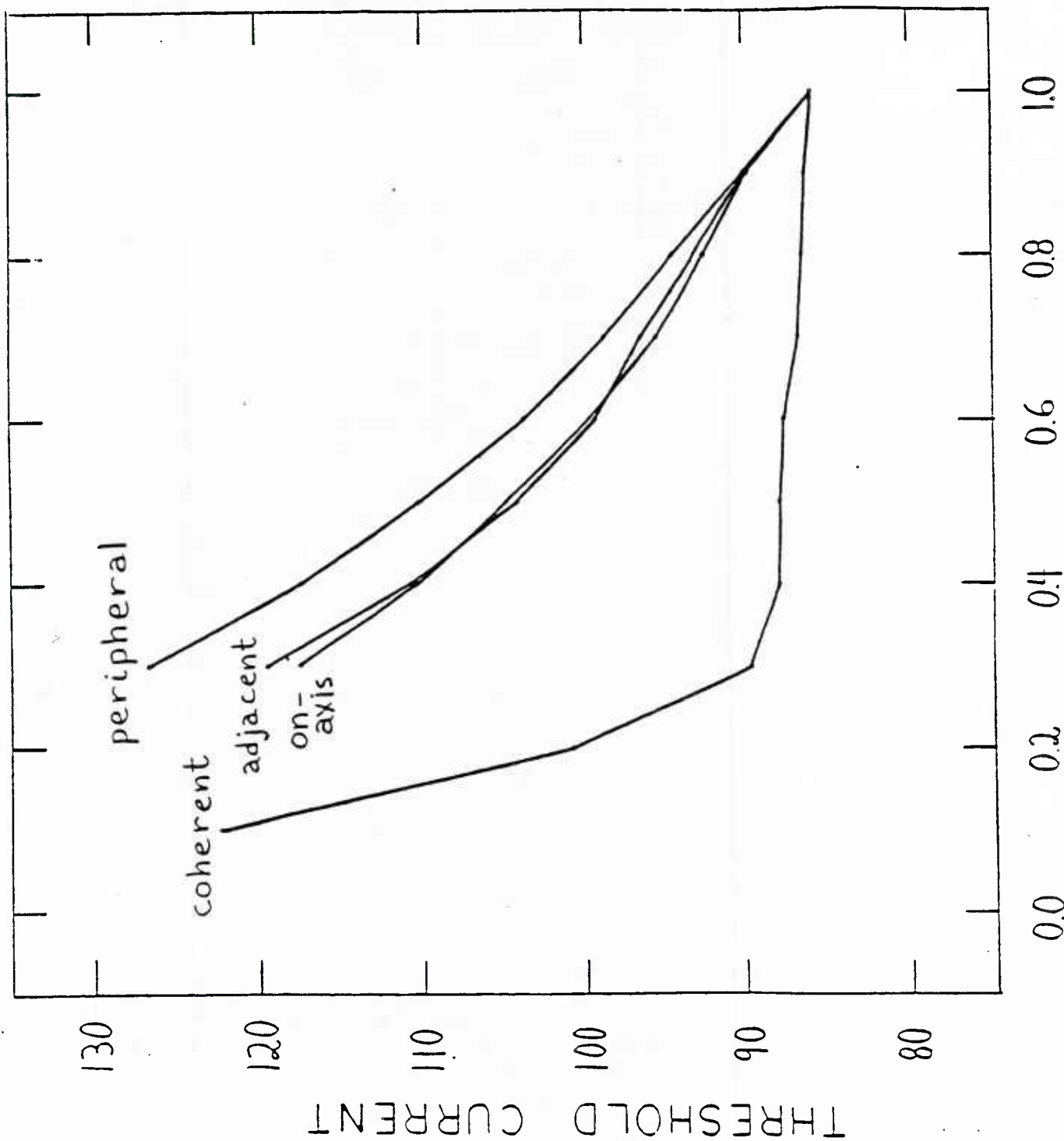


Fig. 3.5 Plot of coherent threshold as a function of spatial filter duty cycle for an equally driven five-element array. For reference, calculated curves are shown for independent operation of the on-axis, adjacent, and peripheral gain elements.

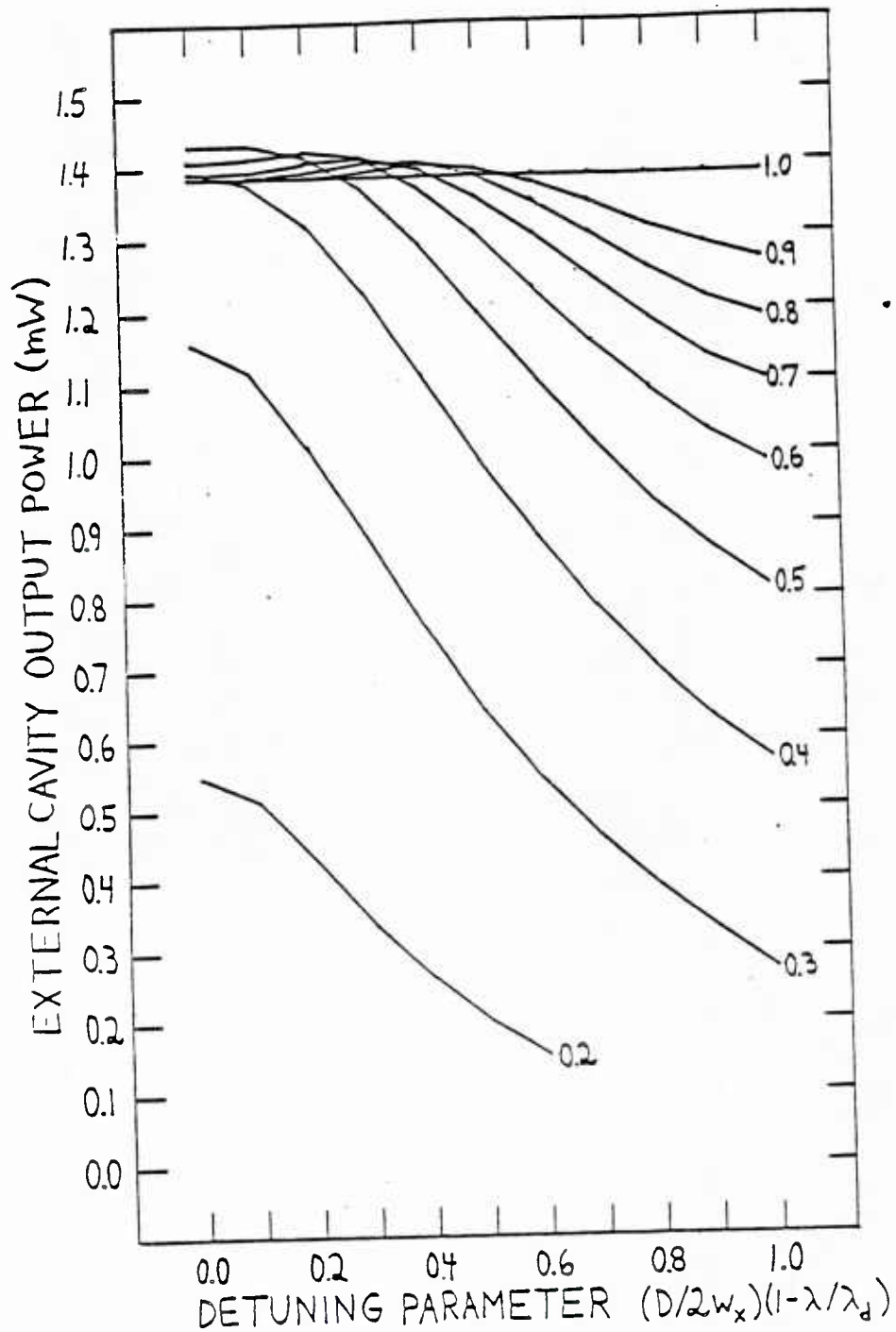


Fig. 3.6 Plot of external cavity laser output power as a function of detuning for fixed gain-element currents and with spatial filter duty cycle as a parameter. For duty cycles less than 50 percent, the output power monotonically decreases as the detuning increases from zero, while for duty cycles between 50 and 100 percent, there is a slight increase in output power for small detuning but a decrease for large detuning.

The final result defines ranges of values of the β factor that produce a stable solution for cavity output for three different input currents — equal in all five elements — above threshold. The result provides important insight to system stability. From the results shown in Fig. 3.7, it is apparent that the system has a larger stability range for filters with 30-40% duty cycles, and the size of this region increases with increasing levels of current.

The theoretical results that the filter duty cycle of 30-40% was optimum agrees with the result that would be predicted by intuition. Referring to Fig. 3.3, the high intensity lobes of the magnitude-squared Fourier transform of the near-field of the five-element array, which occurs in the plane of the spatial filter, extend for about 30-40% of their center-to-center distance. For duty cycles smaller than this range of values the opaque regions of the filter will block an increasingly larger amount of the light produced by the coherent ensemble reducing the feedback from the cavity mirror and the output power. For duty cycles larger than this range of values, the selectivity of the spatial filter will be greatly reduced and the magnitude-squared Fourier transforms of a large range of laser wavelengths can be transmitted by the filter with nearly equal attenuation. It should be pointed out that the small number of five gain elements in our experiment is a more strenuous test of practicality than if a larger number were used. If the five element array were replaced by a twenty-five element array as shown in Fig. 3.8 both the duty cycle and the amount of radiation obstructed by the struts could be significantly reduced. The difference between the coherent ensemble threshold and that of the individual lasers would increase dramatically, the percentage power out would greatly increase and the regions for stable operation would increase.

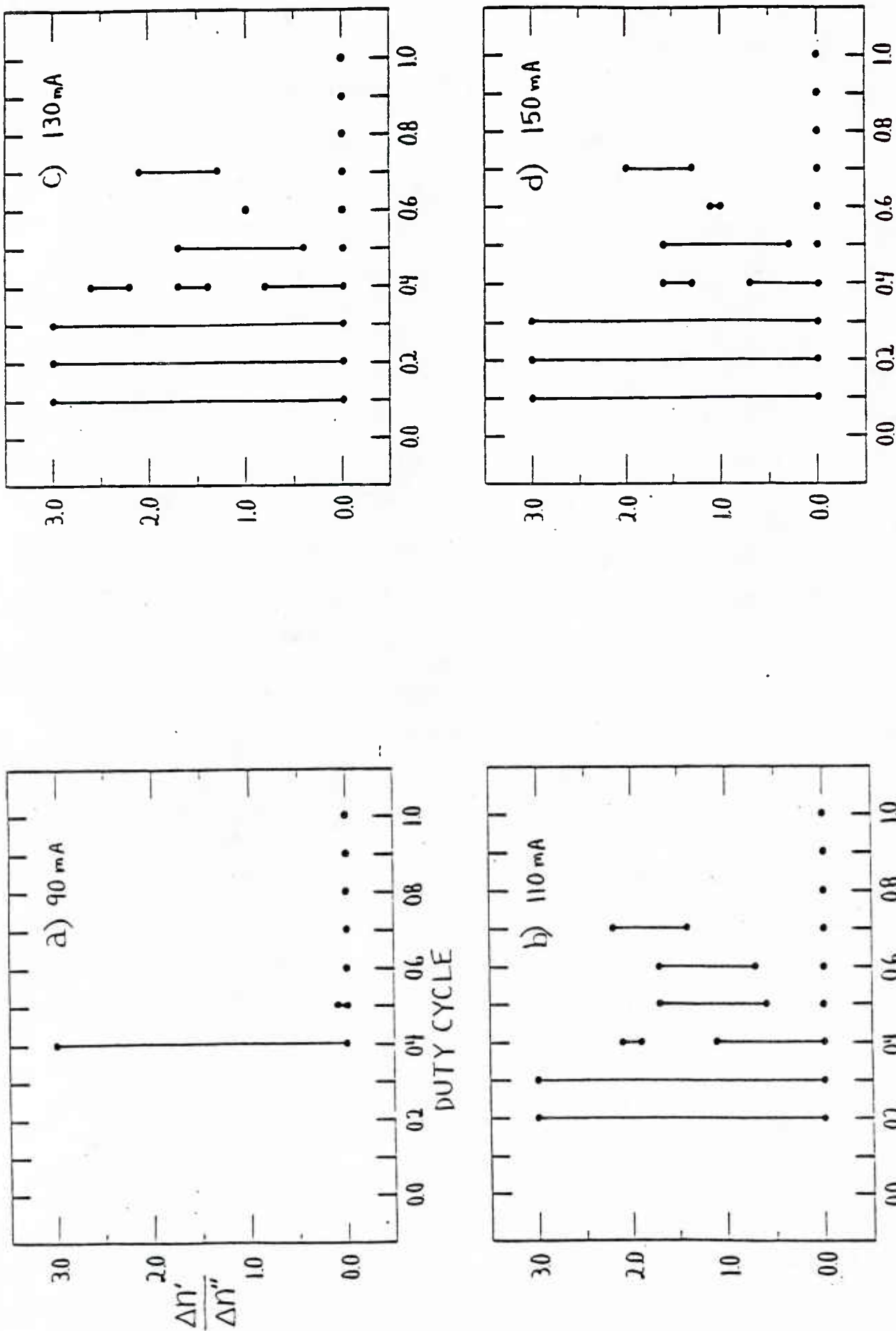


Fig. 3.7 Plots of the ranges of $\Delta n'/\Delta n''$ between 0 and 3 vs. spatial filter duty cycle for which the computer simulation of the external cavity laser converges to a solution. Four cases are considered where the gain elements are equally driven at: a) 90 mA; b) 110 mA; c) 130 mA; and d) 150 mA. This important result indicates that, for sufficient current, operation with large duty cycle spatial filters is more likely to result in instability than with small duty cycle spatial filters.

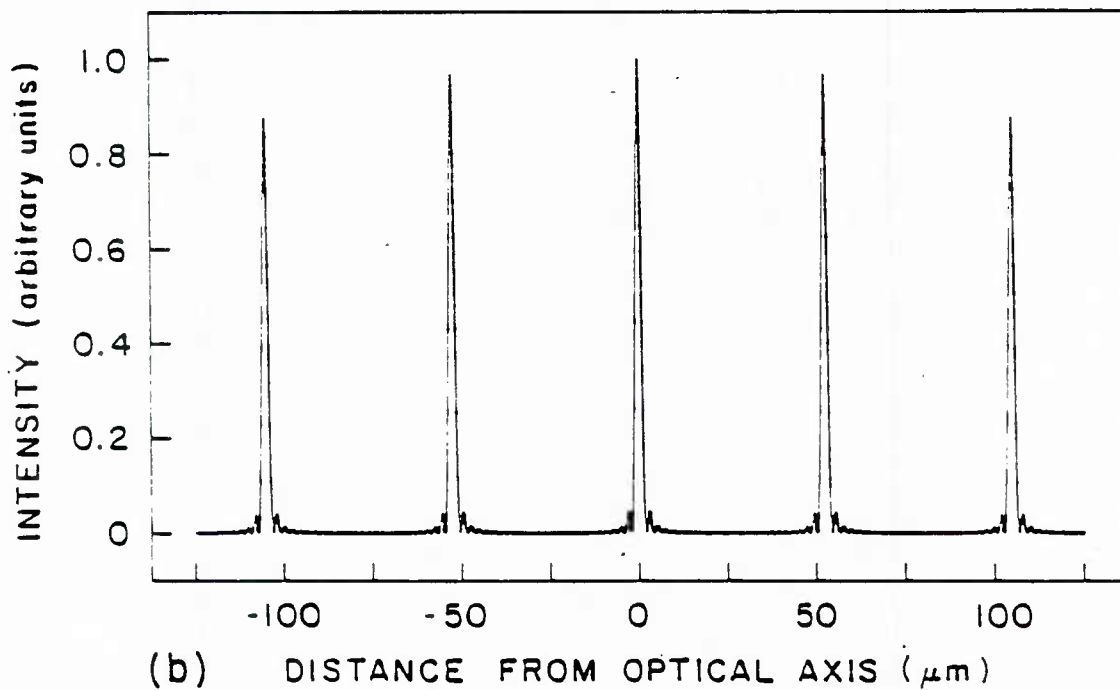
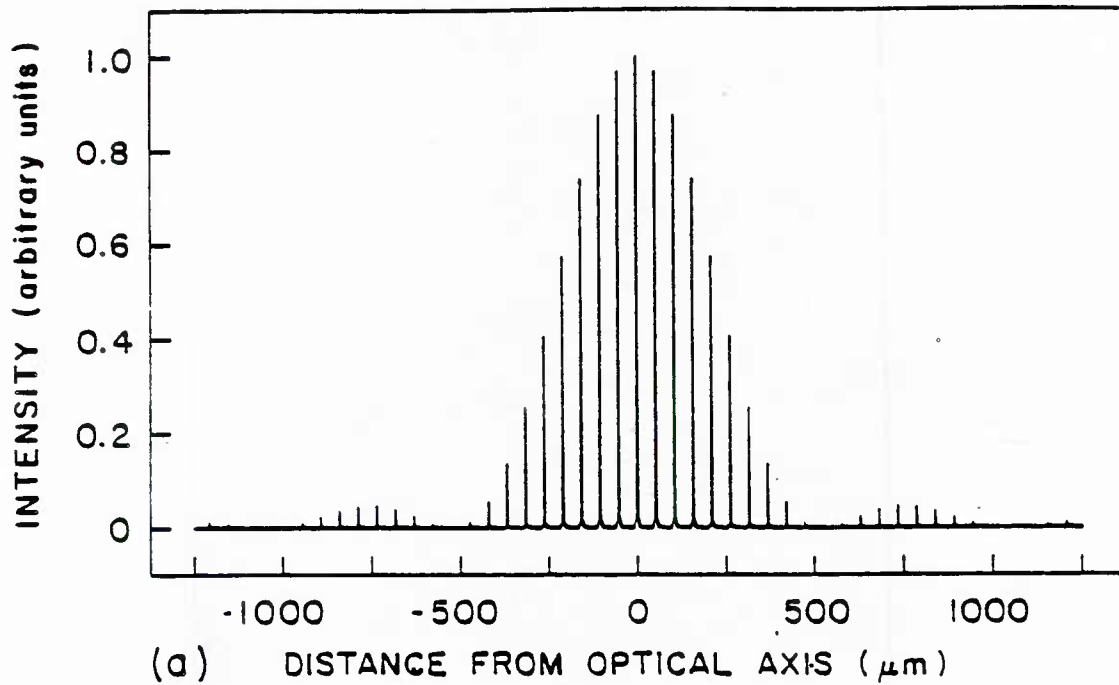


Fig. 3.8 a) Magnitude-squared Fourier transform of near-field of twenty-five element array. Equal excitation, 0.04 cm element width, flat-top element profile, 0.4 cm element spacing, and 0.84 μm wavelength are assumed. Abscissa is transverse dimension in focal plane of 25 cm focal length lens.
b) Expanded plot of central portion of pattern.

References — Section III

1. D.T. Cassidy, "Analytic Description of a Homogeneously Broadened Injection Laser," IEEE J. Quantum Electron., vol. QE-20, p. 913 (1984).
2. D.T. Cassidy, "Consequences of a Lower Level Population on the Modeling of a Homogeneously Broadened Injection Laser," Appl. Phys. Lett., Vol. 44, p. 489 (1984).
3. I.P. Kaminow, G. Eisenstein and L.W. Stulz, "Measurement of the Modal Reflectivity of an Antireflection Coating on a Superluminescent Diode," IEEE J. Quantum Electron., vol. QE-19, p. 493 (1983).

IV. High-Spectral-Purity cw and Pulse Operation of the Coherent Ensemble

A. Improvements to the Experimental Apparatus

The major improvement to the experimental apparatus was the extremely careful alignment of the Tropel model 240 scanning Fabry-Perot interferometer done at no cost to the contract in collaboration with F. Walther at Lincoln Laboratory using an available extremely high quality dye laser as source. This scanning spectrum analyzer was optimized so it met or exceeded its specified 7.5-MHz instrument resolution. Its free spectral range was 1.5 GHz.

B. Improvements to the External Cavity

With the success of the operation of the external cavity described in Section III above, R.W. Mountain of the VLSI group at Lincoln Laboratory who had provided the prototype spatial filter agreed to provide a large series of spatial filters again at no cost to the contract. The basic fabrication of the filters was no different than that of the prototype described in Section III B except that both faces of the filter were blackened. Three wafers each consisting of ninety-six spatial filters were produced. The center-to-center distance of the slits, the duty-cycle of the slit openings and the number of slits was varied. In most of the filters there were 41 slits (rather than the eleven of the prototype slit used above) which was much larger than the lateral extent of the Fourier transform. In the experiments described in Section C below the spatial filter used consisted of a series of forty-one 3.1- μm slits whose center-to-center spacing, D , is 10.47 μm . In addition, the spatial filter holder in the external cavity was modified to accept the new sets of spatial filters.

C. Experimental Results — High spectral purity

Figure 4.1 is a simplified drawing of the optics of the external cavity which has been used during the program in explanation of the experimental results. The gain elements (AR coated laser diodes) now numbered 1 through 5, are spaced with a center-to-center distance, d , equal to 1.98 cm. The three-to-one demagnification of the image from the gain elements to the semitransparent mirror as shown in Figs. 3.1 and 3.2 is neglected for pedagogical reasons because it is irrelevant to any explanation of cavity operation. The light makes the round trip through the cavity. Since all the distances between objects and lenses correspond to the focal length F of the respective lenses, the radiation from the diode lasers is Fourier transformed four times (an identity operation) as it makes the round trip through the cavity for a spatial filter that would pass the exact Fourier transform of the geometry of the diode laser array. In this case the wavelength for maximum filter transmission is:

$$\lambda = dD/F . \quad (1)$$

For equal power from each gain element, and for the spatial filter geometry used in these experiments, calculations predict a single-pass maximum transmission of 90% through the filter because the subsidiary maxima between the large peaks in the Fourier transform are blocked by the opaque struts of the filter.

With no spatial filter in the cavity, each of the five elements operates independently as an external cavity laser. The operating wavelengths of the individual lasers used in the experiments described in this section are separated by more than 60\AA . With the spatial filter in place, output was measured on the 7.5-MHz [$2.7 \times 10^{-4} \text{\AA}$] resolution Tropel model 240 Fabry-Perot Scanning Spectrum Analyzer with 1.5 GHz [$5.4 \times 10^{-2} \text{\AA}$] free spectral

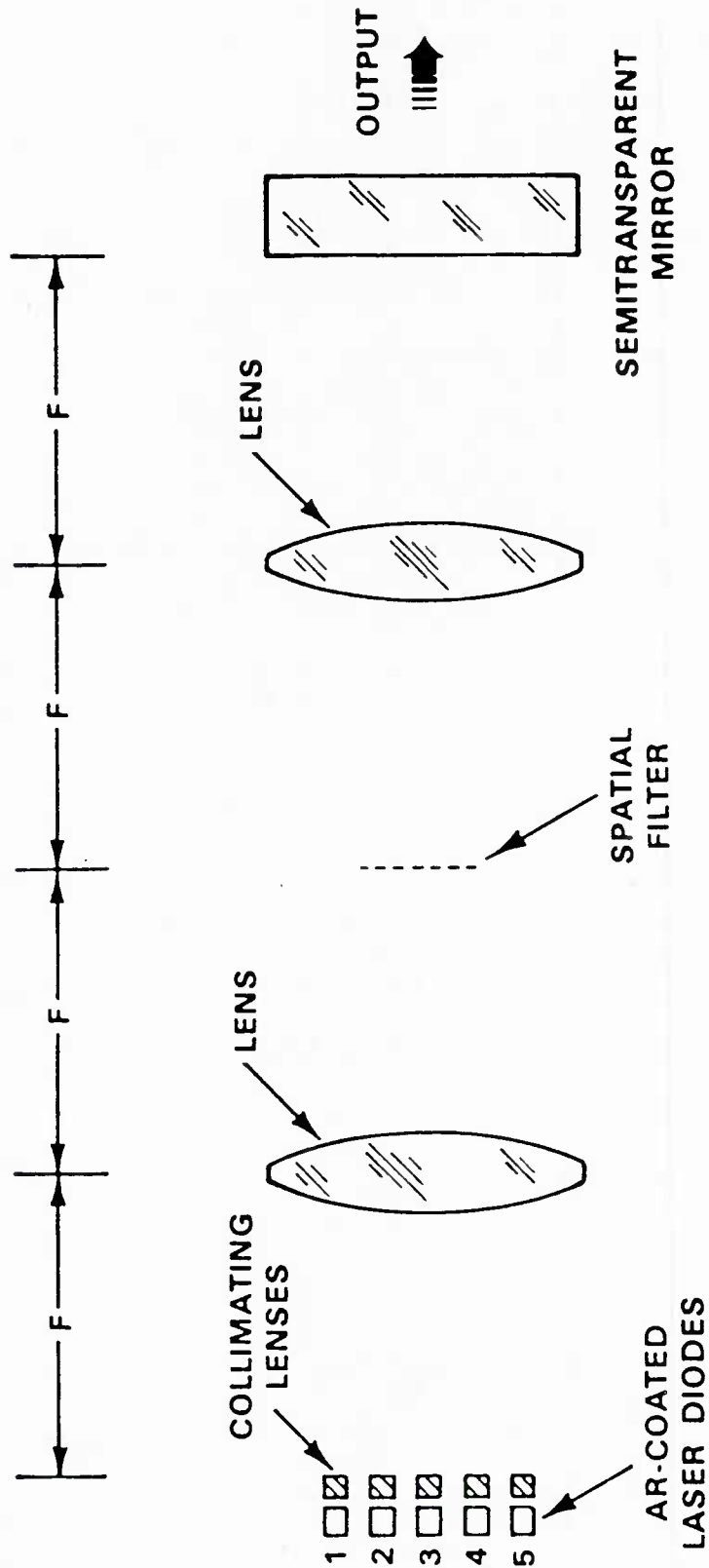


Fig. 4.1 Schematic of multiple-element external-cavity arrangement showing the placement of the five antireflection-coated diode lasers, the associated collimating optics, the two lenses, spatial filter, and end mirror. As indicated on the figure, the elements are separated by the focal length of the lenses so the light undergoes a Fourier transform four times during one round trip through the cavity.

76204.3

range. Figure 4.2 is an oscilloscope trace of the output from this instrument scanning one complete free spectral range. The top trace indicates the output is in a single external cavity spectral mode (longitudinal mode spacing of the external cavity is 250 MHz). As shown in the expanded scale of the lower trace, the linewidth is within the 7.5-MHz instrument resolution. The wavelength corresponding to the results of Fig. 4.2(b) is 8318 \AA , consistent, to the absolute accuracy of the geometric dimensions of the components in the cavity, with the wavelength predicted by Eq. 1. (The operating wavelength, of course, will be affected by the effective gain curve of the coherent ensemble.)

The external-cavity laser has also been operated in the pulse mode with output linewidths of the order of the 7.5-MHz instrument resolution. To achieve this high spectral purity in a pulse mode of operation, three alternate gain elements (elements number one, three and five in Fig. 4.1) are operated cw and the intermediate two elements are pulsed. For a coherent ensemble of only three alternate gain elements, the spacing between the major intensity maxima in the Fourier plane (the filter plane) is decreased by a factor of two relative to the spacing with all five elements operating coherently. As a result, the lasing threshold for the three-element ensemble is much higher because significant radiation hits the opaque areas of the filter. A calculation of the single-pass filter transmission for this case yields a value of 0.48 as compared to the transmission, as described above, of 0.90 when all five elements are running.

The spectral output of the ensemble when operated with current pulses applied to elements number two and four and cw excitation to the other three was measured for two different cases. First, the dc biases on the two pulsed

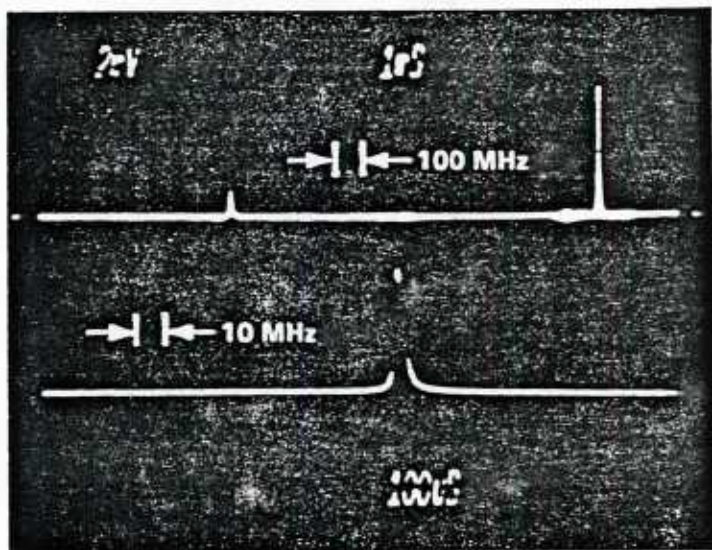


Fig. 4.2 Fabry-Perot scanning-spectrum-analyzer trace of output from multiple-element external-cavity system with spatial filter in place. Top trace covers one free spectral range showing there are no other spectral lines. Lower trace on expanded scale shows linewidth limited by 7.5-MHz ($1.7 \times 10^{-4} \text{ \AA}$) instrument resolution.

elements were set so the laser ensemble was just above threshold when the pulse was off. In this case, the spectrum for the pulse output remains at the value set by the low-level cw output of the external cavity, and the resulting spectrum, shown in Fig. 4.3(a), is a single spectral mode. The linewidth in this case is within the 7.5-MHz instrument resolution. It should be pointed out that if any of the five external-cavity lasers operating independently without the spatial filter are pulsed from below threshold, there is a 1\AA ($\approx 40\text{ GHz}$) output-frequency shift (chirp) during the pulse, and there is still a chirp larger than 1.5 GHz if all five elements of the coherent ensemble with the spatial filter are pulsed simultaneously from above the ensemble threshold.

For the second case, the dc biases on the two pulsed elements were reduced to a point where the ensemble was well below threshold with the pulse off. The spectrum for this case is again a single spectral mode, shown in Fig. 4.3(b), with an apparent linewidth of approximately 9 MHz. These narrow linewidth pulses can be explained by a compensation effect. Refractive index and gain in pulsed elements two and four are changing because of increased temperatures and carriers caused by the increased current. In the other three elements, however, changes occur in the opposite direction because of decreased temperatures and carriers caused by the increase in coherently emitted power output and the simultaneous decrease in carrier lifetime. The parameter space where this compensation is effective in maintaining the narrow linewidth reported here has not been fully explored, but results indicate that it is broad enough to ensure reproducibility to the available instrumental resolution. Since the measured linewidth of all the spectra shown in this paper are less than or close to the specification of the instrument resolution, the actual linewidths cannot be accurately quantified.

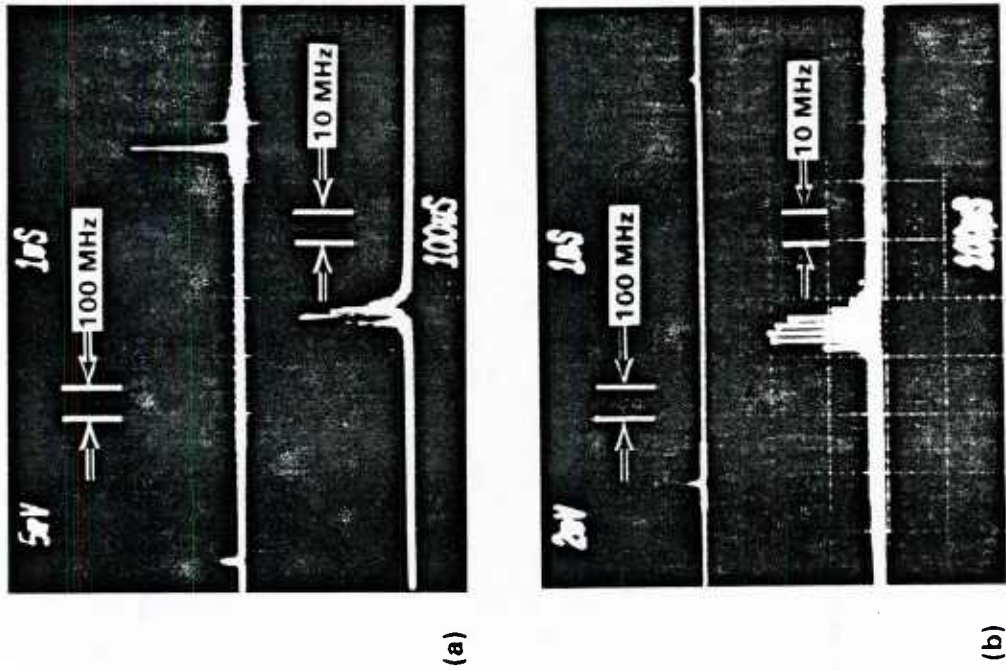


Fig. 4.3 Spectra of pulse output for external cavity as measured using Fabry-Perot scanning-interferometer spectrum analyzer. Alternate gain elements (#1, #3, #5) operated cw. The two intermediate gain elements pulsed from cw bias. (a) Pulse operation when bias is set so external-cavity laser is just above threshold cw. (b) Pulse operation when bias is set so laser ensemble is well below threshold cw. Envelope of pulses indicates linewidth (pulse rate faster than Fabry-Perot scan).

D. Experimental Results — Power Amplification

An interesting result that was obtained in the study of pulse operation of the coherent ensemble was that a small input could greatly increase the output power from the ensemble. The bias on elements two and four is kept at the reduced level of the second case discussed in Section C above, but the pulse height is also reduced to the point where the elements operating independently in the cavity are no longer above threshold. The dc current to elements one, three and five is increased so the ensemble is closer to threshold when no pulse is applied to elements two and four.

For this particular experiment, high spectral purity was not emphasized, though coherent operation and a single longitudinal mode as measured by the spectrometer of the ensemble was required. A filter with a duty cycle of 70% was used. Similar results occur with smaller duty cycle filters, but the effect was not as dramatic. With the spatial filter removed from the cavity, the spontaneous emission output power pulse height from elements two and four is measured. Then the spatial filter is placed in the cavity. The coherent ensemble is not above threshold during the part of the cycle when the pulse is off, but during the pulse part of the cycle, coherent output is evident because of the lowering of the system threshold due to the coupling action of the filter. The output power pulse height is measured with the filter in place. Figure 4.4 shows the experimental result comparing the two pulse heights. There is significant ($>10X$) pulse height amplification seen. This result is interesting because the small increase in power of the two intermediate pens which ordinarily only produces a small amount of spontaneous emission, in this coupled case provides substantial increase in total coherent power output. This result indicates for coherent ensembles with a spatial filter, a small amount of light injected from one element (possibly the output

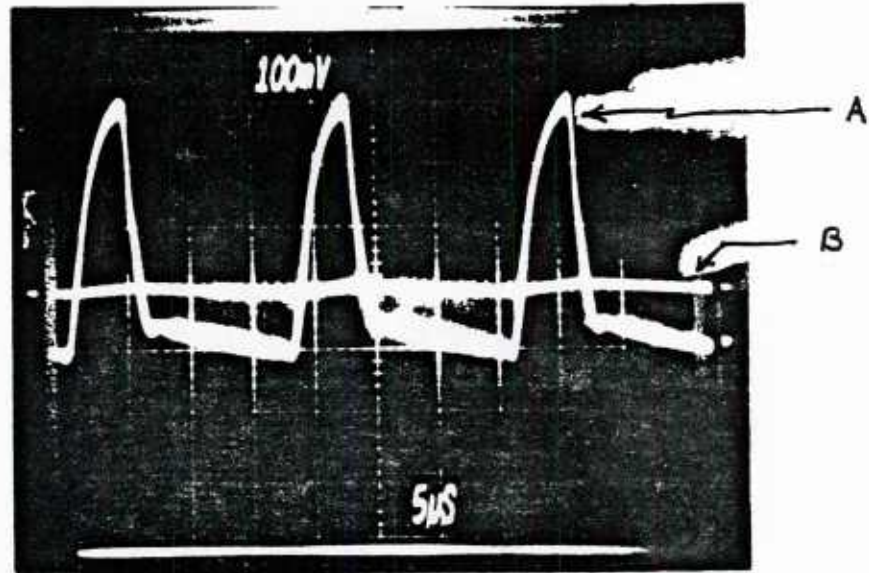


Fig. 4.4 Total power out — scope a.c. coupled. Pulses on pens two and four; D.C. on pens one, three and five.
A: spatial filter in (single frequency spectrum);
B: no spatial filter.

from a long distance fiber) can be significantly amplified using as source, the light from the other elements of the coherent ensemble. Thus an all-optical amplifier based on this principle may be feasible. This possibility has not been exploited any further to date in this program.

V. Validation of the Model of the External-Cavity Semiconductor Laser

A. Improvements to the Experimental Apparatus

A new spectrometer system was obtained for use in the program at no cost to the contract. The spectrometer is a Spex model 1870 and is driven by stepping motor controlled by a CD2A Compudrive. The output from the spectrometer system is digital and one of the more difficult items to obtain was an Allen Chart Recorder which converted the digital drive to an analog signal. This obviated the need for a computer which could not be obtained at no cost to the program. The spectrometer included an internal dither mirror which made it possible to obtain spectra as required in the order of a second on an oscilloscope. This capability insured that drifts did not occur during the taking of spectra and also enabled us to eliminate the cause of any drifts. The granite slab optical table shown in the photograph in Fig. 3.1 was replaced also at no cost to the contract with a new NRC, model RS 48-12, 4 foot x 8 foot optical table. Five detectors and associated optical trains were obtained and used to simultaneously monitor the outputs of the five elements of the coherent ensemble as seen through the semitransparent mirror at the end of the cavity (see Fig. 5.1). [Fig. 5.1 is similar to Fig. 4.1 but illustrates that the external cavity as now configured has five distinct outputs.] The optical train contained beam-splitters and flip-mirrors so one could take simultaneously two of the following three measurements: spectrum from the spectrometer; higher resolution spectrum from the scanning Fabry-Perot; and intensity measurements from the five detectors.

B. Improvements to the External Cavity

The spatial filter holder in the external cavity which previously was modified to accept the new sets of spatial filters was further modified. The

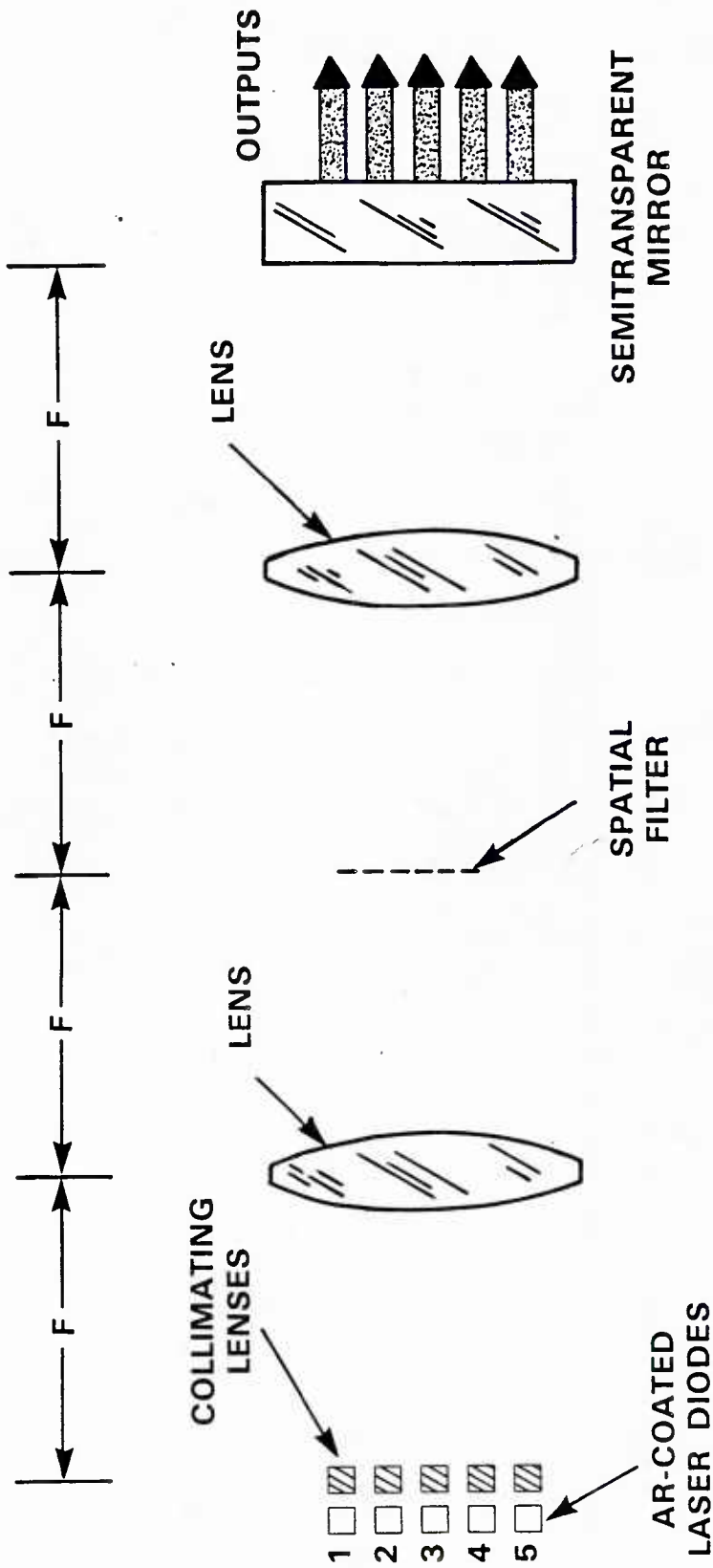


Fig. 5.1 Schematic of multiple-element external-cavity arrangement showing the placement of the five antireflection-coated diode lasers, the associated collimating optics, the two lenses, spatial filter, and end mirror. As indicated on the figure, the elements are separated by the focal length of the lenses so the light undergoes a Fourier transform four times during one round trip through the cavity. This figure illustrates that the external cavity as configured has five distinct outputs.

structure was made more rugged and a stepping motor drive for the tilt controlled from outside the plexiglass enclosure was added. This eliminated the "friendly effect" when one removed fingers from the micrometer, which was the weakest link in optimizing the alignment of the optical system.

C. The Experimental Results — The Intensity Distribution

For 30% duty cycle filters and the five gain elements, the predictions of the many-pass model described in Section III D above are well approximated by requiring that the single-pass transmission through the spatial filter be at its maximum. In this section experimental results are presented for the output intensity distribution between the five gain elements and compared with the distribution predicted by the theory of maximum single-pass transmission. For the intensity measurements, the intensity of the radiation from each of the "images" of the gain elements at the semitransparent mirror was measured with the array of five Si detectors. These intensities would be the same as the intensities from each of the gain elements assuming steady state and perfect symmetry of the cavity. To obtain the theoretical distribution, the amplitude distribution of the output from the ensemble of the gain elements was smoothly varied from a uniform to a Gaussian envelope function. The intensity distribution at the spatial filter was determined from the magnitude-squared Fourier transform of the gain element distribution. The transmission through the spatial filter was calculated for each distribution. The intensity at the spatial filter for the maximum transmission (0.9) is shown in Fig. 5.2. (While the figure shows that secondary interference maxima are blocked by opaque regions of the spatial filter, we corroborate what is well known by microwave engineers, i.e., that the intensity distribution which has nearly zero energy in the side lobes has a wider main lobe, wider than the slit

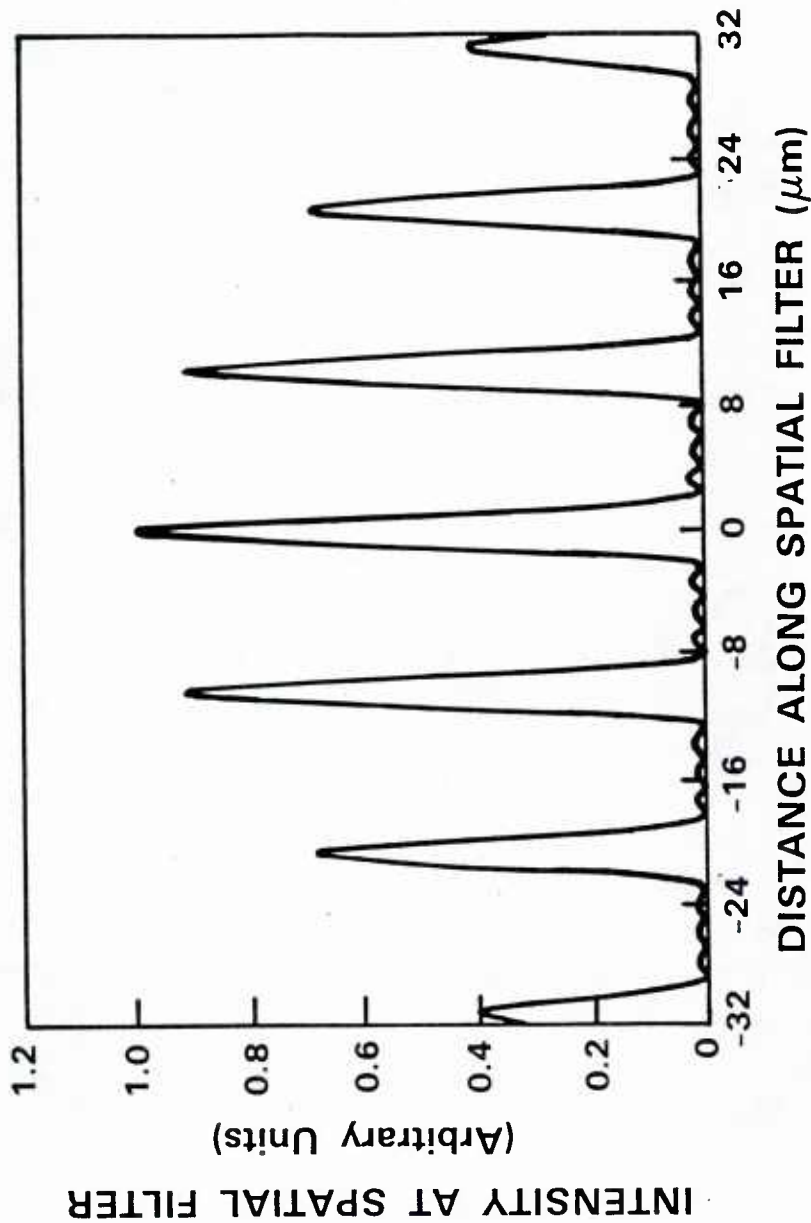


Fig. 5.2 Interference pattern at spatial filter for gain-element amplitude distribution of (0.64, 0.90, 1.0, 0.90, 0.64) which has maximum one-pass transmission through 30% duty cycle filter. Results are shown for the symmetric normal mode (all elements in phase) in which case the zero distance along the filter is on the optic axis of the cavity. The corresponding gain-element intensity distribution is (0.41, 0.81, 1.0, 0.81, 0.41).

opening, and has less transmission through the filter than the intensity distribution of Fig. 5.2. Such an intensity distribution with zero side lobes is illustrated in Fig. 5.3).

In Fig. 5.4 are plotted the experimental intensity distributions at the cavity end mirror for the various gain elements with the cavity "optimally" aligned as determined from spectral linewidth of <7.5 MHz. Also plotted on the figure is the intensity distribution corresponding to the amplitude distribution whose Fourier transform gave the intensity distribution at the spatial filter shown in Fig. 5.2. The experimental points were obtained over a period of days with misalignment and subsequent realignment to take each set of points. The scatter in the points can be attributed to precision in realignment. As can be inferred from Fig. 5.2, the spot size at the spatial filter in the focal (also Fourier) plane for emission from only one gain element has a FWHM about $60 \mu\text{m}$ and perfect overlap of the five focal spots is required for perfect alignment. In extrapolating from five to a multiplicity of gain elements (or their fiber links) with a concomitant increase in element density, much smaller diameter optics would be used in collimation (see Fig. 5.1) and the focal spot would be larger. Thus, the precision required in realignment, as evidenced by the scatter of points in Fig. 5.4, is a worst case in the program to go to a multiplicity of fiber-coupled gain elements feeding the external cavity. This issue is specifically mentioned in this report because for the success of the program it is better that the feasibility experiments be worst cases.

D. The Experimental Results — The Phase Distribution

The theoretical model used to explain the earlier results predicts that with the spatial filter, two modes of operation of the external cavity can be selected. In one, the outputs from adjacent diodes are in phase (defined

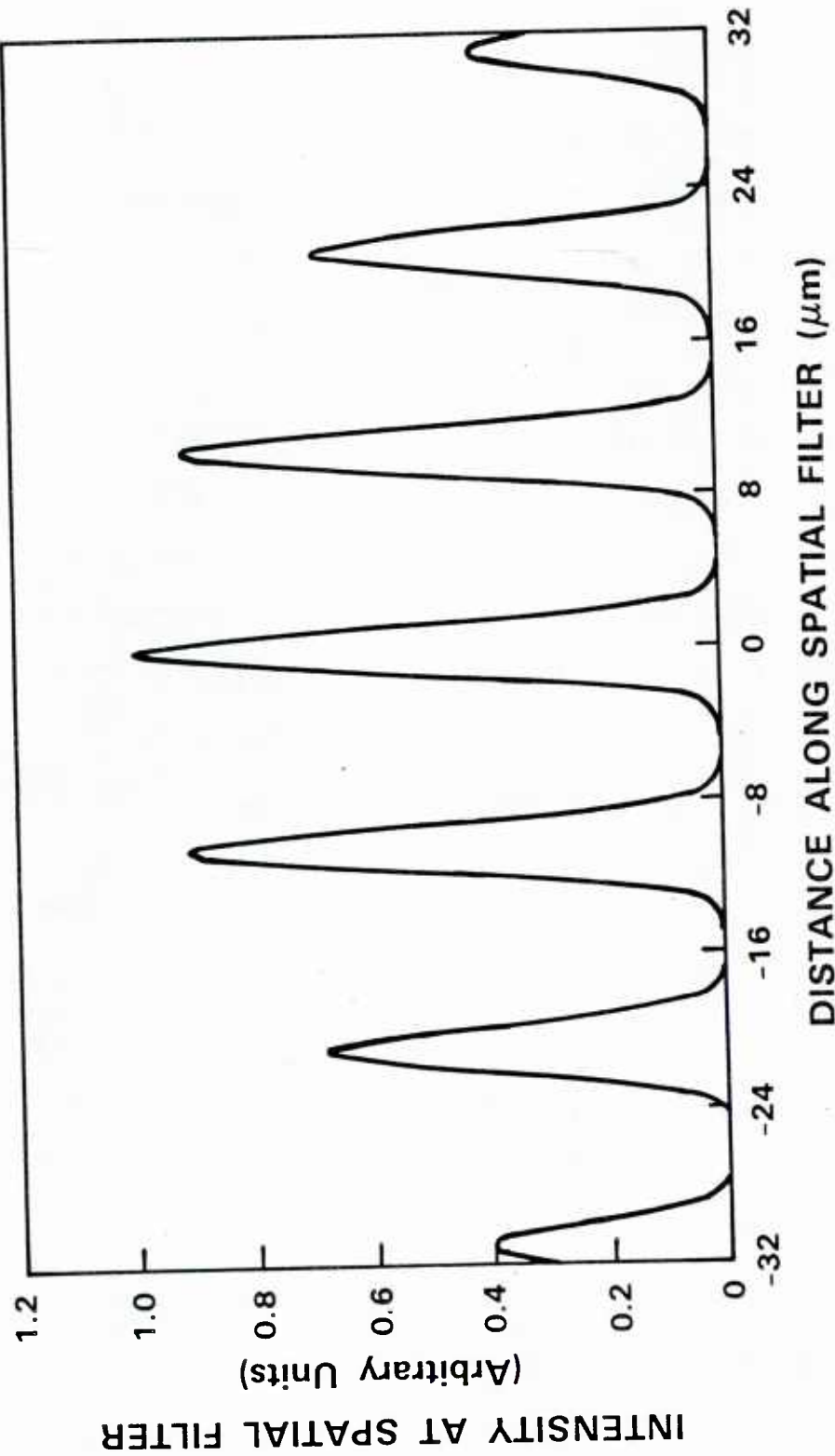


Fig. 5.3 Interference pattern at spatial filter for binomial gain-element amplitude distribution (1/6, 2/3, 1.0, 2/3, 1/6), for which there are no side lobes. Note that the main lobes are wider than those in Fig. 5.2.

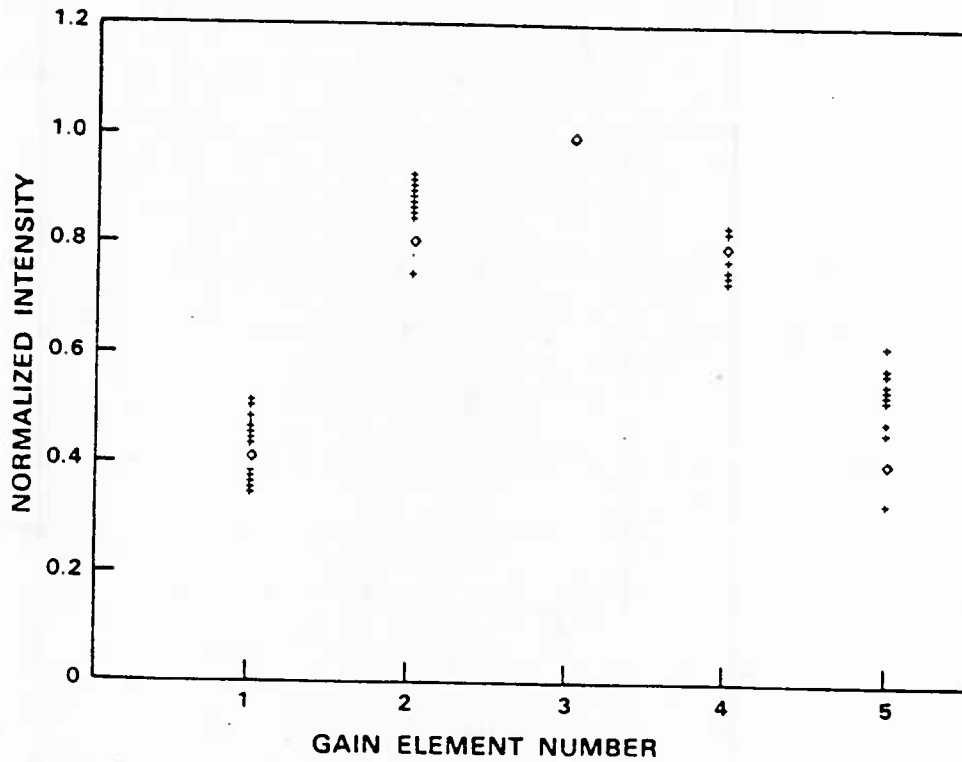


Fig. 5.4 Experimental values (+) for the intensity from each gain element of ensemble as measured at the cavity end mirror are compared to the expected values (◇) if the steady state intensities corresponded to maximum one-pass transmission through the spatial filter.

here as the symmetric mode); in the other, they are 180° out of phase (defined here as the antisymmetric mode). The model predicts that these modes are switched by moving the filter laterally by half the spacing between the center of its slits. The phase between diodes, as well as measurement of the coherence between the outputs of the various diodes, was measured using the two-slit modified Young's experiment illustrated in Fig. 5.5. The results are shown in Fig. 5.6. The symmetric mode, the mode in which adjacent diodes are in phase, was identified by using a two-slit experiment in which the two slits were close together so that the output from one gain element (obviously in phase with itself) interfered with itself. Note in Fig. 5.6 the switching from symmetric to antisymmetric mode when the spatial filter is translated by $1/2$ of the center-to-center slit spacing. For any given current distribution to the five gain elements above the threshold for ensemble lasing, when one switches from one mode to the other mode, the cavity output power remains the same. The current excitations were increased and other modes were searched for as the spatial filter was translated. None were found. These results are evidence that laser oscillation is not due to any parasitic feedback and that the cavity operation is controlled, as was predicted, by the spatial filter. The model is validated and can be used to extrapolate to coherent ensembles of a multiplicity of discrete diodes and/or wafer scale integrated diode lasers. The high fringe visibility in Fig. 5.6 is an indication of the high degree of coherence between the outputs from the various diodes.

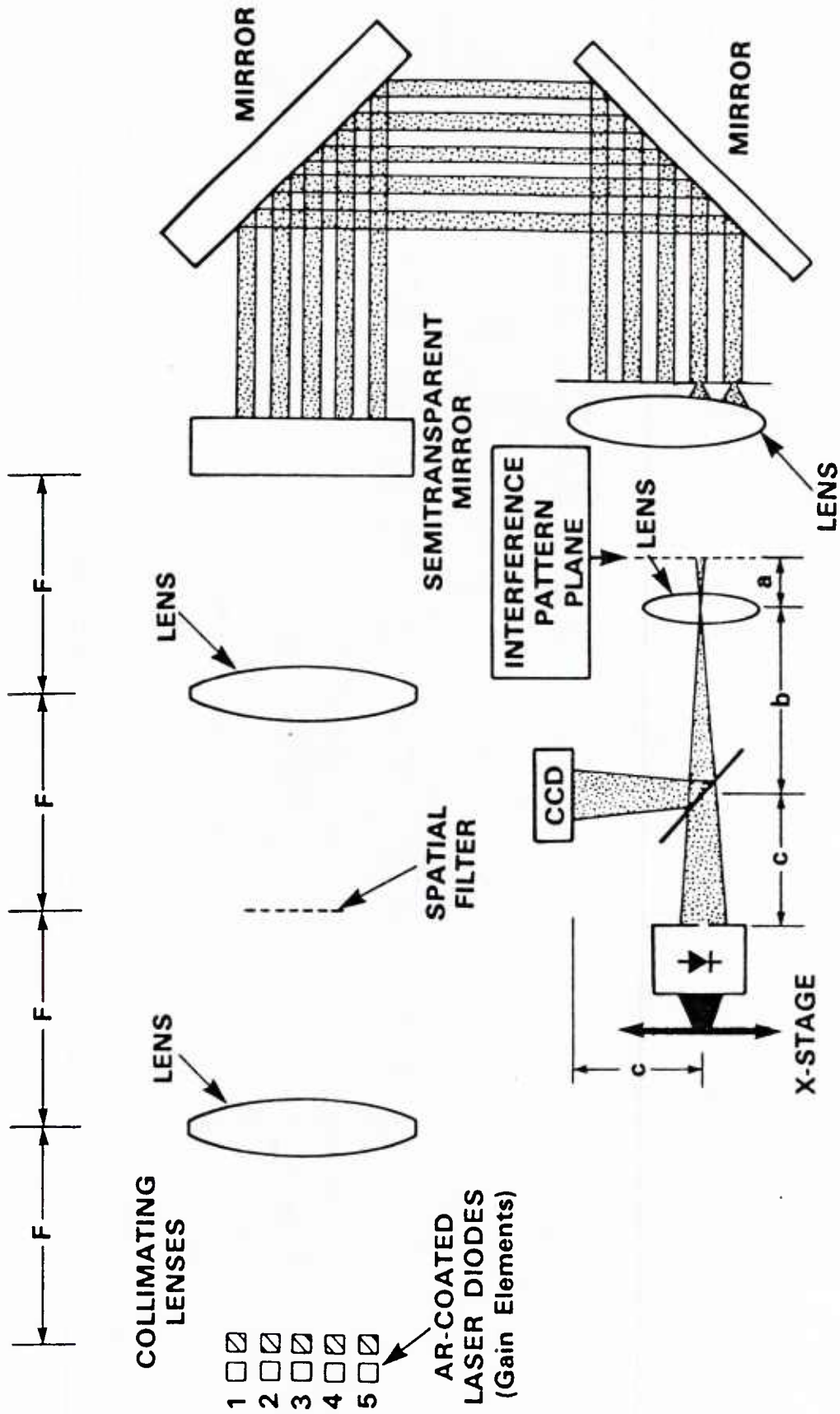


Fig. 5.5 Experimental arrangement for two-slit interference measurement. The external cavity is shown schematically in the upper left with the AR-coated laser diodes numbered and distance F being the focal length of the lenses. The optics to the left of the interference pattern plane magnify the pattern at the detector and the CCD camera. 108030-1

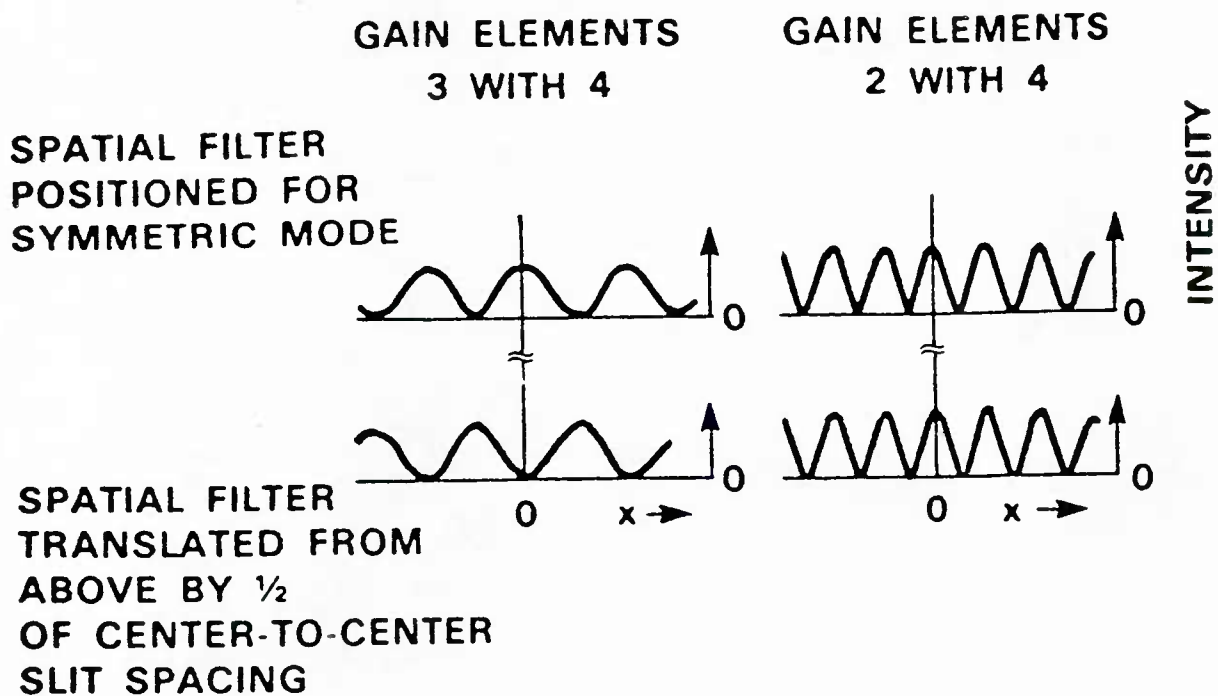


Fig. 5.6 Two-slit interference pattern illustrating the symmetric and the antisymmetric normal modes of the cavity. The intensities at the slits from the gain elements are adjusted to be equal. The high visibility of the fringes is an indication of the coherence between the outputs from the elements.

VI. Preparations for Fiber-Coupled Operation

A. Effect of Changing the Polarization of the Radiation at the Input to the Cavity

Since placing a single-mode fiber in series between the gain element and the input to the cavity may change the polarization of the radiation into the cavity, before removing the gain elements from within the cavity, it was felt important to simulate this polarization change by inserting a half-wave plate in series with gain element #4 as shown in Fig. 6.1. The polarization of the five "images" at the semitransparent mirror was measured and found to be identical. It should be emphasized that as long as the optics in the cavity are properly aligned for optimum lasing, the intensity distribution among the gain elements is independent of relatively large variations of the current in each element. There is feedback between all the elements and the intensities adjust. In either the symmetric or anti-symmetric modes of operation (see Fig. 5.6), the all gain elements produce TE-polarized radiation. This state of polarization was changed by the insertion of the half-wave plate in series with gain element #4. Since the spatial filter was designed to optimally transmit the interference pattern of the five gain elements, when the half-wave plate was set to rotate the polarization by 90° , the radiation from all of the elements remained TE at the spatial filter in the Fourier (also focal) plane. (TM and TE radiation are orthonormal and do not interfere.) Thus, for these experimental conditions the interference pattern had maximum transmission through the spatial filter and the ensemble threshold for the external cavity laser was a minimum. In this case, the current of gain element #4 which is in series with the half-wave plate had to be increased to reach ensemble threshold because it operates TM. By raising the operating currents of the other four gain elements, the threshold current of gain element #4

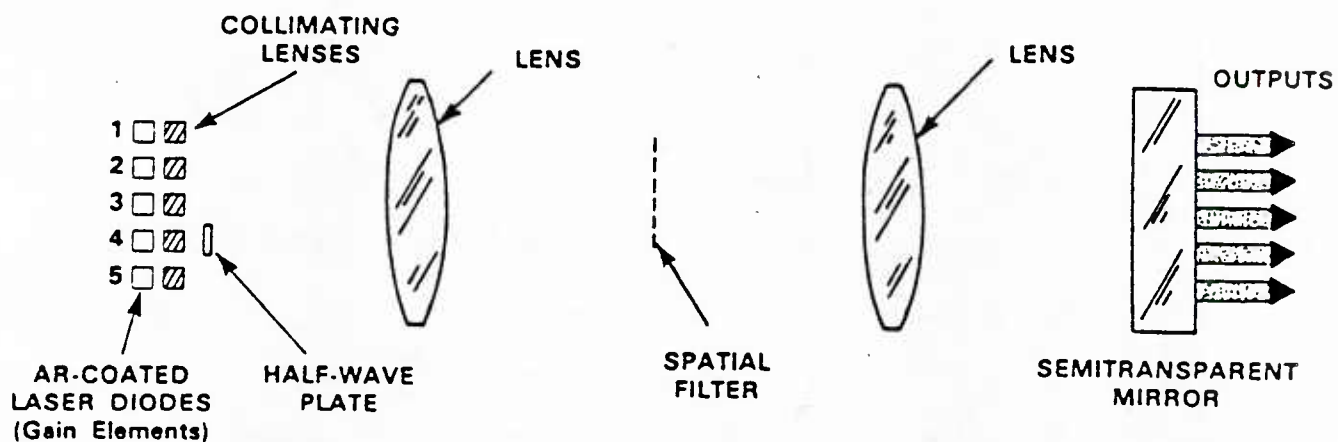
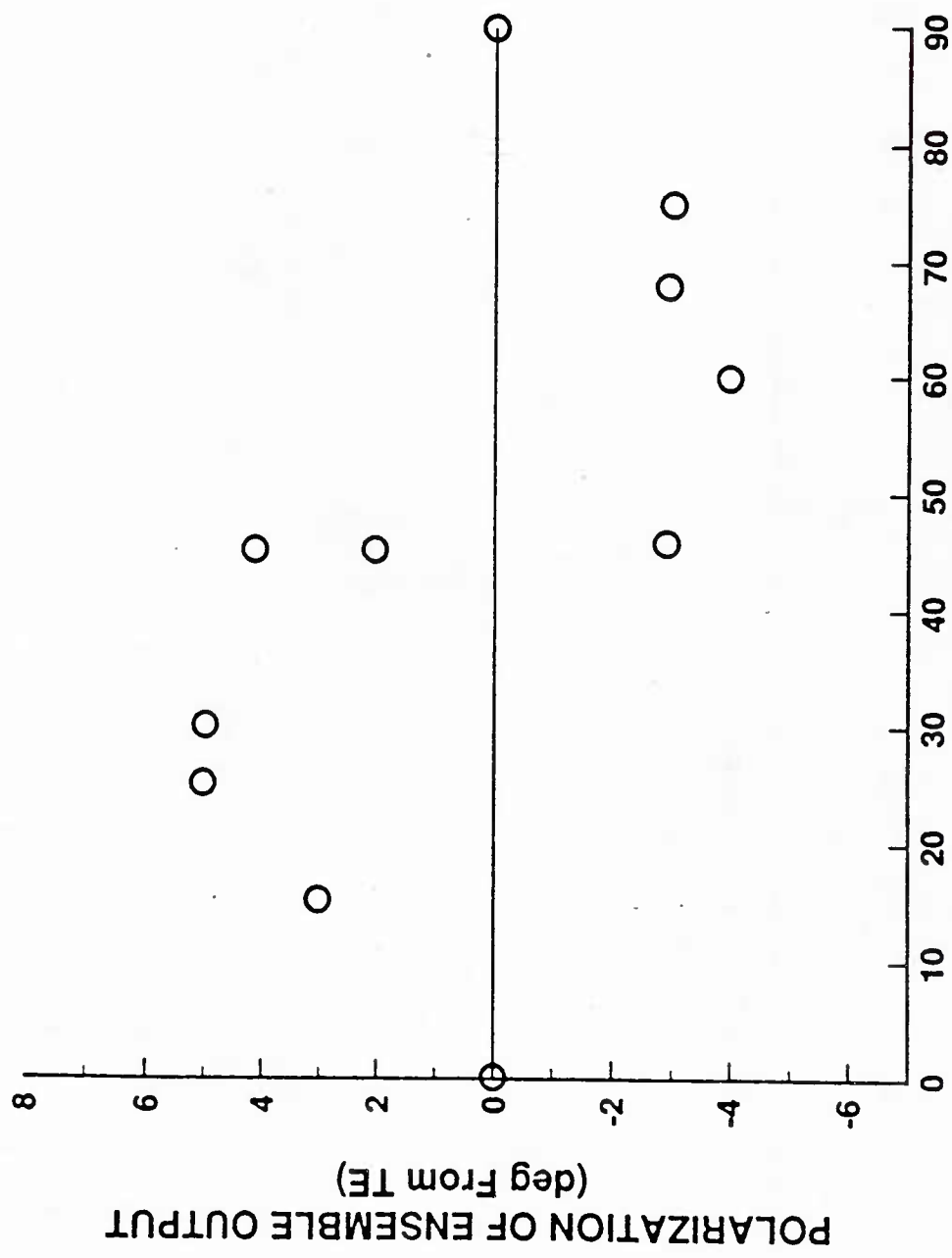


Fig. 6.1 Schematic drawing of the optical system for polarization measurements of coherent array. The half-wave plate rotates polarization of output from gain element #4.

operating TM could be reduced to or below its threshold with the half-wave plate removed and it operating TE. This demonstrates the cooperative nature of the coupled feedback. The ensemble threshold currents are, however, increased over the case for the half-wave plate set to rotate the polarization by 0° with all the gain elements operating TE.

The ensemble operation was studied as the half-wave plate was set to rotate the polarization of the radiation from gain element #4 by various angles between 0° and 90° . The results shown in Fig. 6.2 exhibit a polarization pulling of up to 5° from TE, as measured for each of the five outputs at the cavity end mirror and switching at 45° polarization rotation in the half-wave plate. The switching is due to the changing of the output of gain element #4 between TE and TM operation. This is consistent with the gain element exhibiting a self-stabilization effect in which the lasing polarization mode suppresses the onset (and gain) of oscillation in the other polarization mode¹. Two points should be noted from the experiment: 1) the ensemble continued lasing, albeit at lower power for all polarization rotations, and 2) the results are consistent with the model of ensemble operation.

The polarization experiments described above were performed in spite of the fact that at the same time precautions were taken to eliminate the steady-state variation in polarization of the outputs of the fibers^{2,3}. As shown in Fig. 6.3 each of the five fibers now contains three loops which use the linear birefringence induced by coiling the fiber, so two of the loops are quarter-wave plates and one of them is a half-wave plate. The fibers which are lensed at the gain element end and AR coated at the cavity end have been shown to perform as expected. By adjusting the angle of the loops, the polarization of the fiber outputs has been controlled to compensate for all effects on the polarization, either unavoidably present or intentionally introduced in the rest of the fiber-coupling system. As described above in this section,



ROTATION OF POLARIZATION OF RADIATION FROM GAIN ELEMENT No. 4 (deg)



Fig. 6.2 Polarization of the ensemble output as a function of the rotation by the half-wave plate of the radiation from gain element #4. Before each experimental point was obtained, the spatial filter was removed and the polarization rotation of the half-wave plate was measured. Thus hysteresis, if it occurred, would not be observed.

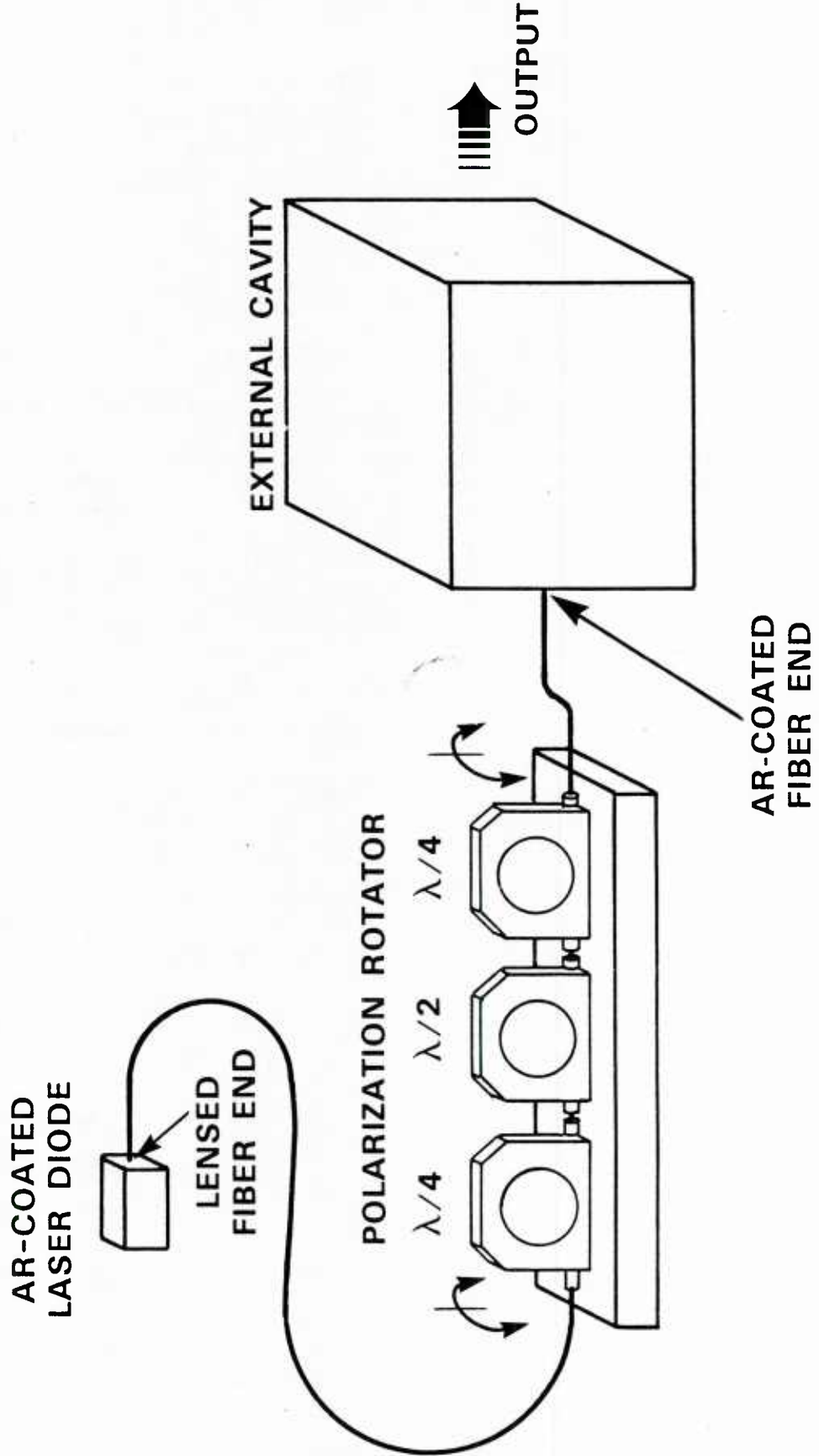


Fig. 6.3 Gain element coupled into external cavity with single-mode fiber. The output from the gain element (AR-coated laser diode) has TE polarization. The polarization rotator assures that the input to the cavity is also TE, compensating for effects on the polarization introduced by the rest of the fiber-coupling system.

for optimum operation of the external cavity laser the outputs of all the gain elements at the spatial filter must be of the same polarization.

B. Quantification of Coupling with One-Meter Fiber

In this experiment a single element external cavity consisting of a microscope objective to collimate the output of the fiber and a partially reflecting end mirror was used in the arrangement shown in Fig. 6.3. In order to efficiently couple the output of the AR coated gain element into the fiber, the end of the fiber was shaped into a lens as shown in Fig. 6.4. The lens was formed by first etching the bare fiber end in an acid solution proprietary to AT&T Bell Laboratories. The tip was then melted into a rounded ball with a chosen radius of curvature to form a lens with an appropriate focal length. By maximizing the overlap integral of the radiation pattern of this lens to that of the radiation exiting the laser diode facet, a high collection efficiency was obtained.

As a preliminary experiment in order to optimize the shape of the fiber lens, the collection efficiency was measured by collecting the output of a laser diode that was not AR coated. Results are presented in Fig. 6.5 in which the collection efficiency is plotted as a function of the radius of curvature of the fiber lens. The optimum radius of curvature was found to be $9\mu\text{m}$ resulting in a collection efficiency of 63%. (In the results described below for an AR coated laser (gain element), a similar collection efficiency was obtained with a $9\mu\text{m}$ radius of curvature fiber). In order to accurately align the fiber tip with respect to the gain-element facet, the lensed fiber was positioned using a 3-axis micromanipulator in combination with a three-axis PZT. The other end of the fiber was AR coated and coupled into the cavity using the Nikon 20X microscope objective.

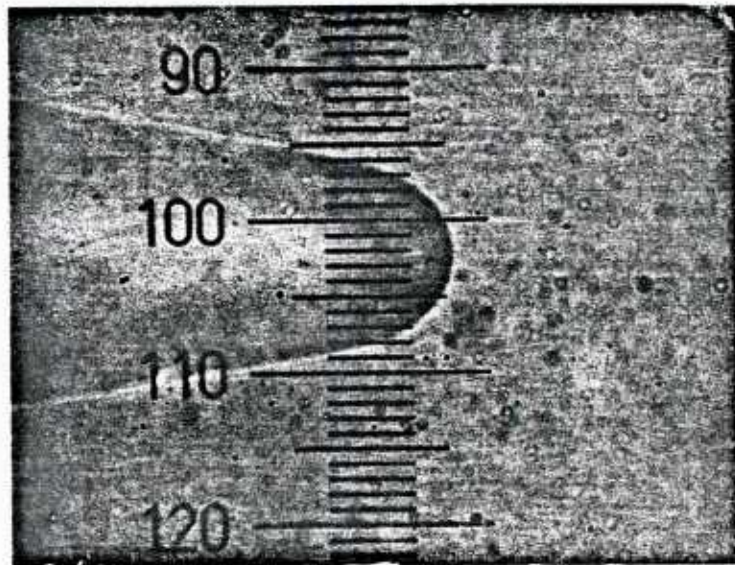


Fig. 6.4 Photograph of the lensed end of single mode fiber. Microscope reticle has scale of $2\mu\text{m}/\text{div}$ showing that lens has a radius of curvature of $12\mu\text{m}$.

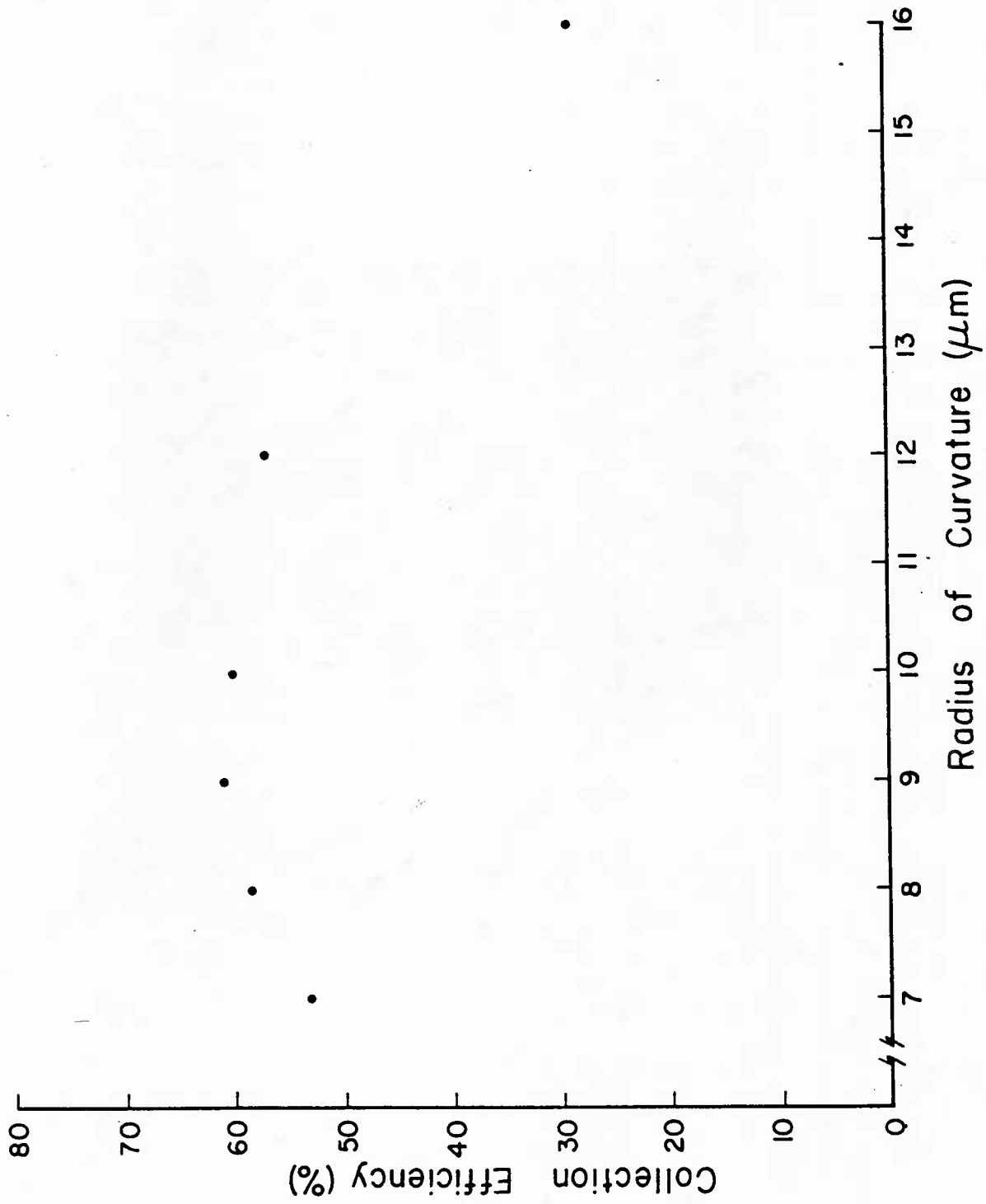


Fig. 6.5 Single mode fiber coupling efficiency as a function of radius of curvature of the lensed fiber end. Data was taken using a diode laser that was not AR coated.

Great care is being taken to make sure that the AR coated diode facet will not contribute any significant reflection into the laser-diode. Feedback from the right facet in Fig. 6.3 would compete with the external cavity feedback, (now reduced by the laser to fiber coupling loss), not allowing external cavity control of the laser output (one of the major goals of this program). In collaboration with Lincoln Laboratory, an AR coating facility has been developed. The coating is $\lambda/4$ of ZrO_2 deposited in a high vacuum e-beam evaporator with a small partial pressure of O_2 . To properly AR coat this facet, a circuit was built which monitors the output power of the laser diode while it is in the evaporator with a photo-detector also inside the evaporator. The laser was pulsed with a 10% duty cycle to reduce any possible self heating. With this arrangement the threshold current was measured as the coating was applied. When the threshold began to approach its maximum the evaporation rate was reduced to $2\text{\AA}/\text{sec}$. The shutter between the source and the laser was closed when the threshold reached its maximum.

Figure 6.6 shows the output power as a function of the input current during operation of the laser diode in the single-element external cavity for four different configurations. Curve (a) is for the laser diode operating independently before AR coating its front facet. Curve (b) is for the same diode, now an AR coated gain-element, placed directly at the input to the single-element external cavity. Curve (c) shows the effect of using a single mode fiber to couple the gain element into the external cavity as shown in Fig. 6.3. The fiber lens used has a radius of curvature of $9\mu\text{m}$. Curve (d) has the same configuration as (c) except the external cavity is spoiled.

One point that should be noted from comparing curves (a) and (c) is the extremely low coupling efficiency of the spontaneous light from the gain element into the single mode fiber. Only when the gain element emits coherent radiation does it efficiently couple into the fiber.

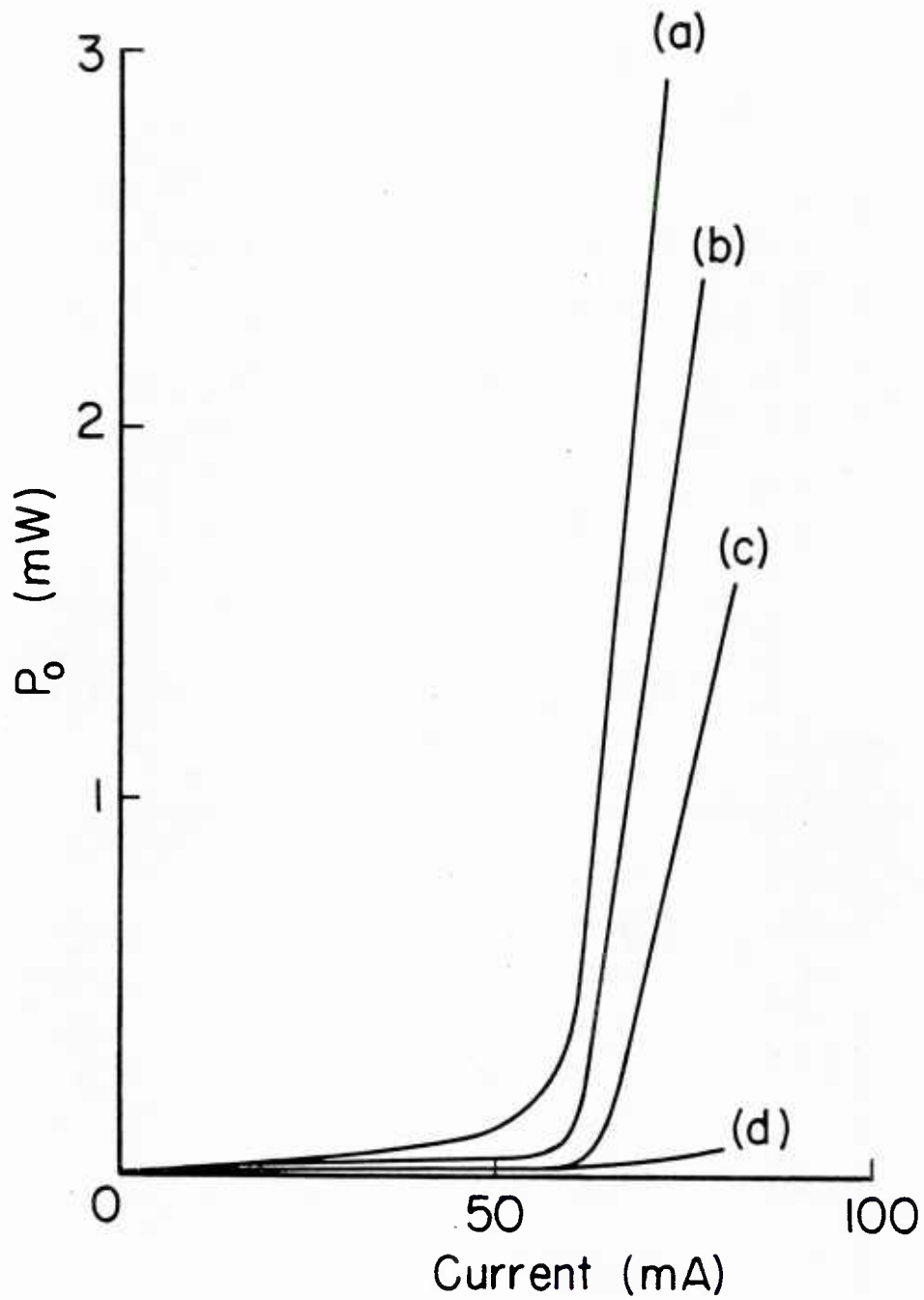


Fig. 6.6 Single-ended power output as a function of gain-element current, for four experimental configurations: (a) Diode laser before being AR coated; (b) gain element AR coated and placed directly at input to the external cavity; (c) gain element coupled into external cavity using a lensed fiber as shown in Fig. 6.3; (d) fiber coupled into spoiled cavity.

Using the model developed in Section II.C, values can be obtained for losses of the various elements in the cavity from the changes in threshold shown in Fig. 6.6. The model used is shown in Fig. 6.7. The values of T are the transmissions of the different loss elements inside the cavity and κ is the geometric mean of the coupling between a loss element and its two neighbors.

Using the fact that the total round trip gain in the cavity must equal unity, we obtain

$$I_t = A \left[\alpha l + J_0 \beta \Gamma l - \ln \sqrt{R_1 R_2 \kappa_1^2 \kappa_2^2 T_1^2 T_2^2} \right]. \quad (1)$$

For various sets of components within the cavity, the different thresholds are related by the equation

$$\exp \frac{I_t - I_t'}{A} = \sqrt{\frac{R_1' R_2' \kappa_1'^2 \kappa_2'^2 T_1'^2 T_2'^2}{R_1 R_2 \kappa_1^2 \kappa_2^2 T_1^2 T_2^2}}. \quad (2)$$

In order to solve this equation and calculate the different losses in the cavity, the constant A must first be determined for the type of laser used in this project.

To do this, an experiment was performed that determined the threshold current of the AR coated gain element in the external cavity for different neutral density filters with known loss inserted into the cavity. In Fig. 6.8, the output power of the cavity is plotted as a function of the input current for three cases. Curve (a) is for the AR coated laser diode in the external cavity with no additional loss ($T=1$). For curve (b), a neutral density filter of $ND=0.3$ ($T=0.50$) is inserted into the cavity. In curve (c), the neutral density filter has an $ND=0.5$ ($T=0.32$). In Fig. 6.9 the threshold current is plotted as a function of the $\ln(T)$ for the three different configurations. The least squares fit to these three data points shown in the figure has a slope of 9.9 mA.

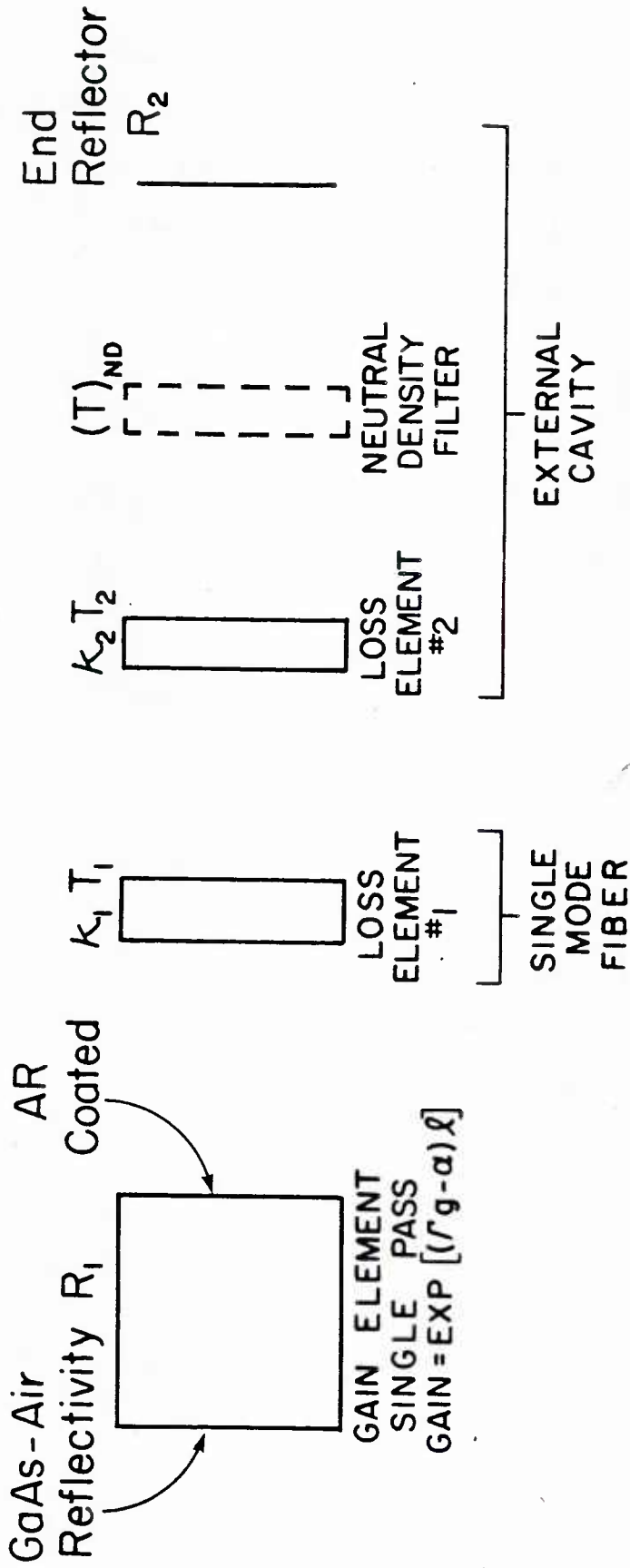


Fig. 6.7 Simple model of external cavity laser used in analyzing threshold currents for various configurations. Loss elements have a transmission T and a coupling coefficient κ which is the geometric mean of the coupling between the element and its two nearest neighbors.

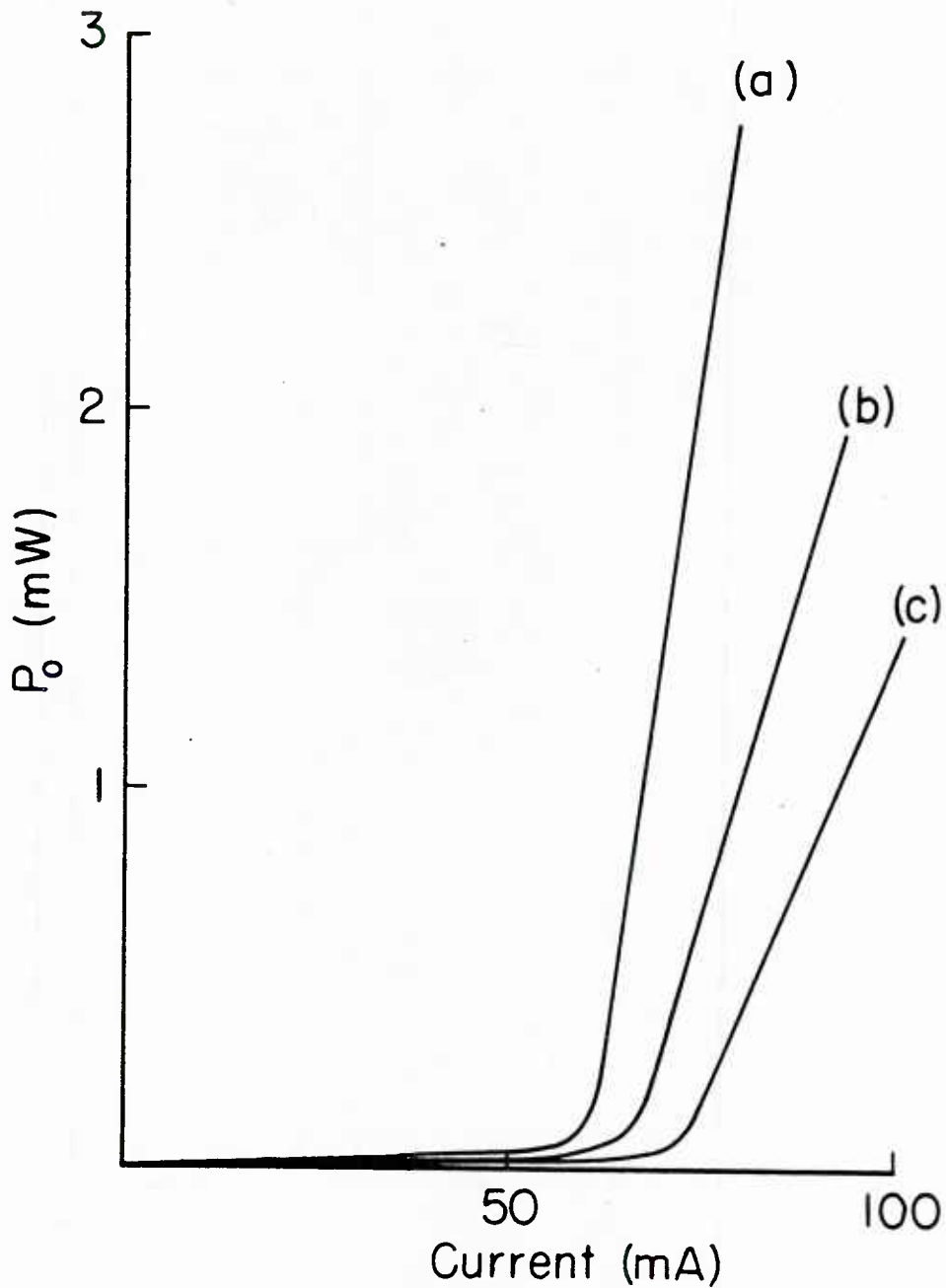


Fig. 6.8 Laser output power as a function of input current for different neutral density (ND) filters placed inside the single-element external cavity: (a) gain element coupled into external cavity with no additional loss: (b) gain element coupled into cavity with an additional ND = 0.3 filter ($T = 0.50$) placed inside the cavity: (c) gain element coupled into cavity with ND = 0.5 filter ($T = 0.32$) placed inside cavity.

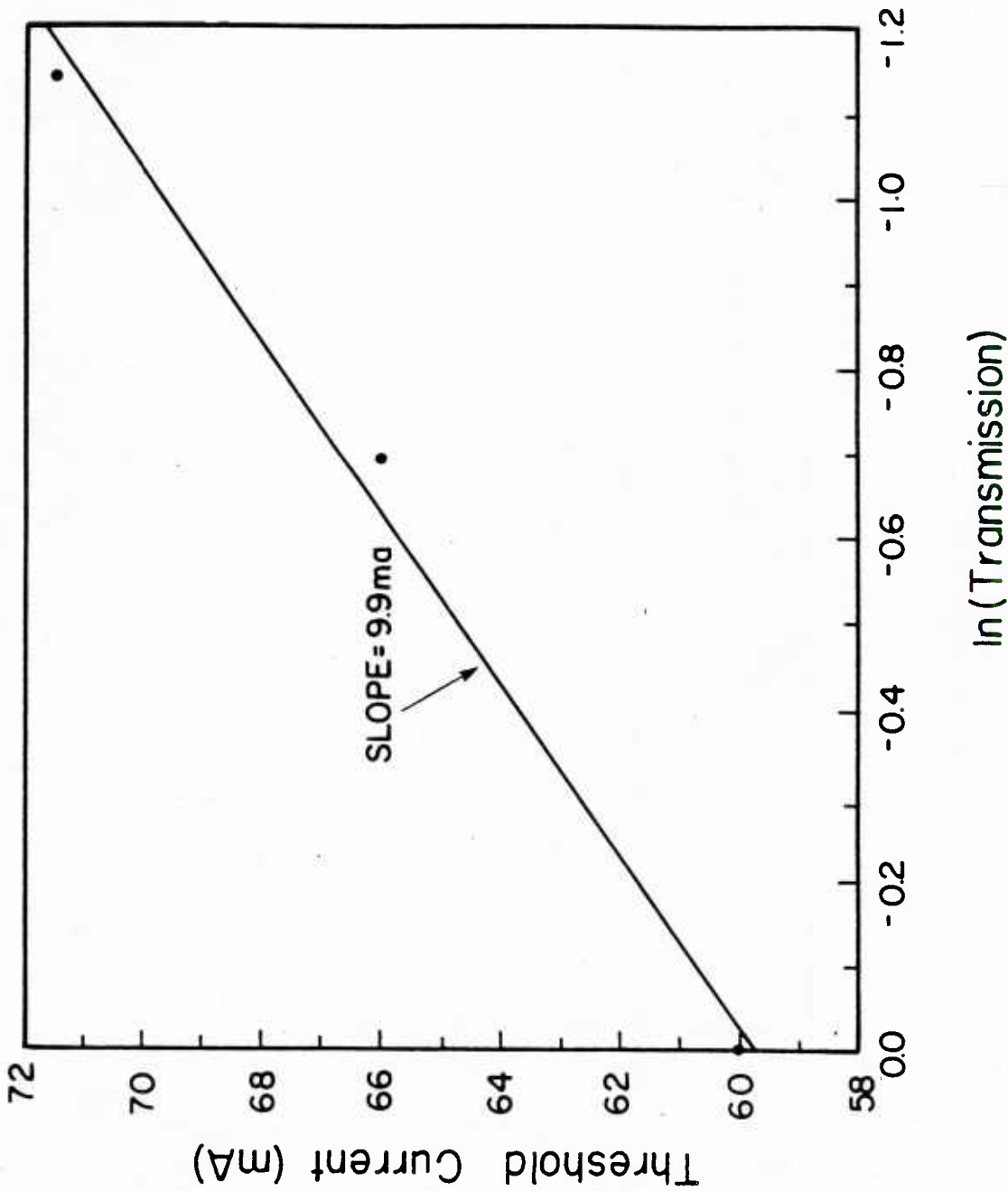


Fig. 6.9 Threshold current as a function of the natural logarithm of the transmission of the neutral density filters for the three different experimental configurations described in Fig. 6.8. Slope of the line that is the least-squares fit to the data is value of A and is equal to 9.9 mA.

It should be noted from Eq. (1) that for different loss elements inserted into the cavity, the threshold current is a linear function of $\ln(T)$, with a slope of A. Thus, the slope of the line in Fig. 6.9 is the value of A, which equals 9.9 mA.

With this value of A, we can now evaluate what the different losses in the system are by following the analysis in Section II.C. Looking back to Fig. 6.6 and using the uncoated laser diode as a reference, we have for configuration (a),

$$R_1' = R_2' = 0.32$$

$$T_1' = T_2' = 1.0$$

$$\kappa_1' = \kappa_2' = 1.0$$

$$I_t' = 59 \text{ mA}$$

The values used in the configuration (b) are as follows,

$$R_1 = 0.32$$

$$R_2 = 0.90$$

$$T_1 = \kappa_1 = 1.0$$

$$I_t = 60 \text{ mA}$$

Inserting these values into Eq. (2), the value of the product $\kappa_2 T_2$ for the microscope objective in the external cavity is calculated to be 0.54.

To evaluate the coupling losses for the single mode fiber ($\kappa_1 T_1$), the data obtained from curve (c) is used along with the values,

$$R_1 = 0.32$$

$$R_2 = 0.90$$

$$\kappa_2 T_2 = 0.54$$

$$I_t = 64 \text{ mA}$$

The value of $\kappa_1 T_1$ for the single mode fiber is then obtained to be 0.64 averaged in the forward and backward directions. This value agrees well with results described above for unidirectional coupling from a diode laser into a single mode fiber.

These quantitative results showing the high coupling efficiency from a laser diode to a single mode fiber are very promising and indicate that the fiber coupling will present no obstacle to the multi-element fiber-coupled external cavity laser. Together with the demonstration of polarization control and the validation of the model of the external cavity, they point to the feasibility of the multi-element laser as proposed earlier in the program.

C. Modifications to the Five-Element External Cavity

A major modification has been made to the first plate of the external cavity which is described as it was in its original form in Section IIIB and shown in Figs. 3.1 and 3.2. The plates still hold the micromanipulators and the piezoelectric transducers (PZT's) used to properly orient the five collimator pen assemblies. The collimator pen now contains the AR coated end of the fiber and the original collimating optic. This collimating optic is a 20x microscope objective, its lenses having been transferred to a customized barrel in the interests of compactness and part count reduction. The AR coated end of the fiber is epoxied into a glass ferrule in a newly designed subassembly. Centering of the fiber relative to the collimating optic is done as before in a special pre-alignment jig, and then locked prior to insertion of the collimator pen into the cavity. Final focussing of the collimator optic is done after the pen is in the cavity. Five laser-to-fiber coupling jigs have been designed and built. The laser is stationary and the fiber is aligned to the laser using a Line Tool XYZ manipulator on which an XYZ PZT, to which the lensed fiber is attached, is mounted.

Since the spacing and the aperture of the collimator pens are unchanged in this modification, no changes are required to any of the other plates in the cavity nor to the spatial filter.

The redesign of the external cavity so the output of 15 fibers can be fed into the cavity has been initiated. In this modification special small collimating lenses for fibers, such as are made by Corning Glass Co., have been obtained at no cost to the contract and will be evaluated. Long lead time items such as miniature PZTs and flexure mounts have been obtained. Theory presented in this report predicts that with the increased number of elements the spatial filter will both have higher transmission and be more selective. It is very desirable to prove the point that the concept improves as the multiplicity of inputs increases with the concomitant higher output power, leading towards practical applications based on the physics learned in this contract.

References — Section VI

1. T. Fugita, A. Schremer, and C.L. Tang, "Polarization instability in external cavity semiconductor lasers," Appl. Phys. Lett., vol. 51, pp. 392-394, 1987.
2. H.C. Lefevre, "Single mode fibre fractional wave devices and polarization controllers," Electron. Lett., vol. 16, pp. 778-780, 1980.
3. B.G. Koehler and J.E. Bowers, "In-line single-mode fiber polarization controllers at 1.55, 1.30 and 0.63 μm ," Appl. Opt., vol. 24, pp. 349-353, 1985.

VII. Epilogue

When this program, "Communications: Fiber-Coupled External Cavity Semiconductor High-Power Laser" started in July 1980, with the goal to show the feasibility of obtaining the 1 kW average power coherent laser beam from an array of semiconductor lasers, it was considered by the community as an extremely long shot. In my talk that was video-taped for the 100-year anniversary of Electrical Engineering at M.I.T., with the tape to be placed in a capsule for posterity, I stated that many were laughing at this goal. I then took out a pocket calculator and stated that those who proposed such a large array of transistors in such a small package were laughed at a decade earlier. No one is now laughing at obtaining a 1 kW average power coherent laser beam from an array of semiconductor lasers, although an array is still far from producing such a high coherent power. A major issue is how to dissipate the heat from such an array. This issue was well understood by the principal investigator in 1980. A patent covering the idea of fiber coupling a spatially distributed array and thus greatly reducing the power-dissipation density, the concept of this program, was issued in 1984 (U.S. Patent #4,479,224). This program is being continued under sponsorship by the Office of Naval Research under ONR Grant N00014-89-J-112, and in this next year the feasibility of fiber coupling and obtaining a coherent output beam will be demonstrated. The physics issues will be studied and operation optimized. For 1 kW average coherent power output, the alternative of the required active cooling system with fluid flowing through a sophisticated network of microchannels, if at all feasible, will be far more complex than the addition of the external cavity to the semiconductor gain-element system. The fiber coupling allows for geometric flexibility, for example, an annular input from an array of fibers into the external cavity with a simple spatial filter (see Fig. 1.1) would produce a coherent beam with high beam quality.

U241299